PHOTOCHEMISTRY OF SILYLCARBENE PRECURSORS AND MECHANISMS OF METALLAENE REACTIVITY

By

TRACY LEAH ANNE MORKIN, B. Sc.

A Thesis

Submitted to the School of Graduate Studies

In Partial Fulfillment of the Requirements

For the Degree

Doctor of Philosophy

McMaster University

MECHANISMS OF METALLAENE REACTIVITY

DOCTOR OF PHILOSOPHY (2001) McMaster University

(Chemistry) Hamilton, Ontario

TITLE: Photochemistry of Silylcarbene Precursors and Mechanisms of Metallaene Reactivity

AUTHOR: Tracy Leah Anne Morkin, B.Sc.

(Mount Allison University)

SUPERVISOR: Professor William J. Leigh

NUMBER OF PAGES: xix, 190

ABSTRACT

The photochemistry of a series of α-silylcarbene precursors has been studied by steady state and nanosecond laser flash photolysis (NLFP) techniques. Direct irradiation of (trimethylsilyl)ketene and –diazirine in hydrocarbon solution results in the formation of 1,1,2-trimethylsilene. Flash photolysis of (trimethylsilyl)ketene and –diazirine yield singlet trimethylsilylcarbene as the direct precursor to the silene, as illustrated by pyridine trapping experiments. On the other hand, irradiation of (trimethylsilyl)diazomethane results in photoisomerization to the diazirine or silene formation from the excited state of the precursor, depending on the wavelength of irradiation.

Photolysis of (pentamethyl)(trimethylsilyl)diazomethane or –ketene in methanolic hexane solution yields four methoxysilane isomers. 1,1-Dimethyl-2,2-bis(trimethylsilyl)silene (**11a**) is formed in the highest yield and is accompanied by the formation of three other silenes: *E*- and *Z*-1,2-dimethyl-1,2-bis(trimethylsilyl)silene and 1,1,2-trimethyl-2-pentamethyldisilanylsilene. Silene **11a** is the most electrophilic silene studied to date and its absolute kinetics with a number of nucleophiles in hexane and THF solution at 24°C were determined. The results were compared with relative rate data for the same silene determined by N. Wiberg in diethyl ether at 100°C.

1,1-Diphenylsilene, and its germanium analogue 1,1-diphenylgermene, were generated by photolysis of the corresponding 1,1-diphenylmetallacyclobutanes in hexane solution. Laser flash photolysis techniques were used to determine the absolute rate

constants and Arrhenius parameters for the head-to-tail dimerizations of these species. The dimerizations occur at nearly the diffusion limit and are among the fastest reactions known for these two species under these conditions. The photochemistry of the 1,1,3,3-tetraphenyl-1,3-dimetallacyclobutane dimers has been done in an effort to propose a possible mechanism for the dimerization of metallaenes.

ACKNOWLEDGEMENTS

Call it a network,
Call it a tribe,
Call it a family.
Whatever you call it,
Whoever you are,
You need one.
- Jane Howard

There is no way this work could have been done without the support of many scientists, colleagues, and friends. When choosing a school for graduate school five years ago, the best advice I ever received was to "pick a supervisor, not a school." Following this advice has been one of the best decisions I could have made. The enthusiasm, excitement, integrity, and tireless commitment to scientific excellence of my supervisor, Willie Leigh, have been sources of inspiration over the last five years. His well-timed pep talks and many chats over a beer or two are among my favourite McMaster memories.

Special thanks to Professors John Warkentin and Brian McCarry for their involvement on my thesis committee, and for helpful suggestions and comments during the writing of this thesis. I am also pleased to acknowledge Professor Tom Tidwell and Annette Allen at the University of Toronto for fruitful collaborations in the area of α-silylketenes.

The people I have worked with during my time at McMaster have made the Leigh lab the best possible place to work. Thanks to Drs. Rabah Boukkerroub, Corinna Kerst, Christine Bradaric, Nick Toltl, Bruce Cook and Ed Lathioor, former labmates who were instrumental in getting me on the right track when I first started. The current Leigh lab members, including Cam Harrington, Tom Owens, Greg Potter and Drs. Xiaojing Li and Dino Mangion have perpetuated the laughter and great working environment and I feel fortunate to have worked with all of them.

I thank Don Hughes and Brian Sayer for their patience during NMR experiments. Also, much gratitude goes to Mike Mallott for his selfless willingness to help during times of major computer catastrophes. I'd also like to extend my sincere gratitude to

Professors Paul Berti and Alex Adronov for insightful discussions and advice about life after Mac. This type of mentoring has made some important decision making easier.

Thanks to Professor Keith Kinder and the McMaster Concert Band for allowing me to play clarinet with them for five seasons. The musical outlet always made the long days in the lab more worthwhile. And thanks to the IR Sox, Bricklayers, Easy Lay-Ins and Chemical Waste for providing a recreational outlet through intramural sports. And of course, the Anal Chemists – one of the best memories I will cherish long after my days at Mac is winning the 2001 Phoenix Cup!

To some of the friends I have made at McMaster: Chris McCrory, Mustafa Mohamed, Marcus Kim, Paul Zelisko, Pippa Lock, John Lehmann, Feride Serefiddin, Arnold Kell, and Krista Kerr. Thanks for the countless beers on the Phoenix patio, late night chats, bike rides, bonfires, too many hands of cards, and for always believing in me.

To Stacey Brydges: I feel as though we have both danced our way through this journey and also dragged each other through it at times! With the "wisdom" exchanged, pizzas from Valentinos, cliché screw-ups and other ups and downs along the way, I celebrate reaching the end of this road together with more success, laughter and grace than I ever thought possible. Your spirit and selflessness are treasured gifts in my life.

To Shanda, Michelle, Jen, Emily, Aalim, Dave, Katie, Lynne and Janet: your listening ears and endless cheerleading during this process have been a blessing. And to Colleen Rapaich and Krista McAllister: you will never know how much your support, advice, and loyalty have made a difference in my life. You are indeed the angels in my life who have picked me up when my wings forgot how to fly.

To Mom, Dad, Scott, Daryl and Kelly: there is a piece of each one of you in every page that follows this one. I share this achievement with you, because every boat ride, birthday party, road trip, camping trip, every phone call across the miles and every late night around the kitchen table have carried me to this point. I love you all.

For Grandma and Grandpa Joe and Grandma and Grandpa Tom,
with love.

"Nothing great was ever achieved without enthusiasm."
Ralph Waldo Emerson

TABLE OF CONTENTS

LIST OF TABLES

LIST OF FIGURES

LIST OF SCHEMES

Prelude

When many people think about chemicals, one of the images that comes to mind are the rows of bottles that are stored on the shelves of science laboratories. However, there are many examples of molecules that are exceptionally high in energy and therefore very reactive, making their isolation and storage impossible. These species are known as ***reactive intermediates***. In the condensed phase, reactive intermediates range in lifetime from femtoseconds (10^{-15} s) to seconds and require sophisticated techniques to see them directly.

The reactive and short-lived nature of these intermediates is attributed to their instability in their environment, a lack or excess of electrons, or weak bonds between some of their constituent atoms. There are numerous examples of organic reactive intermediates. Free radicals (**1a**), carbenes (**2a**), and carbocations (**3a**) are electron deficient, whereas carbanions (**4a**) are examples of electron rich reactive intermediates.

1a

2a

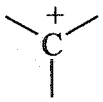

3a

4a

Reactive intermediates have been studied thoroughly to better understand not only chemical processes, but biological and environmental processes as well. For example, oxidative damage, which has been used to explain the effects of aging, heart disease, and

sunburns, has been found to involve free radicals.[1] Reactive intermediates also play a crucial role in the synthesis of polymers. Free radicals are utilized in the formation of polystyrene (used in food packaging materials) and polymethylmethacrylate (the plastic used in the lenses of eyeglasses); carbocations are used in the formation of polyisobutylene (used in the rubber industry for car tires); carbanions are important in the polymerization of caprolactone (a polymer used for biomedical applications as feeding tubes and drug delivery).[2] Carbon-based reactive intermediates have been studied since the early 1900s and continue to play a key role in relevant discoveries in modern chemical laboratories.

A much newer area in this field is the study of other Group XIV reactive intermediates. Silicon, germanium, tin and lead are in the same group as carbon. Tin and lead tend to favour the M(II) oxidation state, but silicon and germanium typically resemble carbon and favour the M(IV) oxidation state. The focus of this thesis is on some of the reactive intermediates of silicon and germanium. For each reactive intermediate in organic chemistry there is a metallic analogue, such as silyl or germyl radicals (**1b,c**), silylenes or germylenes (**2b,c**), silyl and germyl cations (**3b,c**) and silyl or germyl anions (**4b,c**).

1

2

3

4

b. M = Si
c. M = Ge

Organosilicon and organogermanium reactive intermediates have been studied much less extensively than their carbon-based counterparts. Silylenes[3] and silyl radicals[4] have been shown to play a role in the photolysis of polysilanes, a class of polymers that have unique physical and electronic properties. The chemistry of silylenes is analogous to many aspects of silicon surface chemistry, a field which is important in the areas of nanotechnology and the photolithographic manufacture of microchips and semiconductors.[5,6] Silyl anions have an important role in the synthesis of "nanowires."[7] Evidence for the first stable silyl cation has been reported recently.[8] The corresponding germanium species, such as germyl radicals, germylenes and germyl cations and anions have been investigated much less extensively.

The focus of this thesis is on a specific class of organometallic reactive intermediates whose carbon-based analogues (**5a**) are stable molecules. Silenes and germenes are organometallic compounds that contain a metal-carbon double bond (**5b,c**). Unlike the other reactive intermediates that have been discussed, these species are neither electron deficient nor electron rich: their reactivity is a result of other factors that will be discussed in upcoming chapters.

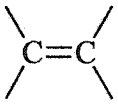

5a

5b

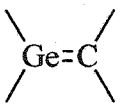

5c

The study of organosilicon and organogermanium reactive intermediates is a field of growing importance as our society and economy become increasingly centred on technological and scientific developments, particularly in the areas of materials, silicon

surface science and photolithography. Researching the principles that govern the reactivity of these species leads to a better awareness of what certain silicon and germanium containing materials can achieve and contribute to the latest developments at the scientific frontier.

Chapter 1

Introduction

1.1 Properties of Silenes and Germenes

Before the mid-1900s, it was widely believed that silicon-carbon and germanium-carbon double bonds could not exist. "The double bond rule," stating that elements outside the second row of the periodic table would not form double bonds, was published in numerous textbooks and upheld by many top scientists.[9] There were many reasons to suspect that species containing double bonds with third or fourth row elements, such as silenes and germenes (**5b,c**), would not form at all. The π bond between the metal and carbon was predicted to be very weak due to poor overlap between the 2p orbital on carbon and the 3p or 4p orbitals on silicon or germanium, respectively. The greater bond length of the metal-carbon bond was also predicted to weaken the bonding between the two centres. Furthermore, there is an electronegativity difference between carbon and the metal that makes the double bond polar ($^{\delta+}M{=}C^{\delta-}$). None of these unfavourable features are associated with alkenes (**5a**), where the double bond is formed between two 2p orbitals, the bond distance is shorter and there is no difference in electronegativity between the bonding atoms.

In 1967, Gusel'nikov and Flowers studied the gas-phase thermolysis of 1,1-dimethylsilacyclobutane (**6a**).[10] The product of the reaction was 1,1,3,3-tetramethyl-1,3-disilacyclobutane (**8a**, equation 1.1), which was proposed to form via the dimerization of the reactive intermediate 1,1-dimethylsilene (**7a**).

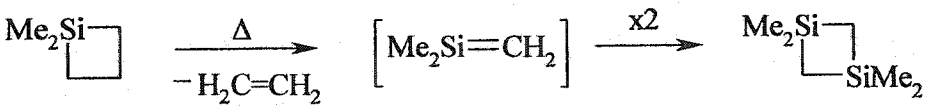

6a **7a** **8a** **1.1**

Since this discovery, numerous examples of metallaenes have been studied. Silenes have been studied most extensively and the area has been frequently reviewed.[11-15] More recently, organogermanium chemistry has become more prominent and germene chemistry has been reviewed as well.[16-18] The physical properties of both silene (**9a**) and germene (**9b**) have been well characterized and are outlined in Table 1.1. Interestingly, the longer bonds, dipole moments, π-bond energies (E_π) and infrared stretching frequencies ($\nu_{M=C}$) of **9a,b** support the characteristics that were originally thought to make silenes and germenes non-existent! These properties also make the reactivity of metallaenes exceptionally different from that of their carbon analogues (**9c**).

Table 1.1 A Comparison of the Physical Properties of Ethylene, Silene and Germene, as Predicted by Theoretical Calculations

	$H_2Si{=}CH_2$ **(9a)**[19,20,21]	$H_2Ge{=}CH_2$ **(9b)**[22]	$H_2C{=}CH_2$ **(9c)**[23]
M=C Bond Length/ Å	1.70	1.78	1.33
Dipole Moment	0.84	–	0
E_π /kcal mol^{-1}	38	33	65
$\nu_{M=C}$ / cm^{-1}	985	814	1645

1.2 Generation of Metallaenes

Silenes and germenes are formed from the thermolysis or photolysis of a wide variety of precursors. The precursor employed is determined by the metallaene substituents that are ultimately desired on the double bond. The synthesis of silenes[14] has been more thoroughly developed than the synthesis of germenes,[17] but in general, organosilicon compounds that have been shown to generate silenes have organogermanium analogues that often generate the corresponding germene. Metallaenes have most frequently been characterized as their adducts with nucleophiles (section 1.3.2.2).[14,24] However, kinetic studies and the use of time-resolved spectroscopy have further developed what is known about silene reactivity, stability and structure.[25] The majority of metallaene syntheses fall into one of five general categories: thermal salt

eliminations, *t*-butyllithium addition to chlorovinylsilanes, 1,3-sigmatropic shifts of disilanes, [4+2]- or [2+2]-cycloreversions and thermolysis or photolysis of α-silylcarbene precursors.

1.2.1 Thermal Salt Eliminations

The formation of unsaturated silicon or germanium compounds by this method requires that the precursor have a halogen (X) on the metal and lithium bound to the adjacent carbon, as in **10**. Upon thermolysis of **10** in the presence of butadiene, LiX salts are extruded and metallaene **11** is formed (equation 1.2), characterized by formation of **12**. N Wiberg and coworkers have illustrated that this type of reaction works well for generating 1,1-dimethyl-2,2-bis(trialkylsilyl)substituted silenes [26,27] and germenes.[28-30] The 1,1-dimethyl substituted derivatives (**11a,b**) were the original metallaenes studied, but Wiberg and coworkers more recently have extended this method to the generation of 1,1-diphenyl-[31,32] and 1,1-bis(*tert*-butyl)-2,2-bis(trimethylsilyl)silene[33] as well.

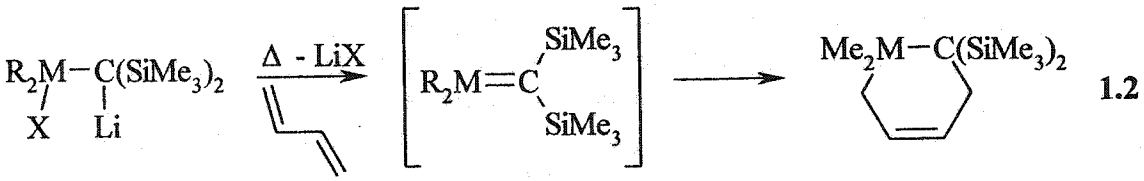

1.2

10 **11** **12**

a. M = Si
b. M = Ge

All of the silenes generated by this method have alkylsilyl groups at carbon, presumably because the precursor has a high degree of negative charge, which is stabilized by α-silyl groups.[34] There is one example of metallaene formation that does

not have this substituent pattern. Couret and coworkers generated the first isolable, stable germene (**14**) from the thermolysis of **13** (equation 1.3).[35]

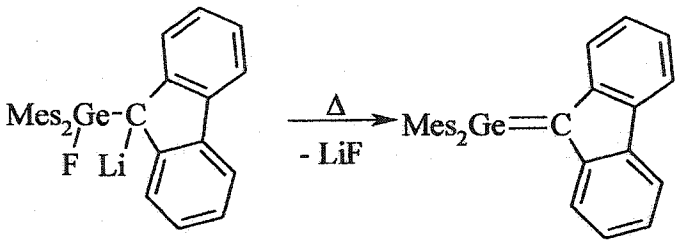

13 **14** 1.3

1.2.2 *t*-Butyllithium Addition to Chlorovinylsilanes

Silenes that have neopentyl groups at carbon can be easily generated from the nucleophilic addition of *t*-butyllithium to chlorovinylsilanes. Jones and coworkers were the first to add *t*-butyllithium to chlorodimethylvinylsilane (**15**) to yield 1,1-dimethyl-2-neopentylsilene (**16**, equation 1.4).[36-39] The silenes were proposed as intermediates on the basis of the observation of *cis*- and *trans*-1,3-disilacyclobutanes **17**.

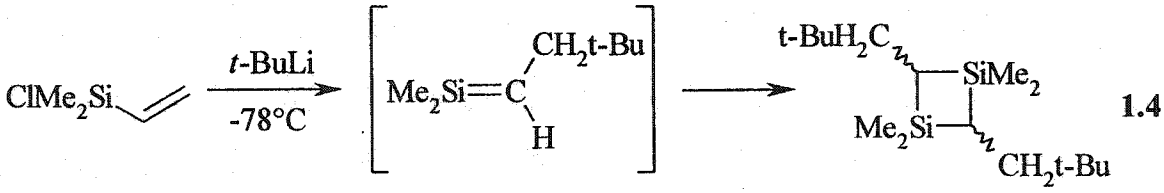

15 **16** ***cis/trans*-17** 1.4

Auner developed the method further and showed that a series of 1,1-dichloro- and 1,1-dimethyl-2-substituted silenes (**19a** and **b**) could be synthesized by the addition of *t*-butyllithium to the appropriate vinylsilane (**18a** or **b**,equation 1.5).[14,40-45] The silenes were characterized as their disilacyclobutane dimers or their adducts (**20**) with alcohols or

trimethylmethoxysilane.

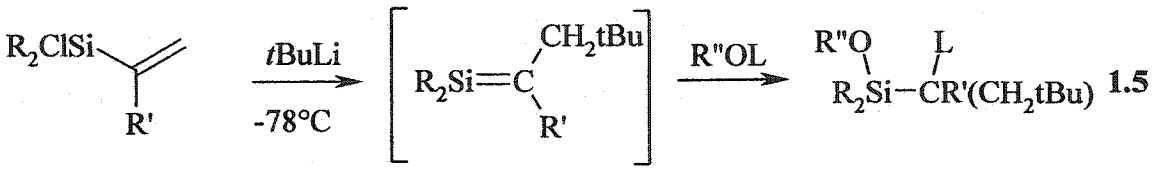

18 **19** **20**

a. R = Cl R' = H, Ph, $SiMe_3$, $SiMe_2OCMe_3$
b. R = Me R" = Me, Et L = H, D, $SiMe_3$

1.2.3 1,3-Sigmatropic Shifts in Disilanes

1,3-Sigmatropic shifts are a class of pericyclic reactions that involve four π electrons in the transition state and therefore are thermally forbidden to occur suprafacially and require a photon for the reaction to occur.[46] Vinyl-, phenyl-, alkynyl- and acyldisilanes are effective photochemical precursors to silenes via this pathway.[47] For example, the photolysis of pentamethylvinyldisilane **21** leads to 1,1-dimethyl-2-methyltrimethylsilylsilene **22**, as shown initially by Ishikawa and coworkers (equation 1.6).[48-50] Leigh,[51] Conlin[52] and Kira[53] have also used this method to generate other silenes from various vinyldisilane derivatives.

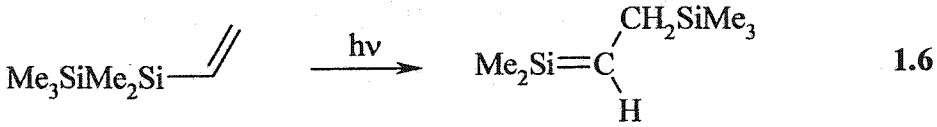

21 **22**

Aryldisilanes undergo an analogous photochemical rearrangement.[50,54-58] Photolysis of phenylpentamethyldisilane **23**, results in a [1,3]-migration of a trimethylsilyl group into the aromatic ring to yield a 1,3,5-(1-sila)hexatriene **24** (equation

1.7), which has been detected directly using time-resolved UV spectroscopy. Arylgermasilanes and aryldigermanes react similarly.[59]

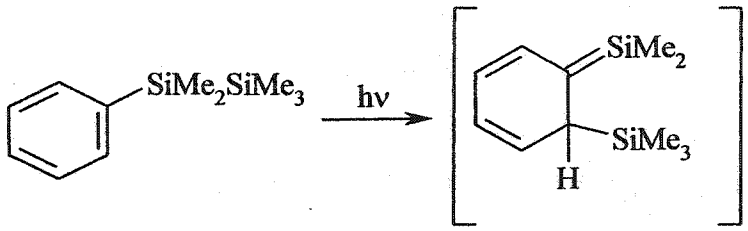

23 **24** **1.7**

[1,3]-Silyl migrations also occur upon photolysis of alkynyldisilanes, yielding 1-silaallene derivatives.[60,61-64] Photolysis of (phenylethynyl)pentamethyldisilane **25** affords 1-silaallene **26**, whose formation is support by the observation of adduct **27** (equation 1.8).[65] Like all of the metallaenes discussed so far, 1-silaallenes are typically reactive intermediates, although there are stable examples known.[66]

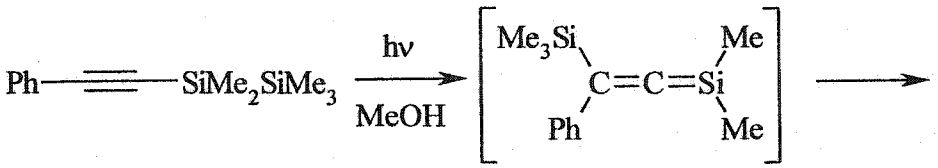

25 **26** **1.8**

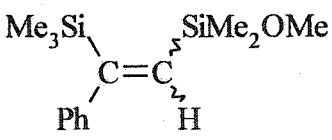

27

A significant class of silenes has been generated from the photolysis of acylpolysilanes.[14] Upon photolysis of acylpolysilanes such as **28**, one of the trimethylsilyl groups undergoes a [1,3]-migration to oxygen to yield silene **29** (equation 1.9).[67-70] It was the first stable, isolable silene and was characterized by NMR, IR and X-

ray crystallography. The reasons for its exceptional stability certainly involve the steric effects of the adamantyl and trimethylsilyl groups, but electronic factors are also important (*vide infra*, section 1.5).

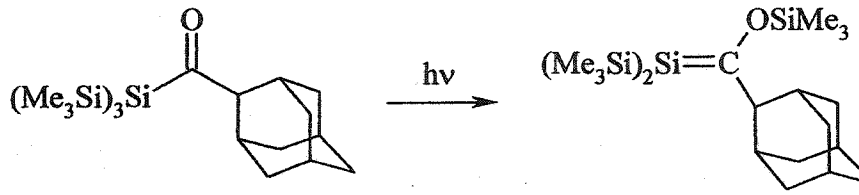

28 **29** **1.9**

1.2.4 [2+2]- and [2+4]-Cycloreversions

Thermolysis or photolysis of silacyclobutanes has been used to generate a variety of metallaenes in the gas phase[71-79] and condensed phase.[80-84] Ring opening proceeds via homolytic cleavage of an Si-C bond to form a 1,4-biradical intermediate.[85-87] This method has proven to be convenient for generating 1,1-disubstituted silenes (recall equation 1.1) and 1,1-disubstituted germenes (equation 1.10), as illustrated in the gas phase thermolysis of 1,1-dimethylgermacyclobutane **6b**.[88] This reaction has also been demonstrated to work well in the condensed phase photolyses of 1,1-diphenylmetallacyclobutanes **30a,b**.[84] The formation of the metallaenes (**31a,b**) is supported by the characterization of their adducts with methanol (**32a,b**, equation 1.11)[89,90] and by their head-to-tail dimers (**33a,b**).[91]

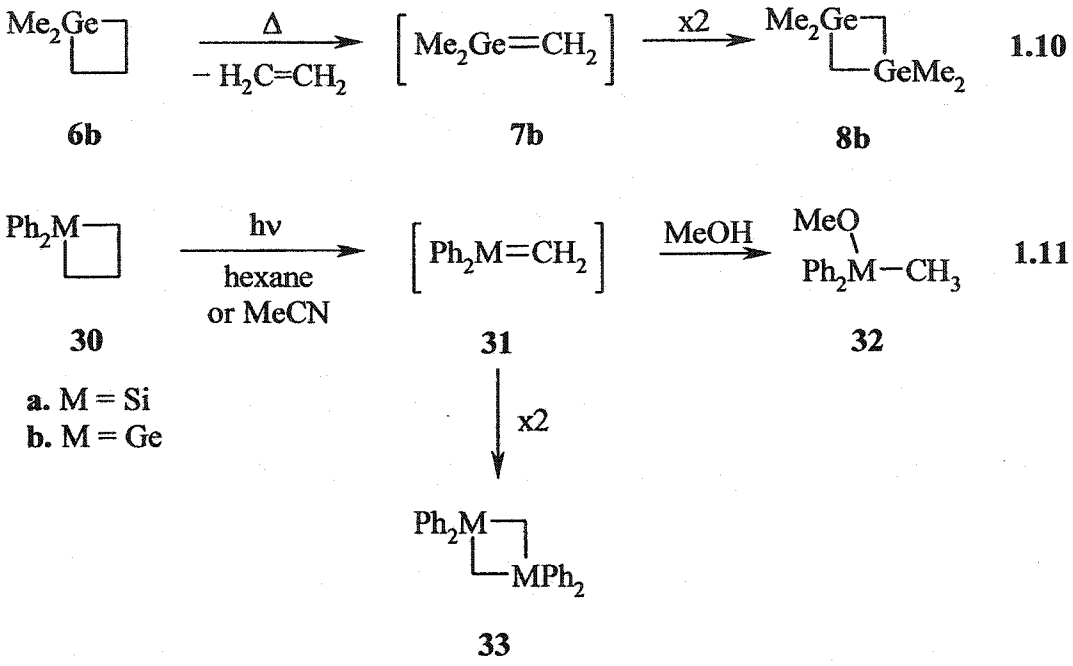

The photolysis or thermolysis of dimetallacyclobutanes has been shown to lead to metallaenes in certain cases.[92] Apeloig, Leigh and coworkers studied the thermal and photochemical decomposition of 1,2-dimetallacyclobutanes **34a,b**.[93] Thermolysis of **34a** in methanolic hexane leads to the exclusive cleavage of the silicon-silicon bond to form two molecules of silene **35a**, identified as the cycloaddition product with phenylacetylene (**38a**, Scheme 1.1). On the other hand, photolysis of **34a** in the presence of butadiene affords **39** and 2,2'-biadamantylidene (**37**) in quantitative yield, indicating that tetrakis(trimethylsilyl)disilene **36a** is formed. Interestingly, neither thermolysis nor photolysis of **34b** produces the analogous germene **35b**. Instead, the formation of **37** was observed, supporting the formation of digermene **36b** (Scheme 1.1).

Scheme 1.1 Photolysis and Thermolysis of 1,1,2,2-Tetrakis(trimethylsilyl)dispiro[3,3',4,4'-biadamantane-1,2-dimetallacyclobutanes] (34)

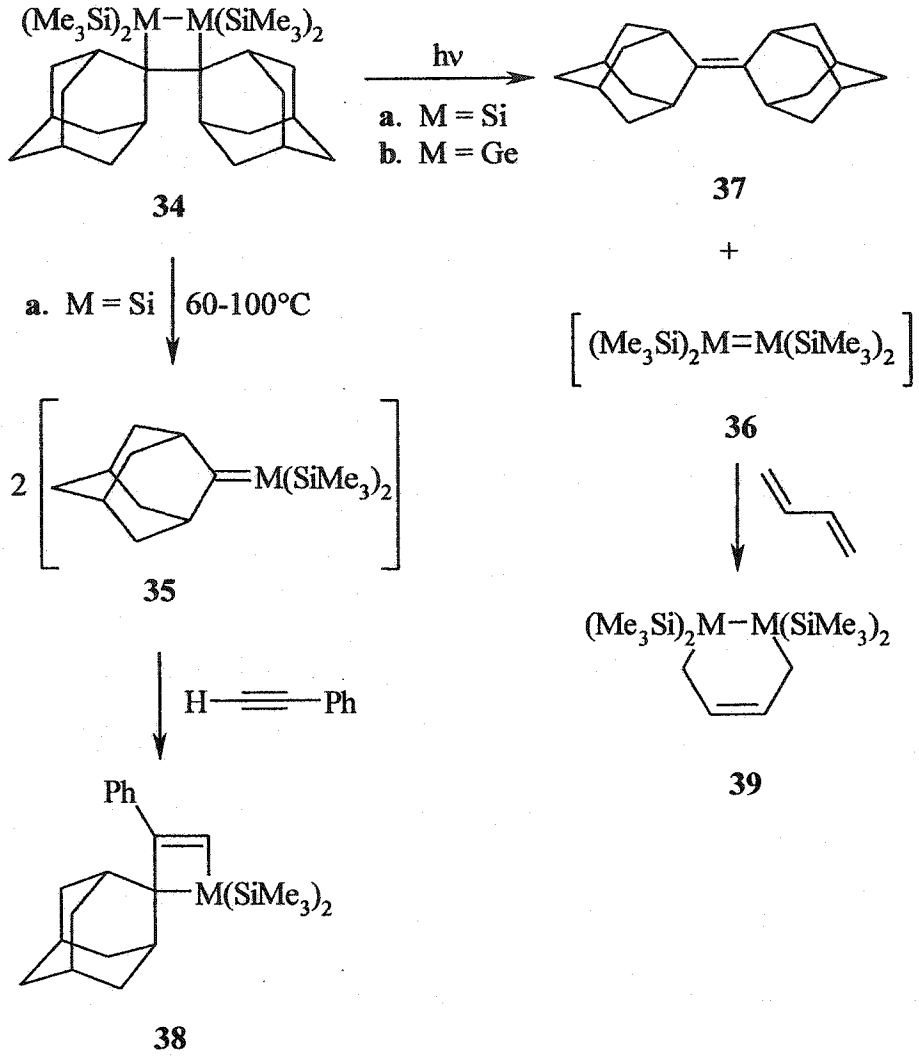

Jones and coworkers found that the retro-Diels-Alder reaction of **40** resulted in the formation of a mixture of 1,3-disilacyclobutanes (**42**), suggesting that silene **41** was formed as an intermediate (equation 1.12).[38] [2+4]-Cycloreversions have also been

shown to form germenes, in the thermolysis of bicyclic germanium compound **43** (equation 1.13).[94]

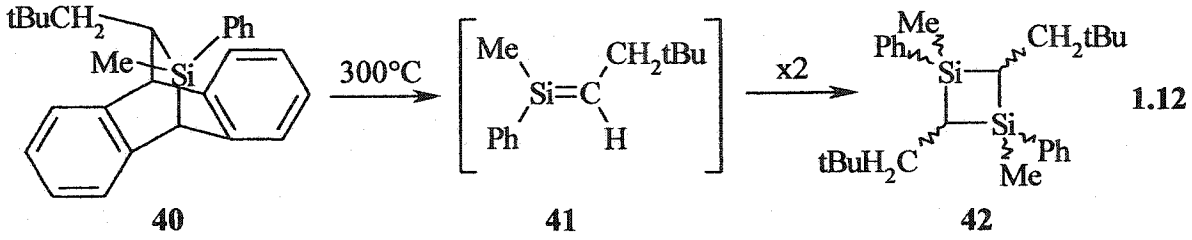

40 **41** **42** **1.12**

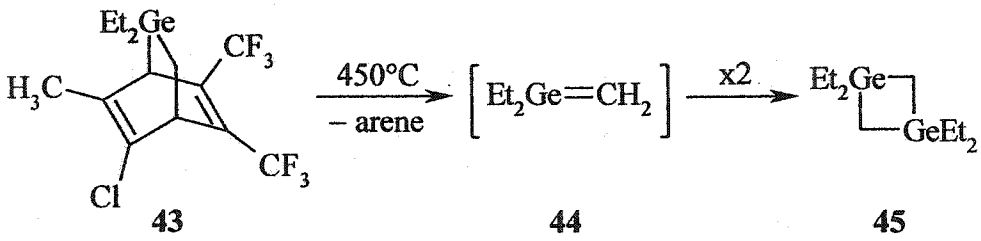

43 **44** **45** **1.13**

1.2.5 Thermolysis and Photolysis of α-Silyl- or α-Germylcarbene Precursors

Photolysis or thermolysis α-silyldiazomethanes is a well-established method for silene generation,[95-100] but there has been only one corresponding study involving α-germyldiazomethanes.[101] For example, photolysis and thermolysis of diazomethanes **46a,b** yields metallaenes **47a,b** (equation 1.14).[101] The metallaenes were proposed to result from the rearrangement of a carbene intermediate. The mechanism for silene formation from α-silyldiazomethanes will be discussed further in Chapter 2.

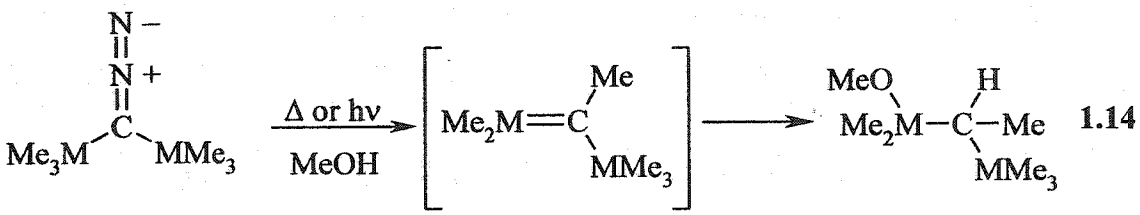

1.14

46

a. M = Si

b. M = Ge

47

48

For unsymmetrical diazomethanes, products of competitive migration are observed. For example, Oku and co-workers studied the migratory aptitudes of various substituents in the photolysis of **49** (Scheme 1.2).[99] Three silenes are formed that were proposed to arise from various migrations in carbene **50**. The yields of the three silenes were determined by product ratios of their methanol adducts (**51:52:53** = 4.5:1.4:1).

Scheme 1.2 Photolysis of (1-Phenylsilacyclobutyl)(trimethylsilyl)diazomethane (49)

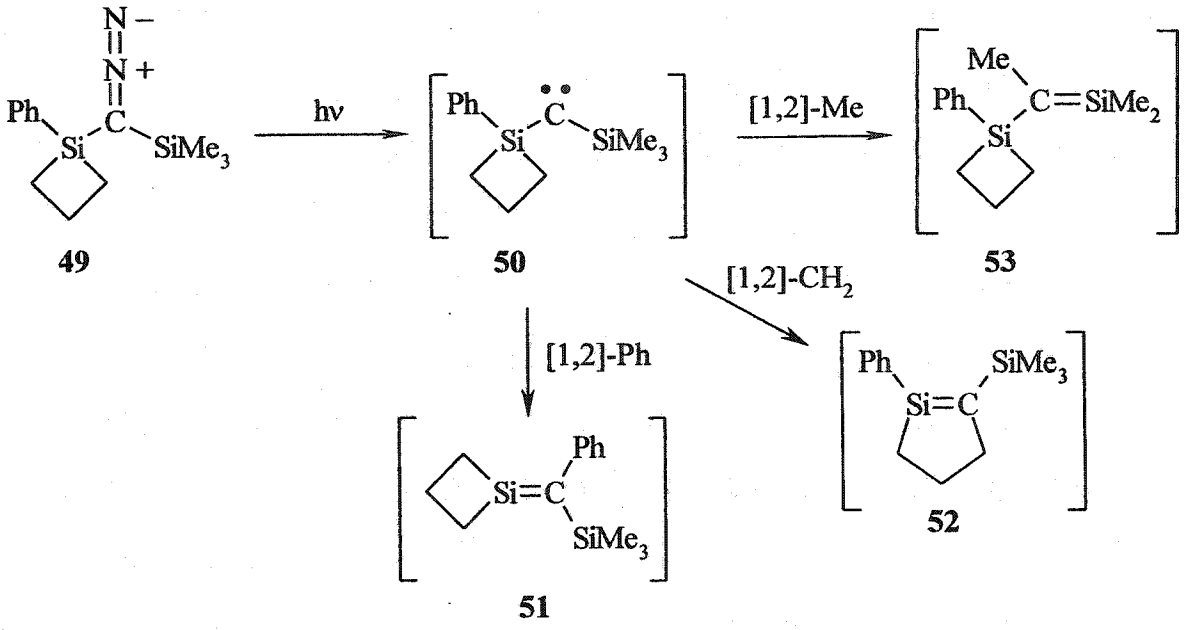

Similar chemistry has been observed for α–silylketenes (*vide infra*).[102] Although there have been many studies to determine the absolute rate constants for rearrangements of carbenes with alkyl or aryl substituents, there have been no analogous studies on the rearrangements of α–silyl or –germylcarbenes.

1.3 Reactivity of Metallaenes

1.3.1 Dimerization

Silenes are known to dimerize by one of three modes: head-to-tail cycloaddition, head-to-head cycloaddition or head-to-head ene-dimerization. Calculations suggest that the course of the reaction is dictated by the electronic nature of the substituents at carbon and silicon, and their effect on the polarity of the $^{\delta+}Si{=}C^{\delta-}$ bond.[102-104] Similar factors appear to control the regiochemistry of dimerization of germenes.[22,101]

Head-to-head regiochemistry is favoured for silenes of reduced polarity and therefore relatively low electrophilicity. For example, silene **55**, generated by the photolysis of acylpolysilane **54**, dimerizes to give two products: 1,2-disilacyclobutane **56** and ene-dimer **57** (equation 1.15).[105] The two products have been proposed to result from either a concerted [2+2]-cycloaddition or ene-reaction respectively, or via a stepwise pathway involving the common 1,4-biradical intermediate **58** (Scheme 1.3). The kinetics of dimerization of **55** have also been studied by Conlin and coworkers.[106] The bimolecular rate constant in cyclohexane solution at 293 K was found to be 1.3×10^7 M^{-1} s^{-1} while a study of the temperature dependence allowed the determination of the Arrhenius parameters: $E_a = 0.2 \pm 0.1$ kcal/mol and $\log (A / M^{-1} s^{-1}) = 7 \pm 1$. These values are most consistent with the stepwise mechanism of Scheme 1.3, provided that the formation of the intermediate (**58**) is reversible. However, the Arrhenius parameters are consistent with an ene-reaction as well. This is the only reported kinetic study for the condensed-phase dimerization of a metallaene until the work of this thesis.

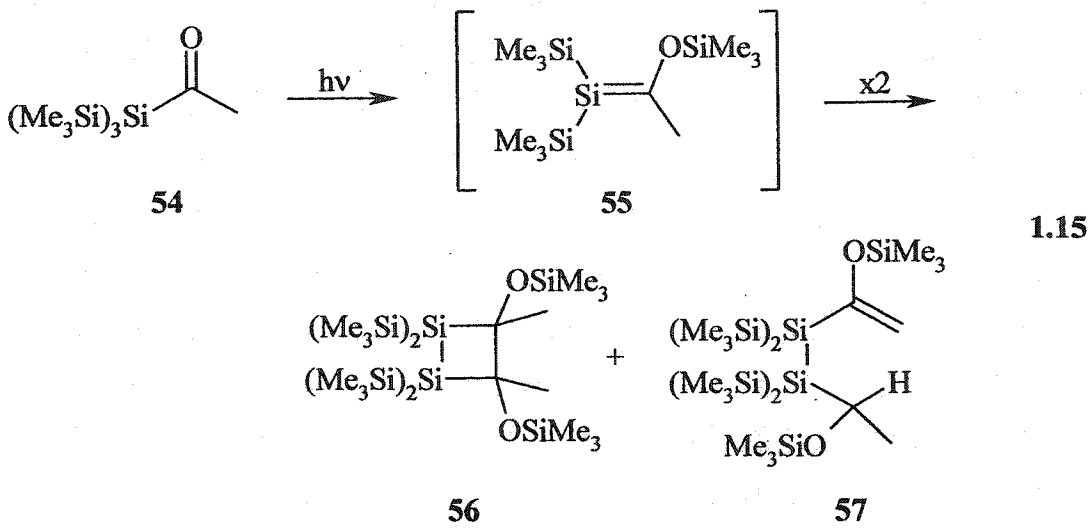

Scheme 1.3 Head-To-Head Dimerization of 1,1-Bis(trimethylsilyl)-2-methyl-2-trimethylsiloxysilene (55)

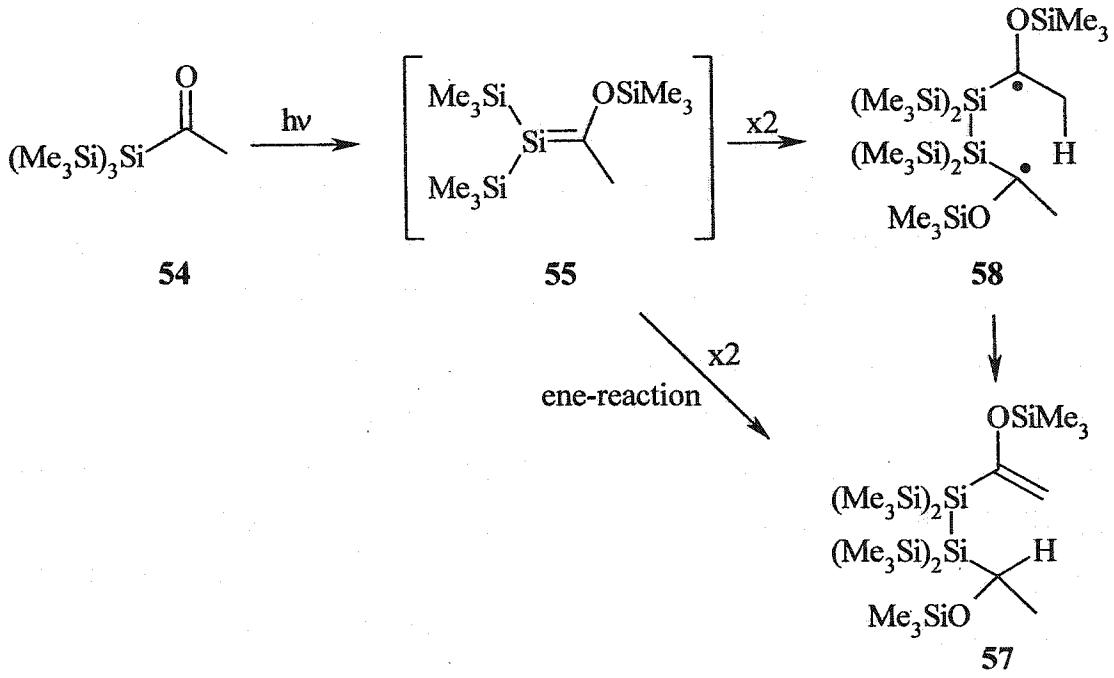

Head-to-head regiochemistry has also been observed in germene dimerization,[101,107] although no kinetic studies on these systems have been done. For example, dimerization of the transient 1,1,2-trimethyl-2-trimethylgermylgermene **47b**, yields the acyclic ene-dimer **59** as the major product (equation 1.16).[101] Similar regiochemistry is observed in the dimerization of silene derivative **47a**.[101]

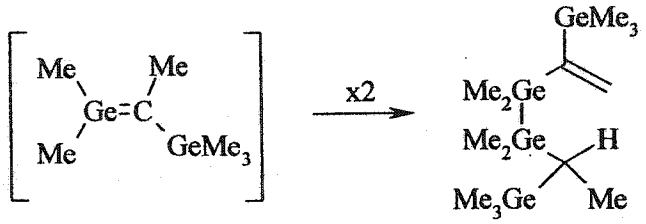

47b **59** **1.16**

Head-to-tail dimers are typically formed from relatively electrophilic silenes such as 1,1-dimethylsilene **7a**, which has been generated by gas-phase thermolysis or photolysis of 1,1-dimethylsilacyclobutane **6a** (equation 1.1).[10,75,76,108,109] The kinetics of dimerization of **7a** have been studied in the gas phase by two groups. Gusel'nikov and coworkers, using gas phase flow pyrolysis techniques,[110] determined a value of k_{dim} = 6.6×10^{-15} cm^3 s^{-1} (corresponding to a solution phase value of 3.55×10^6 M^{-1} s^{-1}) and found the rate constant to be insensitive to temperature over the 25-300°C range. Thus, they reported Arrhenius parameters of $E_a = 0 \pm 1$ kcal/mol and log (A / cm^3 s^{-1} = −14.2) for the dimerization of this silene. It was later shown that the pre-exponential factor determined by Gusel'nikov is incompatible with the thermochemistry of the system,[111] and so Potzinger and coworkers re-examined the dimerization of **7a** using laser flash photolysis techniques.[112] They obtained a value of $k_{dim} = (3.3 \pm 0.8) \times 10^{-11}$ cm^3 s^{-1} at ~298 K (corresponding to a solution phase value of 2×10^{10} M^{-1} s^{-1}), which is consistent with a

more recent determination of the rate constant for head-to-tail dimerization of 1-methylsilene (k_{dim} = (2.4±0.5)x10^{-11} cm^3 s^{-1} at 300 K).[113] Earlier work by Potzinger and coworkers on the photolysis of tetramethylsilane led to the conclusion that the dimerization of **7a** proceeds with a negligible activation energy,[114] in agreement with the conclusions of Gusel'nikov et al.

1,1-Dimethylgermene (**7b**, equation 1.17) has also been shown to dimerize with head-to-tail regiochemistry from the vacuum pyrolyses of 1,1-dimethylgermacyclobutane (**6b**)[115] or 1,1-dimethyl-1-germa-2-thietane (**6c**).[88] Kinetic studies have not been reported.

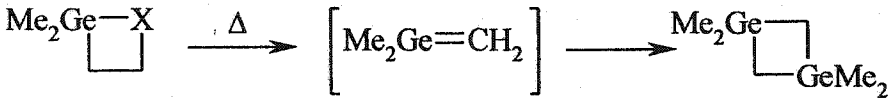

6 **7b** **8b** **1.17**

b. X = CH_2
c. X = S

1.3.2 The Reaction of Metallaenes with Nucleophiles

The reactions of metallaenes with nucleophiles have been studied intensively and their mechanistic behaviour is now well understood.[25,84,116,117] The discussion in this section summarizes what is known about the products formed and the kinetic studies that have been instrumental in elucidating the mechanistic details of metallaene reactions with nucleophiles, particularly alcohols.

1.3.2.1 Metallaene Complexes with Ethers

Lewis bases such as dimethyl ether and tetrahydrofuran (THF) have been shown to form complexes with silenes. At low temperatures, these complexes can be detected spectroscopically. For example, Wiberg has generated silene **60** via thermal salt elimination. Silene **60** is stable, meaning that in the absence of a nucleophile, it does not dimerize.[118,119] In the presence of THF, complex **61** can be isolated (equation 1.18) and identified by X-ray crystallography.[120] Similar types of complexes have also been observed for amines with both silenes[121] and germenes.[35]

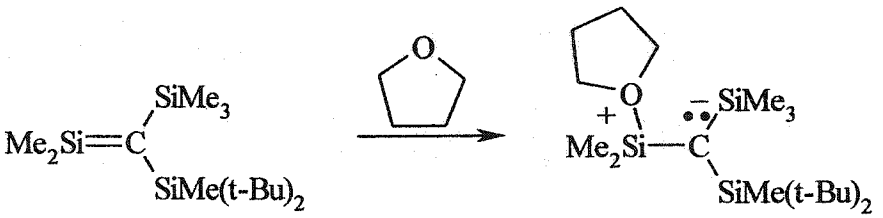

60 **61** **1.18**

There are significant differences in the physical properties of free silene **60** and its complex **61**. Bond angles at the silenic silicon atom are approximately 120°,[118,119] whereas the bond angles at silicon in **61** assume a distorted tetrahedral geometry.[120] Furthermore, the free silene has a ^{29}Si NMR chemical shift of 144.2 ppm, indicative of an sp^2-hybridized silicon. This shifts upfield to 52.39 ppm in complex **61**. The silicon-carbon bond length in **60** (1.702 Å) is significantly shorter than that in **61** (1.747 Å), a further indication that the double bond character of **60** is reduced upon complexation with THF.

Auner and coworkers have also obtained NMR evidence for the complexes of silene (**9a**), 1-methylsilene (**62a**) and 1,1-dimethylsilene (**7a**) with dimethylether-d_6.[73] The ^{29}Si NMR chemical shifts of complexes **63a-c** (equation 1.19) are δ = –25.2, –1.8 and 16.8 ppm respectively, which are significantly upfield from the silenic ^{29}Si resonance in Brook's stable silene **29** (δ ^{29}Si = 41.4 ppm) and δ ^{29}Si for Wiberg's stable silene **60**.[67] The lower chemical shifts illustrate that the planar, sp^2-hybridized character of the silene is lost in the presence of a Lewis base.

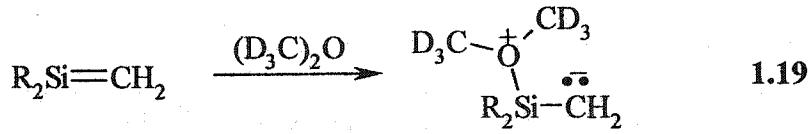

1.19

9a. R = H,H
62a. R = H,Me
7a. R = Me,Me

63 a. R = H,H
b. R = H,Me
c. R = Me,Me

1.3.2.2 Metallaene Reactivity with Alcohols

The formation of a metallaene in a chemical reaction is often characterized by the product that forms when the metallaene (**64**) reacts with a nucleophile. Typical silene traps include alcohols, amines, or dienes to give **65**, **66**, and **67**, respectively. Alkenes and ketones can undergo [2+2]-cycloadditions to yield **68** or ene-reactions to yield **69** (Scheme 1.4).[14,15,17,50,116] The most commonly used traps are aliphatic alcohols. Efforts to determine the mechanism of alcohol addition to silenes and germenes are outlined below.

Scheme 1.4 Trapping Metallaenes with Nucleophiles

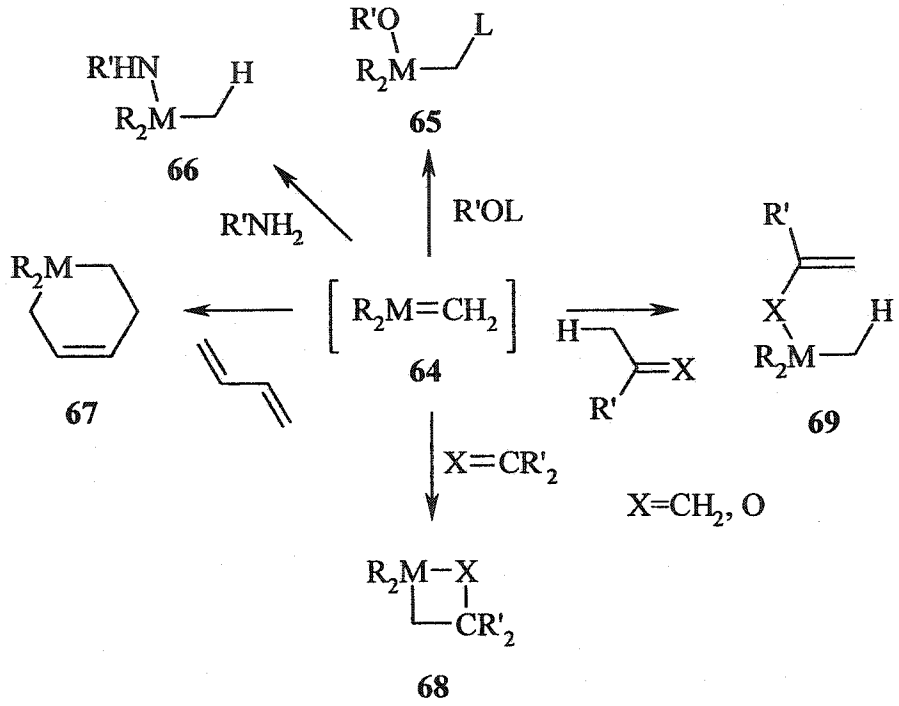

N. Wiberg was the first to study kinetics of silicon-carbon double bond reactions in the condensed phase. Generation of 1,1-dimethyl-2,2-bis(trimethylsilyl)silene (**11a**) by cycloreversion of **70** (equation 1.20) in the presence of a wide variety of nucleophiles allowed the determination of relative rate constants for the reaction of **11a**. The results, some of which are listed in Table 1.2, show that the relative rate of addition increases as a function of nucleophilicity rather than acidity, indicating that the first step of the mechanism is nucleophilic attack at silicon.[30] Davidson and coworkers established the same trends for the addition of nucleophiles to 1,1-dimethylsilene (**7a**) in the gas phase.[76] The fastest rates of addition were observed with aliphatic alcohols and amines, leading to the hypothesis that the first step of the reaction was the formation of a σ-bonded complex between oxygen or nitrogen and silicon, much like the complexes (**63a-c**) that have

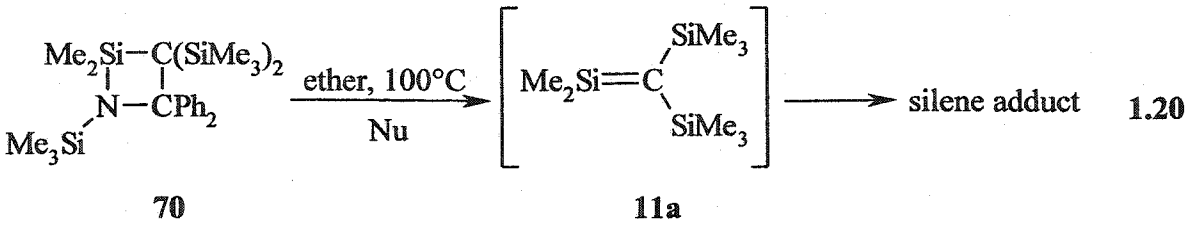

70 **11a** **1.20**

Table 1.2 Relative Rate Constants (k_{rel}) for the Addition of Nucleophiles to 11a[30]

Nucleophile	k_{rel}	Type of Reaction
methanol (MeOH)	10,500	1,2-addition
isopropanol (*i*-PrOH)	5,000	1,2-addition
tert-butyl alcohol (t-BuOH)	3,400	1,2-addition
acetic acid (AcOH)	8,500	ene-addition
acetone	420	ene-addition
tert-butylamine (*t*-BuNH$_2$)	5,500	1,2-addition
tert-butylazide (*t*-BuN$_3$)	115	[2+3]-cycloaddition
2,3-dimethyl-1,3-butadiene (DMB)	4.6	[2+4]-cycloaddition
1,3-butadiene	1	[2+4]-cycloaddition
trans-2-butene	0.31	ene-addition

recently been studied by Auner and coworkers.[73] Table 1.2 also includes data for alkenes and dienes reacting with **11a** in either ene-addition or Diels-Alder cycloaddition.[27,122-124]

A few years later, Kira and coworkers established further mechanistic details for the addition of alcohols to silenes. Photolysis of disilane **71** in the presence of an alcohol was reported to yield products consistent with the initial formation of the cyclic silene (**72**, equation 1.21).[53] A series of product studies examined how the product distribution of stereoisomeric alkoxysilanes **73** and **74** varied as a function of alcohol concentration. As the concentration of alcohol was increased, so did the yield of *anti*-isomer **74**, whereas *syn*-isomer **73** predominated at lower alcohol concentrations. Their results suggest that the initial step is formation of an alcohol-silene complex that collapses to products by two competing pathways. *Intra*molecular proton transfer to yield **73** is the favoured pathway at lower alcohol concentrations whereas *inter*molecular proton transfer yields **74** at higher concentrations, and involves a second molecule of alcohol.

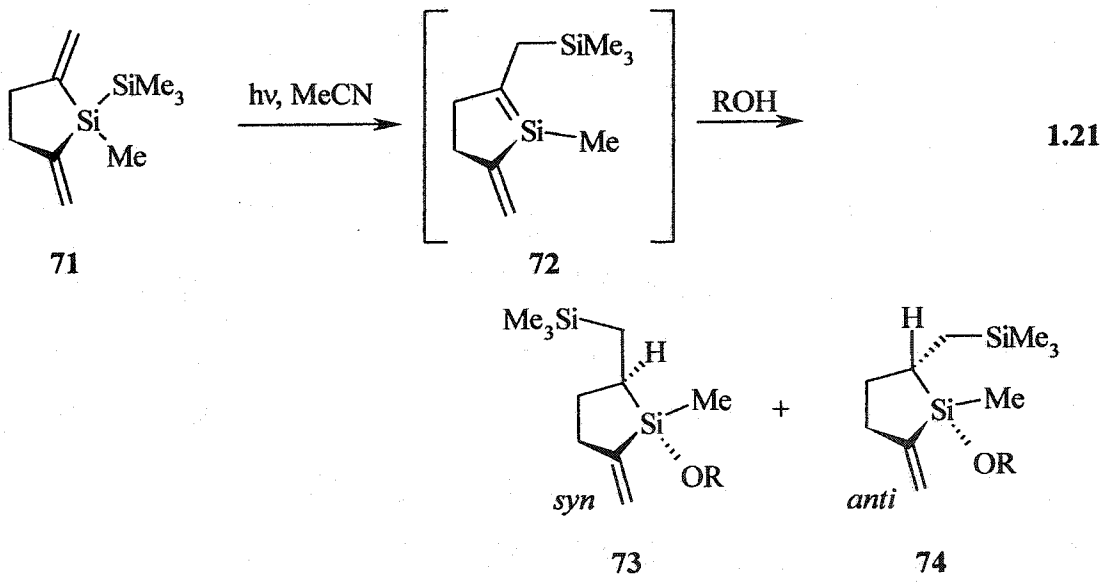

Photolysis of pentamethylphenyldisilane (**23**) results in a [1,3]-sigmatropic shift of a silyl group into the phenyl ring to produce 1,3,5-silahexatriene **24**, which yields a mixture of alkoxysilanes upon reaction with methanol (equation 1.22).[54,57,125,126] The product distribution in the photolysis of **23** varies as a function of methanol concentration, with [1,4]- and [1,6]-regioisomers, **76** and **77**, respectively, predominating at higher methanol concentrations. This is analogous to the higher yield of *anti*-stereoisomer (**74**) observed in Kira's experiment.

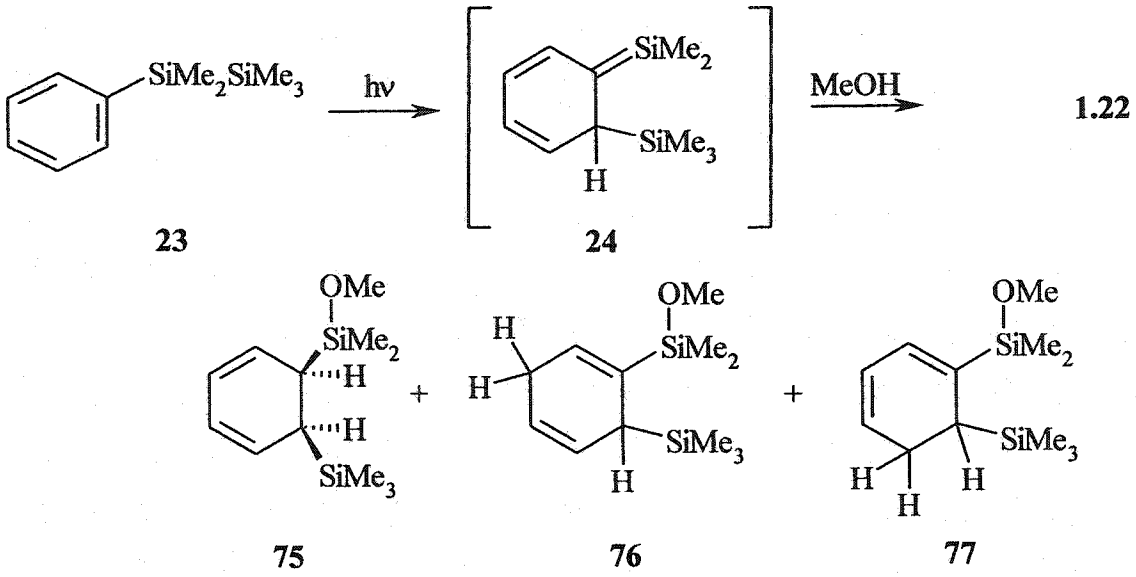

Time-resolved methods have proven to be a valuable tool to probe the silene-alcohol mechanism even further. Nanosecond laser flash photolysis of **23** led to transient absorptions that were attributed to silahexatriene **24**. Addition of methanol shortened the lifetime of **24**, such that under pseudo-first order conditions, rate constants for methanol addition to **24** could be obtained. A plot of the observed rate of decay (k_{decay}) of the silene as a function of methanol concentration (Figure 1.1) is curved. These data were fitted according to the expression of equation 1.23, where k_0 is the pseudo-first order rate

constant for decay of the silene in the absence of methanol, k_{MeOH} is the bimolecular rate constant for reaction of the silene with methanol, and k_{2MeOH} is the third order rate constant for the silene with two molecules of methanol. The quadratic relationship supports Kira's proposal that there are two competing pathways for reaction of the silene: one involving one molecule of ROH and one involving two.

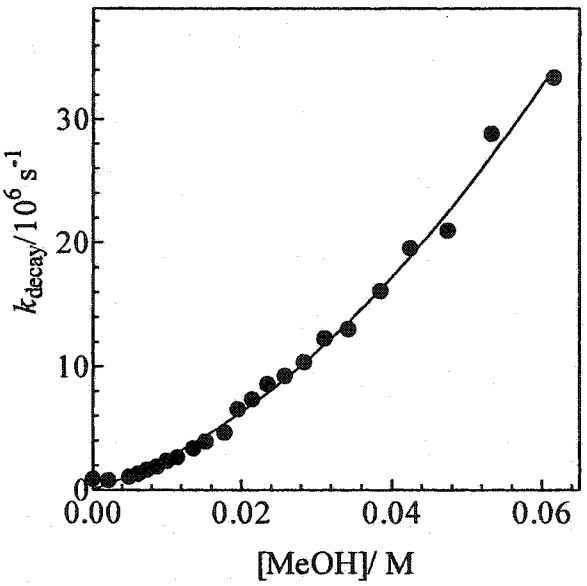

Figure 1.1 A plot of k_{decay} vs. [MeOH] for silene **24** in acetonitrile solution at 24°C.[58]

$$k_{decay} = k_0 + k_{MeOH}[MeOH] + k_{2MeOH}[MeOH]^2 \qquad \textbf{1.23}$$

The curvature of the plots of k_{decay} vs. [MeOH] in Figure 1.1 demand the addition of one more mechanistic feature (Scheme 1.5): the complex formation (k_C) must be reversible – that is, the complex can either revert to free silene and alcohol (k_{-C}) or undergo intra- (k_H) or intermolecular proton transfer ($k_{H'}$) to form the product. Using the

steady-state approximation for the complex, the mechanism for the overall reaction results in the expression of equation 1.24 for the observed rate of decay (k_{decay}), where k_0 is the pseudo-first order decay of the silene in the absence of methanol.

Scheme 1.5 The Mechanism for Addition of Methanol to Silenes

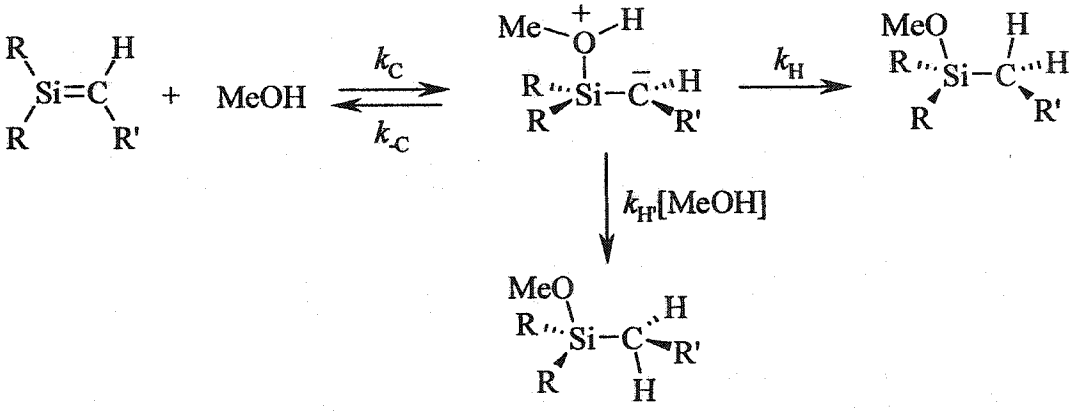

$$k_{decay} = k_0 + \frac{k_C[MeOH]}{k_{-C} + k_H + k_{H'}[MeOH]}(k_H + k_{H'}[MeOH]) \qquad \textbf{1.24}$$

For more reactive silenes, a linear dependence on alcohol concentration is observed (*vide infra*), suggesting that only one molecule of alcohol is involved in the reaction. Under these conditions, the assumption is made that the intermolecular pathway ($k_{H'}$) is slow to relative to the intramolecular pathway (k_H). Using the steady-state approximation for the complex and assuming that intermolecular proton transfer is negligible, equation 1.25 is obtained. The rate constant for methanol addition (k_{MeOH}) depends on the rate constant for the initial complexation k_C and a partitioning ratio for reaction of the complex $k_H/(k_{-C} + k_H)$.

$$k_{decay} = k_0 + k_C \bullet \frac{k_H}{k_{-C} + k_H} [MeOH] \qquad 1.25$$

For example, flash photolysis of 1,1-diphenylsilacyclobutane (**30a**) results in transient absorptions attributed to 1,1-diphenylsilene (**31a**). The rate of decay of **31a** is a linear function of alcohol concentration in acetonitrile (Figure 1.2a; equation 1.26).[82,89] Furthermore, primary kinetic isotope effects are observed (k_H/k_D =1.5) for the addition of deuterated alcohols to **31a**, indicating that proton transfer within the complex to the silenic carbon (k_H) is the rate-determining step. Primary kinetic isotope effects are also observed for the addition of alcohols to 1,1-diphenylgermene (**31b**).[90] However, unlike **31a**, the decay rate of **31b** in acetonitrile solution has a squared dependence on alcohol concentration (Figure 1.2b), indicating that intramolecular proton transfer is so slow compared to intermolecular proton transfer ($k_{H'}$) that it cannot be detected under these conditions. When a more acidic nucleophile is used, such as acetic acid, the intramolecular proton transfer in **31b** is enhanced and a linear dependence on acetic acid is observed. The observed rate constants for reactions of a number of nucleophiles with **31a** and **31b** are listed in Table 1.3.

$$k_{obs} = k_0 + k_{ROH}[ROH] \qquad 1.26$$

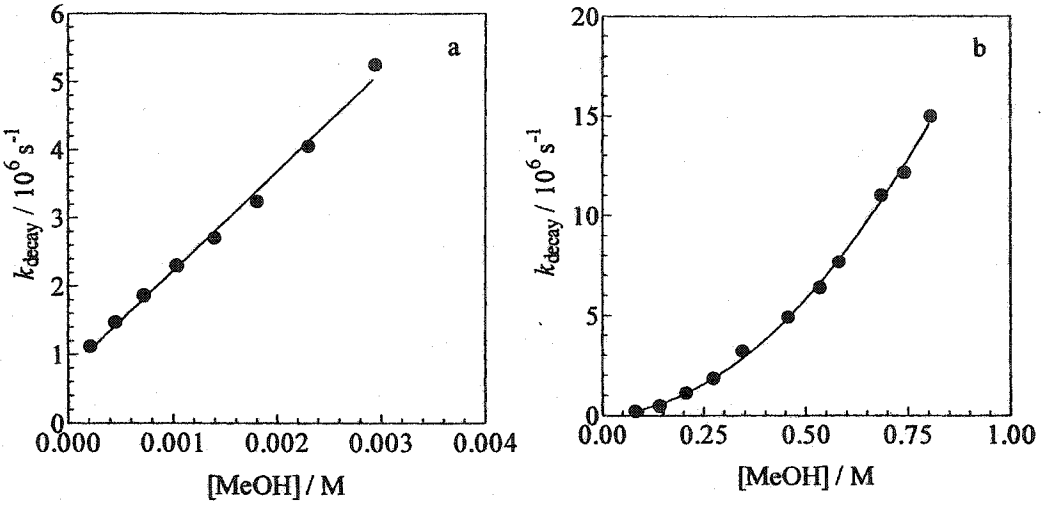

Figure 1.2 Plots of k_{decay} vs. [MeOH] for (a) **31a**[127] and (b) **31b**[90] in acetonitrile at 24-25°C.

Table 1.3 **Rate Constants (k_{ROH}) for the Addition of Nucleophiles to 1,1-Diphenylmetallaenes 31a and 31b in Acetonitrile at 23-25°C**

Nucleophile	$Ph_2Si=CH_2$ (**31a**)	$Ph_2Ge=CH_2$ (**31b**)	
	k_{ROH} / 10^9 M^{-1} s^{-1} [89]	k_{ROH} / 10^7 M^{-1} s^{-1} [90]	k_{2ROH} / 10^7 M^{-2} s^{-1}
MeOH	1.5±0.1	<0.03±0.2	2.2±0.2
EtOH	1.0±0.1	*a*	*a*
i-PrOH	0.72±0.05	*a*	*a*
t-BuOH	0.41±0.02	<0.04±0.3	0.14±0.02
AcOH	1.23±0.07	77±4	*b*

a. not measured. *b*. linear dependence on acetic acid concentration.

By adding different substituents to the *para*-position of the phenyl ring of **31a**, Bradaric and Leigh provided further evidence for the proposed mechanism for alcohol addition to silenes.[83,128] A Hammett study on the rate constants for reaction of a number of *para*-substituted diarylsilenes (equation 1.27) with methanol indicates that electron-releasing groups decrease the reactivity of **31a** ($\rho = +0.31$, Figure 1.3). The smaller rate constant for the addition of methanol to the *para*-methyl derivative **31c** indicates that the initial complexation (k_C) and/or the proton transfer (k_H) must be occurring more slowly in the zwitterionic complex of **31c** as compared to that of **31a**. The opposite is true in the case of *para*-trifluoromethyl substituted **31f**.

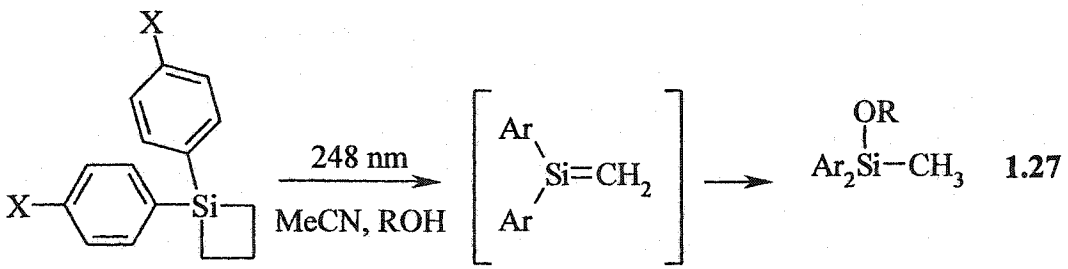

30 **31** **32**

a. X=H
c. X=Me
d. X=F
e. X=Cl
f. X=CF_3

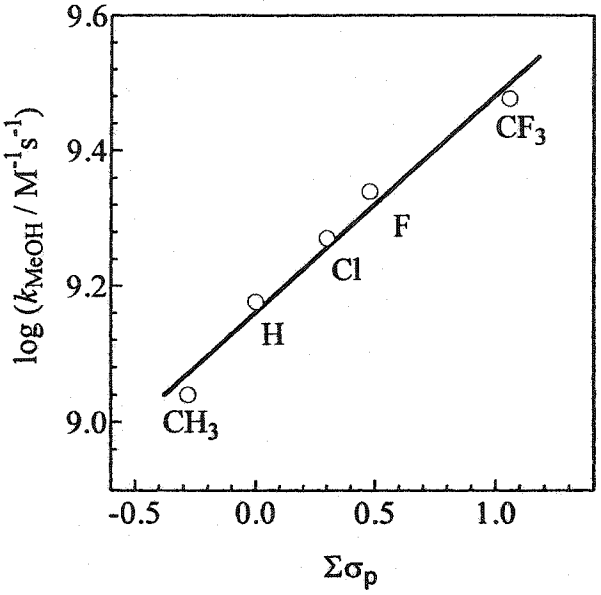

Figure 1.3 Hammett plot for the addition of methanol to 1,1-diarylsilenes (**31a,c-f**). Each point is labelled with the substituent at the *para*-position.[83]

The reversibility of complex formation and the characteristic rate-determining proton transfer are illustrated in the temperature dependence of the rate constant for alcohol addition to the same series of 1,1-diarylsilenes.[83,129,130] At this time, similar studies have not been completed for the corresponding series of 1,1-diarylgermenes. Arrhenius plots show that the reaction exhibits a negative energy of activation over the experimental temperature range, consistent with a two-step mechanism in which the intermediate complex has two reaction pathways available that differ in entropic demand (Scheme 1.5).[84] This can be more easily visualized with a series of reaction coordinate diagrams.

Recall that the rate constant for alcohol addition (k_{ROH}, equation 1.28) is dependent on the initial complexation reaction (k_C) and the ratio of rate constants (k_H / k_H + k_{-C}). Consider a reaction coordinate diagram for the alcohol addition to any silene,

$$k_{ROH} = k_C \bullet \frac{k_H}{k_{-C} + k_H} \qquad \textbf{1.28}$$

where the y-axis is ΔG (Figure 1.4a). The second step of the reaction is the proton transfer within the complex (k_H), which has been shown by kinetic isotope effects to be rate-determining,[83,127] and therefore formation of the alkoxysilane has a larger free energy barrier in comparison to that for reforming the starting materials (k_{-C}). However, if the free energy of activation for proton transfer consists of largely an entropic contribution, the enthalpic barrier to proton transfer ($\Delta H^{\neq}$, Figure 1.4b) is relatively small. A negative activation energy will result if the enthalpic barrier for the rate-determining step is lower than the enthalpy of the starting materials. The relatively large entropic barrier to proton transfer within the intermediate to form products compared to that for reversion to starting materials leads to the experimentally observed negative activation energies for the reaction of most silenes with aliphatic alcohols within the temperature ranges that have been studied.[84] In theory, a very broad temperature range should yield a bell-shaped Arrhenius plot (Figure 1.5 and also see Chapter 3) where $k_H >> k_{-C}$ at low temperatures yields a positive activation energy and where $k_H << k_{-C}$ at higher temperatures yields a negative activation energy.

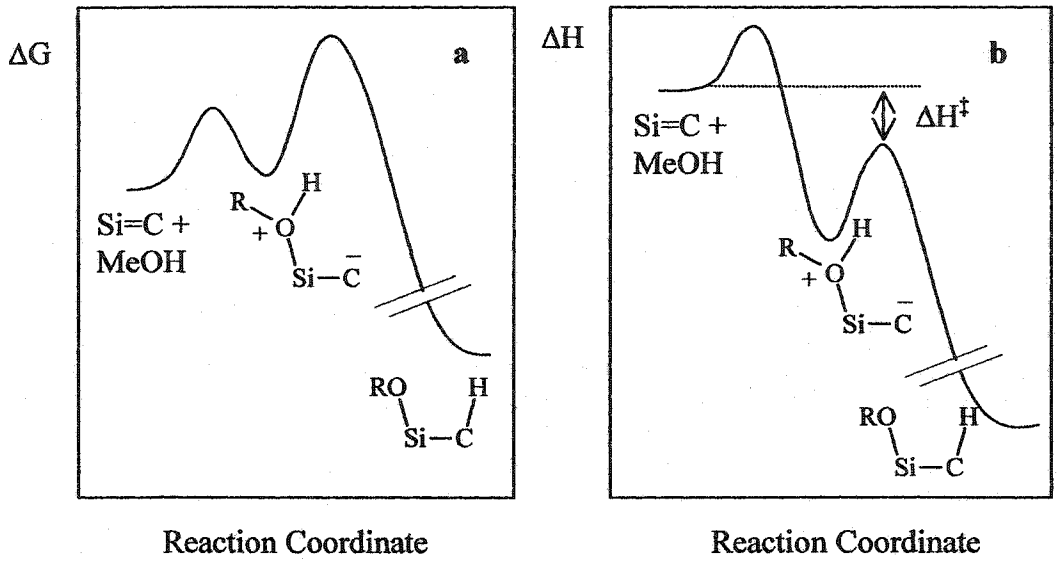

Figure 1.4 a) Free energy (ΔG) vs. reaction coordinate and **b)** enthalpy (ΔH) vs. reaction coordinate for the addition of alcohol to a silene: the origin of a negative activation energy.

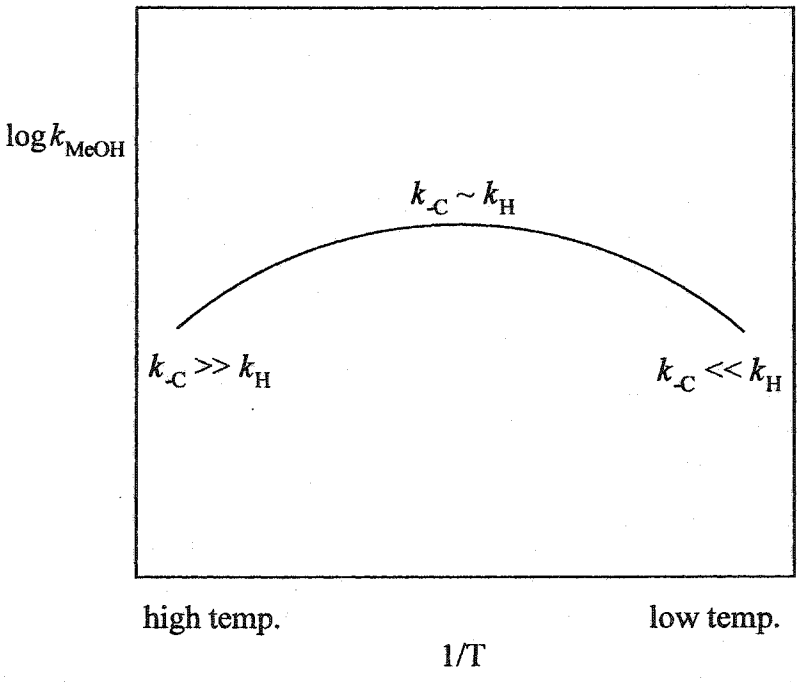

Figure 1.5 Hypothetical bell-shaped Arrhenius plot.

The temperature ranges that have been studied are approximately 0-60°C, and for methanol addition to most silenes, the activation energies are negative. For more acidic nucleophiles such as acetic acid, the activation energy is positive. Essentially, each experiment involves examining a particular window of the bell-shaped plot, where the location of the window in the hypothetical plot depends on the electrophilicity of the silene and the nucleophilicity and acidity of the trap. The area of the bell-shaped plot that is observed in the experimental temperature window is defined by the magnitude of the individual rate constants. The vertical position of the bell primarily depends on k_C, whereas the horizontal domain is defined by the relative magnitudes of k_H and k_{-C}. Table 1.4 summarizes some of the rate constants, activation barriers and kinetic isotope effects observed for **31a, c** and **f**.

Table 1.4 **Absolute Rate Constants, Arrhenius Parameters and Kinetic Isotope Effects for the Addition of Methanol and Acetic Acid to 31a,c and f in Acetonitrile**[83]

Silene	ROH	k_{ROH} / 10^9 M^{-1} s^{-1}	k_H/k_D	E_a / kcal mol^{-1}	log A
31c (X=Me)	MeOH	0.9±0.1	1.9±0.2	-2.7±0.2	6.9±0.3
31a (X=H)	MeOH	1.5±0.1	1.9±0.2	-2.5±0.3	7.3±0.2
	AcOH	1.3±0.3	1.1±0.1	+1.9±0.3	10.5±0.4
31f ($X=CF_3$)	MeOH	2.2±0.3	1.0±0.1	-1.9±0.2	7.9±0.1
	AcOH	2.2±0.2	*a*	+3.6±0.5	12.0±0.4

a. not measured

The data of Table 1.4 illustrate that the most reactive silene in the series (**31f**) has the most positive activation energy, illustrating that k_H is larger and/or k_{-C} is smaller than the corresponding rate constants for **31a**. This is also exemplified in the kinetic isotope effects; as silene reactivity increases (ie. **31f**), k_H/k_D approaches unity. This decrease in the kinetic isotope effect is a result of k_H increasing relative to k_{-C}. Further supporting this mechanism is the kinetic isotope effect of unity and the positive activation energies observed for addition of acetic acid to **31a** and **f**. The k_H/k_D observed with acetic acid is indicative of a fast proton transfer where k_H is not the rate-limiting step. This is also illustrated in the positive activation energy, where $k_H > k_{-C}$ and the observation "window" of Figure 1.5 is at the low temperature end of the plot.

Methanol is the most utilized and best known of the silene and germene traps. Other nucleophiles such as alkenes,[29,131-133] dienes,[123] alkoxysilanes,[38,134,135] amines[121] and carbonyl compounds[61,90,129,136] have also been shown to add to both silenes and germenes. The addition of alkoxysilanes, amines and carbonyl compounds to metallaenes have been shown to proceed via similar stepwise mechanisms.[25]

1.4 Substituent Effects on Silene Reactivity

Initial interest in the area of substituent effects on silene stability and reactivity was aroused by reports on the successful synthesis and characterization of two silenes that were found to be stable towards dimerization. The first of these silenes was **29,** isolated by Brook and coworkers from the photolysis of acylpolysilane **28** (equation 1.9).[67] Shortly thereafter, Wiberg and coworkers reported that silene **60** was also stable.[137] Both **29** and **60** contain bulky substituents on the double bond, which would impede dimerization. However, the role of the electronic properties of the substituents on the double bond was not clear. Both silenes contain trialkylsilyl groups (inductive donors) that are situated on silicon in Brook's silene (**29**), while Wiberg's silene (**60**) has them situated at carbon. Clearly, a better understanding of the effects of substituent on silene reactivity and stability was necessary.

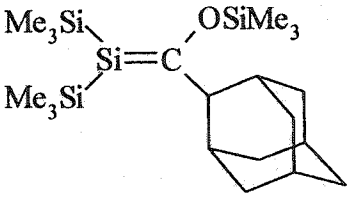

29

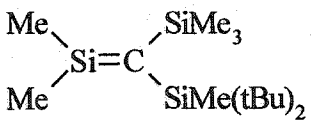

60

To address this problem in a systematic way, three significant studies have been conducted. The first was a theoretical study (RHF/3-21G and 6-31G*) by Apeloig and Karni, investigating the heats of formation, bond lengths and charge distributions in a series of substituted silenes (**78** and **79**).[103] Their results revealed that substitution at silicon or carbon does not affect the heats of formation significantly; however, substantial differences in charge distribution and the length of the Si=C bond were predicted, depending on the substituent and its location (Table 1.5). In general, when π-donors such as $-OSiH_3$ or –OH or σ-acceptors such as –F are situated at carbon, the bond polarity is reduced and a corresponding increase in the calculated Si=C bond length is observed, as compared to the parent silene $H_2C{=}SiH_2$. A similar effect is also observed when σ-donors such as $-SiH_3$ and π-acceptors such as $-NO_2$ are at silicon. Less reactive silenes were predicted to be those with relatively low double bond polarity and longer Si=C bond lengths. This theoretical prediction is reflected in the experimentally determined bond length of Brook's silene (**29**), where the Si=C bond length is 1.764 Å,[67] which is longer than the calculated bond length for $H_2Si{=}CH_2$ of 1.718 Å. The strong polarization ($^{\delta+}Si{=}C^{\delta-}$) of the double bond in Wiberg's silene **60** is reflected in its shorter bond length of 1.702 Å. Electronic effects predict that **60** should be highly reactive, indicating that the steric effect of the *t*-butyl groups must play a significant role in protecting the silene from dimerization.

$RHSi{=}CH_2$ $H_2Si{=}CHR$ R = **a**. H, **b**. CH_3, **c**. SiH_3, **d**. OH,
e. $OSiH_3$, **f**. F, **g**. CN, **h**. NO_2

78 **79**

Table 1.5 **Calculated Charge Densities at Silicon and Carbon and Bond Lengths in Silenes 78 and 79**[103]

	$RHSi{=}CH_2$ (**78**)			$H_2Si{=}CHR$ (**79**)		
R	Charge at C	Charge at Si	Bond Length / Å	Charge at C	Charge at Si	Bond Length / Å
a. H	-0.67	0.46	1.718	–	–	–
b. CH_3	-0.67	0.59	1.716	-0.42	0.42	1.725
c. SiH_3	-0.62	0.28	1.725	-0.75	0.51	1.721
d. OH	-0.73	0.84	1.705	-0.06	0.26	1.746
e. $OSiH_3$	-0.71	0.83	1.705	-0.05	0.28	1.749
f. F	-0.72	0.91	1.698	0.10	0.37	1.730
g. CN	-0.63	0.56	1.711	-0.53	0.59	1.727
h. NO_2	-0.63	0.67	1.702	-0.32	0.64	1.731

The second study involved the photolysis of a series of 1-methyl-1-substituted silacyclobutanes (**80**). These were photolyzed to produce silenes (**81**) that were studied by nanosecond laser flash photolysis at room temperature in hexane solution (equation

1.29) and the absolute rate constants for each silene with methanol were determined.[104] The data from flash photolysis of **6a** to generate **7a** in hexane at room temperature were also included.[138] The rate constants for methanol addition did not vary with either inductive (σ_I) or resonance (σ_{R°) substitutent parameters in a straightforward way. However, a multi-parameter analysis that included both σ_I and σ_{R° as well as the steric substituent parameter E_s, (Figure 1.6) led to a much better fit ($r^2 = 0.977$, 9 points). The coefficients in the substituent parameter function are the ρ values indicating the individual contributions of inductive, resonance and steric factors to silene reactivity. The negative $\rho_{R^\circ} = -3.6$ and positive $\rho_I = 3.1$ values suggest that resonance electron donors and inductive electron acceptors at silicon enhance the reactivity of silenes toward nucleophiles. The relatively small, positive $\rho_S = 0.21$ value indicates that bulkier groups at silicon reduce silene reactivity, but it is electronic effects that primarily determine silene reactivity within this particular series of compounds.

The third study was undertaken to investigate systematically the substituent effects at carbon.[102] Six 1,1-dimethyl-2-substituted silenes were generated using a variety of different silene precursors, and absolute rate constants for their reactions with methanol were measured using nanosecond laser flash photolysis. Three were generated from α-silylketenes (**82a-c**, equation 1.30),[102] which have been shown to extrude carbon monoxide upon photolysis to form a carbene that can rearrange. Silene **83a** was also photochemically generated from (trimethylsilyl)diazomethane (**84**, equation 1.31).

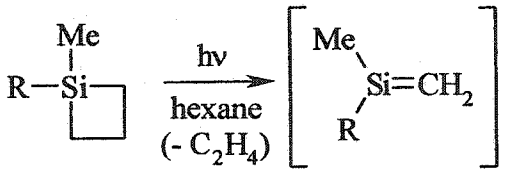

1.29

80 **81**

a. R = Ph
b. R = H
c. R = Et
d. R = *t*-Bu
e. R = CH_2SiMe_3
f. R = $CH{=}CH_2$
g. R = C≡CH
h. R = $SiMe_3$

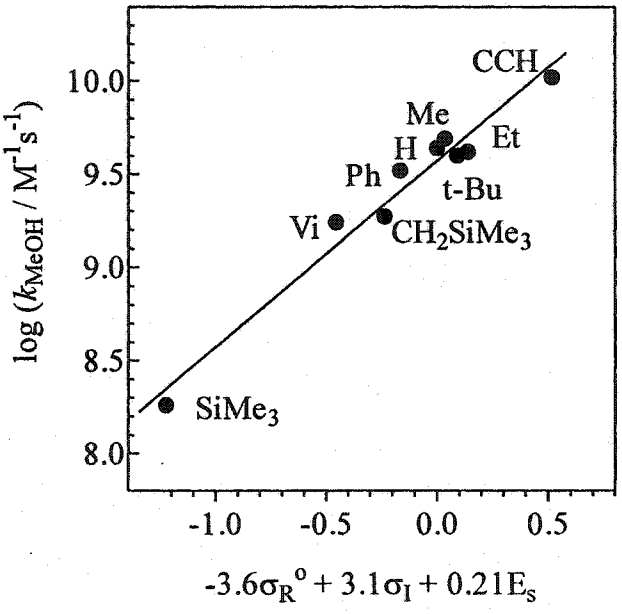

Figure 1.6 Plot of log (k_{MeOH} / M^{-1} s^{-1}) versus the three parameter substituent constant function in hexane solution at 23°C for silenes **81a-h** and **7a.**

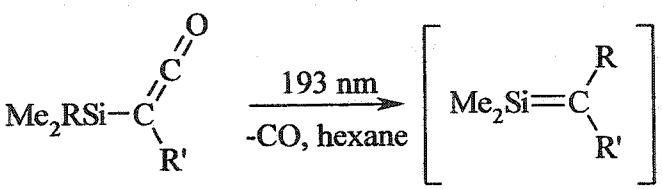

1.30

82 **83**

a. R = Me; R' = H
b. R = Me; R' = $SiMe_3$
c. R = $SiMe_3$; R' = H

a. R = Me; R' = H
b. R = Me; R' = $SiMe_3$
c. R = $SiMe_3$; R' = H

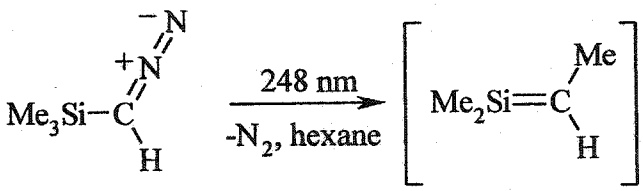

1.31

84 **83a**

Other silenes that were also included in the study were 1,1-dimethylsilene (**7a**),[104] 1,1-dimethyl-2-methyltrimethylsilylsilene (**22**) and 1,1-dimethyl-2-vinylsilene (**86**). Silene **22** was obtained from the 248-nm photolysis of vinylpentamethyldisilane **21** (equation 1.6).[51] Silene **86** was obtained from electrocyclic ring opening of 1,1-dimethyl-(1-sila)cyclobut-2-ene (**85**, equation 1.32), upon 193-nm laser excitation.[139]

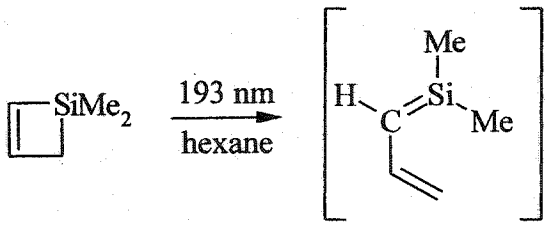

1.32

85 **86**

The k_{MeOH} values for each of the 1,1-dimethyl-2-substituted silenes were plotted as a function of the resonance substituent parameter, σ_{R° (Figure 1.7). Unlike the silicon-substituted derivatives, the correlation between the rate constants and substituent

parameter was not improved upon adding parameters for inductive and steric effects. The slope of the plot afforded a ρ_{R° value of +8.1±1.6, indicating that π-donors at carbon result in kinetic stabilization of the silicon-carbon double bond. This is in agreement with the conclusions of the substituent effect study by Apeloig and Karni.[103]

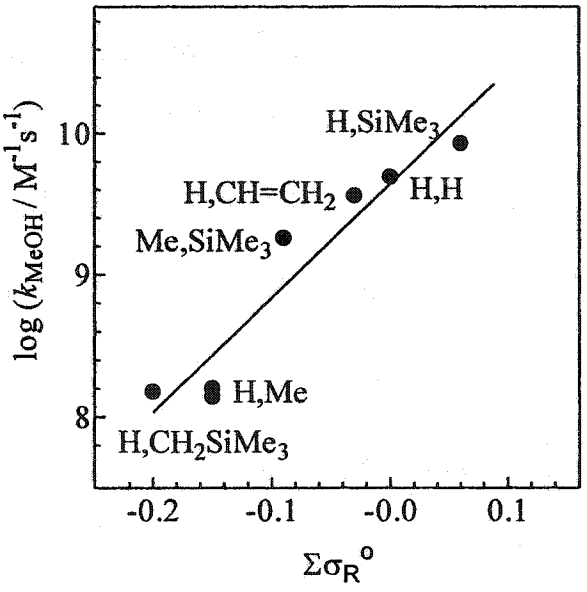

Figure 1.7 Plot of log (k_{MeOH} / M^{-1} s^{-1}) versus σ_{R° for silenes **7a, 83a-c, 22** and **86** in hexane solution at 23°C.

The results of these kinetic and theoretical studies explain the stability of Brook's silene **29**, because it has trialkylsilyl groups (σ-donors) on *silicon*, and a strong π-donor at carbon. Given this, the stability of Wiberg's silene **60** is somewhat surprising because the trialkylsilyl groups are at *carbon*. Although steric factors clearly must play a role in reducing the reactivity of **60**, the extent to which they offset the unfavourable electronic effects of the substituents in this molecule is not clear. Determination of the absolute reactivity of 1,1-dimethyl-2,2-bis(trimethylsilyl)silene (**11a**) with nucleophiles is

an essential contribution to these studies on substituent effects, because its substituent pattern is similar to that of **60**.[140]

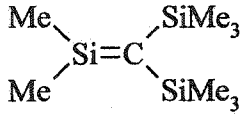

11a

1.5 Goals and Scope of This Thesis

This thesis addresses three aspects of organometallaene chemistry, including the mechanism for formation of silenes from the photolysis of α-silylcarbene precursors, the reactivity of silenes with nucleophiles as a function of substituent and solvent, and the dimerization of silenes and germenes in solution.

Although many reports on absolute rate constants for the rearrangements of alkylcarbenes to alkenes have been made in the literature,[141] absolute rate constants for the analogous rearrangements of α-silylcarbenes to silenes have not been measured before. A better understanding of this type of rearrangement is essential in the field of silene chemistry because the photolysis or thermolysis of α-silyldiazomethanes and –ketenes has become a well-known route to silenes (section 1.3.5). The results of Chapter 2 describe a study of the photochemistry of three simple α-silylcarbene precursors to 1,1,2-trimethylsilene (**83a**): trimethylsilylketene (**82a**), –diazomethane (**84**) and –diazirine (**87**). By using the pyridine probe technique for trapping carbenes,[142] we planned to determine the absolute rate constant for methyl migration to form **83a** from trimethylsilylcarbene.

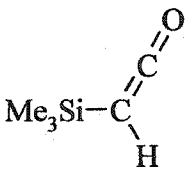

82a

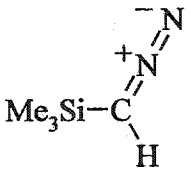

84

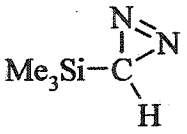

87

To date, there has only been one report of the direct detection of silenes generated from the flash photolysis of α–silylketenes or –diazomethanes.[102] Chapter 3 focuses on the photolysis of two α-silylcarbene precursors (**88a,b**) to Wiberg's transient silene **11a**. The original goal of this work was to generate **11a** in the condensed phase at ambient temperatures under conditions where it could be detected directly, and to determine absolute rate constants for its reaction with some of the nucleophiles previously studied by Wiberg and coworkers. Furthermore, because Wiberg and coworkers performed relative rate experiments at 100°C in diethyl ether, the effect of solvent and temperature on the reaction kinetics of **11a** were also examined.

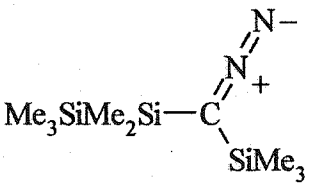

88a

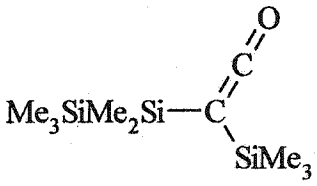

88b

Other than the addition of alcohols, silene dimerization remains as one of the most important and ubiquitous reactions in organometallaene chemistry. Although the mechanisms for the reactions of silenes with nucleophiles are quite well understood, the mechanism by which silenes dimerize is not. The goal of Chapter 4 is to determine the absolute rate constants for dimerization of 1,1-diphenylsilene (**31a**) from the flash

photolysis of 1,1-diphenylsilacyclobutane (**30a**). To further extend what is known about the germanium analogue, 1,1-diphenylgermene (**31b**), its absolute rate constant for dimerization was also determined. These are the first absolute kinetic data to be reported for the head-to-tail dimerization of organometallaenes at ambient temperatures in the condensed phase. In an effort to elucidate the mechanism for dimerization, the Arrhenius parameters for the reaction have also been determined.

Chapter 2

Photochemistry of (Trimethylsilyl)ketene, -diazomethane and -diazirine and the Mechanism of Silene Formation

2.1 Background

Carbenes are a class of carbon-based reactive intermediates that have been the focus of extensive experimental and theoretical investigation over the last fifty years.[143,144] Carbenes can exist as either ground state *singlets* or *triplets*. Singlet carbenes are characterized by an sp^2 hybridized carbon with the lone pair of electrons located in the sp^2 hybridized orbital while the p orbital is vacant (Figure 2.1a). Triplet carbenes have two unpaired, non-bonding electrons which are located in separate orbitals on the carbon centre (Figure 2.1b).

Methylene ($:CH_2$) has been shown experimentally to be a ground state triplet, lower in energy than the singlet by 8.99 kcal/mol.[145] This energy difference is slightly smaller than that predicted by theory (see Table 2.1).[146] The relative energies of the lowest singlet and triplet states are given by the singlet-triplet energy gap (ΔE_{ST}, equation 2.1). The lowest state can be either the singlet or the triplet, depending on the substituents on the carbene centre. Table 2.1 lists several substituted carbenes (**89-97**) along with their calculated singlet-triplet energy gaps. Typically, alkyl carbenes are found to be ground state triplets with relatively small ΔE_{ST}. On the other hand, if there

are π-electron donating groups attached to the carbene centre, as in dimethoxycarbene (**97**), the carbene is a ground state singlet.[147]

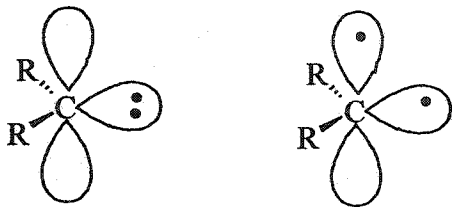

a **b**

Figure 2.1 Electronic distribution in a) singlet carbenes and b) triplet carbenes.

$$\Delta E_{ST} = E_{singlet} - E_{triplet} \qquad \textbf{2.1}$$

Table 2.1 Calculated Singlet-Triplet Gaps (ΔE_{ST} / kcal mol^{-1}) for Various Carbenes

No.	Carbene	ΔE_{ST}	Ref.	No.	Carbene	ΔE_{ST}	Ref.
89	HCH	9.71	146	**94**	HCCl	-6.39	146
90	$HCCH_3$	5.2	148	**95**	HCBr	-4.03	146
91	$(H_3C)_2C$	1.4	149	**96**	$(NHR)_2C$	-76	150a
92	$HCSiH_3$	19.08	146	**97**	$(CH_3O)_2C$	-24.7	150b
93	HCF	-15.83	146				

Carbenes undergo a wide range of intermolecular reactions, depending on the substituents attached to the carbene centre. For example, singlet carbenes bearing π-electron donating groups such as amino-, oxy-, and thioalkoxy groups are nucleophilic and undergo such reactions as insertion into OH bonds and stereospecific addition to alkenes and alkynes.[151] On the other hand, diarylcarbenes are ground state triplets and undergo radical-type reactions such as hydrogen abstraction.[152] Initially, absolute rate constants for carbene reactions could only be determined by flash photolysis if the carbene contained a chromophore, such as an aryl substituent.[153,154] However, in 1988, Jackson et al. introduced the "pyridine-probe" technique for studying the absolute kinetics of the inter- and intramolecular reactions of simple alkyl carbenes.[142] Typically these studies employed diazirines or diazomethanes as carbene precursors.

2.1.1 The Pyridine Probe Technique and Intramolecular Reactions of Carbenes

Flash photolysis of simple alkyldiazirines (**98a**) or –diazomethanes (**98b**) does not lead to the detection of carbene intermediates because they do not contain chromophores suitable for UV-Vis detection. However, if pyridine is added to the reaction, it can add to the empty p orbital on the carbene centre to form a pyridine ylide (**99**, Scheme 2.1), which does absorb (λ_{max} ~360-400 nm). The pyridine acts as a trap that can intercept the carbene intermediate (**100**) in competition with intramolecular rearrangement to form an alkene (**101**).

Scheme 2.1 The Pyridine Probe Method

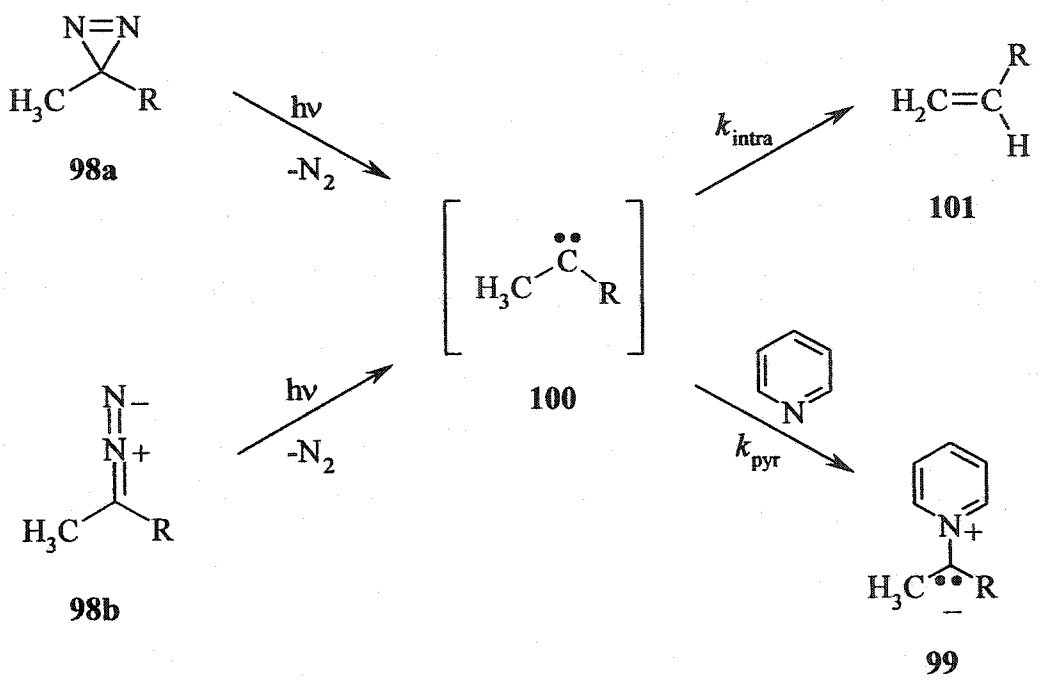

Pyridine is a good carbene trap for nanosecond laser flash photolysis studies of carbenes for a number of reasons.[144] Firstly, it does not react with most carbene precursors in the absence of light. Secondly, the UV spectrum of pyridine is such that is absorbs below 300 nm, so it does not interfere with the laser irradiation of typical carbene precursors, such as diazirines or diazo compounds, which absorb at wavelengths greater than 330 nm. Thirdly, the pyridine ylide produced is easily monitored by its absorption at 360-400 nm. Lastly, pyridine reacts rapidly with most carbenes (k_{pyr} = 1-5 x 10^9 M^{-1} s^{-1})[155] such that trapping competes effectively with intramolecular rearrangement reactions (ie. $k_{pyr} \geq k_{intra}$).

Absolute rate constants for carbene reactions can be determined using two different techniques. The simplest of these methods is to monitor k_{growth} of the ylide as a

function of pyridine concentration (equation 2.2), where Δ-OD_t is the absorbance of the ylide at time t and Δ-OD_{max} is the maximum absorbance of the ylide before it starts to decay.

$$\Delta\text{-}OD_t = \Delta\text{-}OD_{max}\,[1-\exp(-k_{growth}t)] \qquad 2.2$$

The observed rate of growth of the ylide is equal to the sum of the rate constants for all the decay processes available to the carbene,[156] including reaction of pyridine (k_{pyr}), intramolecular rearrangement (k_{intra}) of the carbene, carbene dimerization and any pseudo-first order reactions with adventitious impurities in the reaction medium. Therefore, the growth kinetics of the ylide can be measured to obtain an upper limit for intramolecular rearrangements of carbenes. By plotting k_{growth} as a function of pyridine concentration (equation 2.3), the bimolecular rate constant for the reaction of the carbene with pyridine can be determined from the slope (k_{pyr}). The intercept (k_0) represents the sum of all the other pseudo-first order decay processes available to the carbene, including the rate constant for intramolecular rearrangement (k_{intra}), intersystem crossing to the triplet (k_{ISC}) and rate constants for reaction with the precursor, solvent and any adventitious impurities present in the reaction medium (Σk_d). The lifetime of the carbene ($\tau_{carbene}$, equation 2.4) is the reciprocal of the sum of all of these rate constants.

$$k_{growth} = k_0 + k_{pyr}\,[PYR] \qquad 2.3$$

$$k_0 = k_{intra} + k_{ISC} + \Sigma k_d = \frac{1}{\tau_{carbene}} \qquad 2.4$$

This method has proven to work well for halogenated carbenes,[153,157-159] because these are typically less reactive than simple alkylcarbenes ($k_{intra} \leq 5 \times 10^7\ s^{-1}$, Table 2.2).

This reduction in reactivity is attributed to π-electron donation into the empty p-orbital on the carbene centre from the adjacent halogen or oxygen-containing substituent. However, alkyl-substituted carbenes are so reactive that $k_{intra} > 5 \times 10^7\ s^{-1}$. Under these circumstances, it is impossible to monitor the increase of the ylide absorbance as a function of time using nanosecond laser flash photolysis. In order to determine the lifetimes of these carbenes, it is necessary to monitor the yield of ylide produced as a function of pyridine concentration.[159] This yield is normally estimated by measuring the maximum absorbance of the ylide.

The absorbance of the ylide (Δ-OD_y) is determined by the state efficiency for carbene formation from the photolysis of the precursor ($\phi_{carbene}$), the state efficiency for ylide formation (ϕ_y), and a constant (C, equation 2.5) that includes the laser intensity, the extinction coefficient of the ylide and the static absorbance of the carbene precursor at the laser wavelength. The state efficiency for ylide formation (equation 2.6) is the rate constant ratio for the reaction between the carbene and pyridine (k_{pyr}[PYR]) and the sum of all the decay processes available to the carbene, including k_{pyr}[PYR], k_{intra}, k_{ISC} and Σk_d. Following substitution of equations 2.4 and 2.6 into 2.5, an expression is obtained (equation 2.7, where $C' = C \bullet \phi_{carbene}$) for Δ-OD_y as a function of [PYR]. Non-linear least squares fitting of a plot of Δ-OD_y vs. [PYR] leads to the determination of $k_q\tau_{carbene}$. If the reciprocal of equation 2.7 is taken (equation 2.8), linear least squares analysis of a plot of $1/\Delta$-OD_y vs. 1/[PYR] results in an intercept:slope ratio of $k_{pyr}\tau_{carbene}$. The lifetime is then estimated using a value of $k_{pyr} = (1\text{-}5) \times 10^9\ M^{-1}\ s^{-1}$, the range of k_{pyr} values obtained from study of a wide range of relatively long-lived carbenes. Typically, under the conditions

employed for laser flash photolysis, Σk_d is assumed to be negligible[144,159] and ultimately k_{intra} can be determined.

$$\Delta\text{-OD}_y = C \bullet \phi_{carbene} \bullet \phi_y \qquad \textbf{2.5}$$

$$\phi_y = \frac{k_{pyr}[PYR]}{k_{intra} + \Sigma k_d + k_{pyr}[PYR]} \qquad \textbf{2.6}$$

$$\Delta\text{-OD}_y = \frac{C' k_{pyr} \tau_{carbene}[PYR]}{1 + k_{pyr} \tau_{carbene}[PYR]} \qquad \textbf{2.7}$$

$$\frac{1}{\Delta\text{-OD}_y} = \frac{1}{C'} + \frac{1}{C' k_{pyr} \tau_{carbene}} \bullet \frac{1}{[PYR]} \qquad \textbf{2.8}$$

Carbene rearrangements such as [1,2]–hydrogen and –carbon migrations have been widely studied using the pyridine probe technique.[141,159] The simplest of these reactions is the 1,2–hydrogen shift in methylcarbene (**90**, equation 2.9).[160] Modarelli and Platz unsuccessfully attempted to trap **90** with pyridine in the photolysis of 3-methyldiazirine (**102**). However, they were successful in trapping the perdeuterated isotopomer of **90** (**90-d_4**), which had a lifetime of 500 ps, corresponding to a rate constant for [1,2]-deuterium migration of 2×10^9 s^{-1}.[161] Their results showed that migration occurs faster than (or is at least competitive with) intersystem crossing (ISC) to the triplet ground state of the carbene. This is supported by the theoretical investigations of Evanseck and Houk[162] and Ma and Schaefer[163] who showed that the barrier to H-migration was only 1.2±0.5 kcal/mol and that the singlet state of **90** is indeed a true energy minimum, rather than a transition structure on the reaction pathway to ethylene.[160]

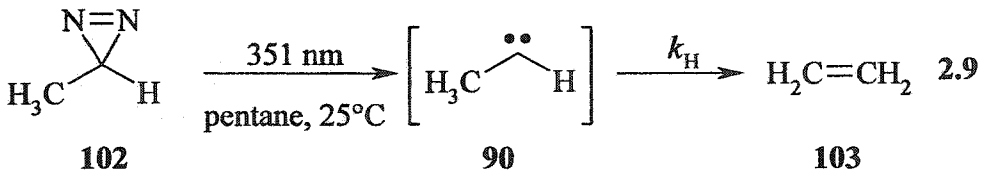

Efforts to study dimethylcarbene (**91**) by nanosecond laser flash photolysis have been more successful,[144] since it is predicted by theory to be slightly less reactive than **90** (E_a for [1,2]-H ~ 5 kcal/mol).[164] The lifetime (τ) was ~5 ns in pentane at 25°C, corresponding to $k_{1,2\text{-H}} \sim 2\text{x}10^8\ s^{-1}$. Table 2.2 summarizes the k_{intra} values for a number of other [1,2]-H migrations that have been determined.

Table 2.2 Rate Constants for [1,2]-Hydrogen Migrations in Carbenes at Ambient Temperature

No.	Carbene	k_H / $10^7\ s^{-1}$	Ref.
90	$HCCH_3$	200	161
91	$(H_3C)_2C$	20	144
104	H_3CCCl	0.2	141
105	$PhCH_2CBr$	5.6	141
106	H_3CCPh	<0.6	141
107	Me_3CCH_2CCl	1.4	141

1.2.2 [1,2]-Carbon Rearrangements and the Role of Excited States

The kinetics of [1,2]-carbon migration in acyclic carbenes have been studied to a lesser extent than those of [1,2]-H migrations.[141,165] *Tert*-butylcarbene (**108**), generated from a number of different photochemical and thermal precursors,[165] rearranges to yield two products: 2-methyl-2-butene (**109**) and 1,1-dimethylcyclopropane (**110**) via methyl migration or γ-CH insertion, respectively (Scheme 2.2). The yields of these two products change as a function of the precursor and the method of generation. For example, the photolysis of either *t*-butyldiazirine or -diazomethane (**111a,b**) in solution at room temperature affords **109** and **110** in a ratio of 49:51.[165,166] On the other hand, thermolysis of **111a** leads to **109:110** = 8:92. Thermolysis of tosylhydrazone salt (**112**) affords the same product ratio as thermolysis of **111a.**[166] The initial hypothesis was that the excited states of **111a,b** that were formed in the photochemical pathways were also contributing to product formation directly, without the intermediacy of carbene **108**. Since this proposal was made, the role of excited states as direct precursors to rearrangement products has been studied extensively.[141,160,165,167,168]

Scheme 2.2 Photochemical or Thermal Decomposition of *tert*-Butyldiazirine (111a), –diazomethane (111b) and Tosylhydrazone Sodium Salt (112)

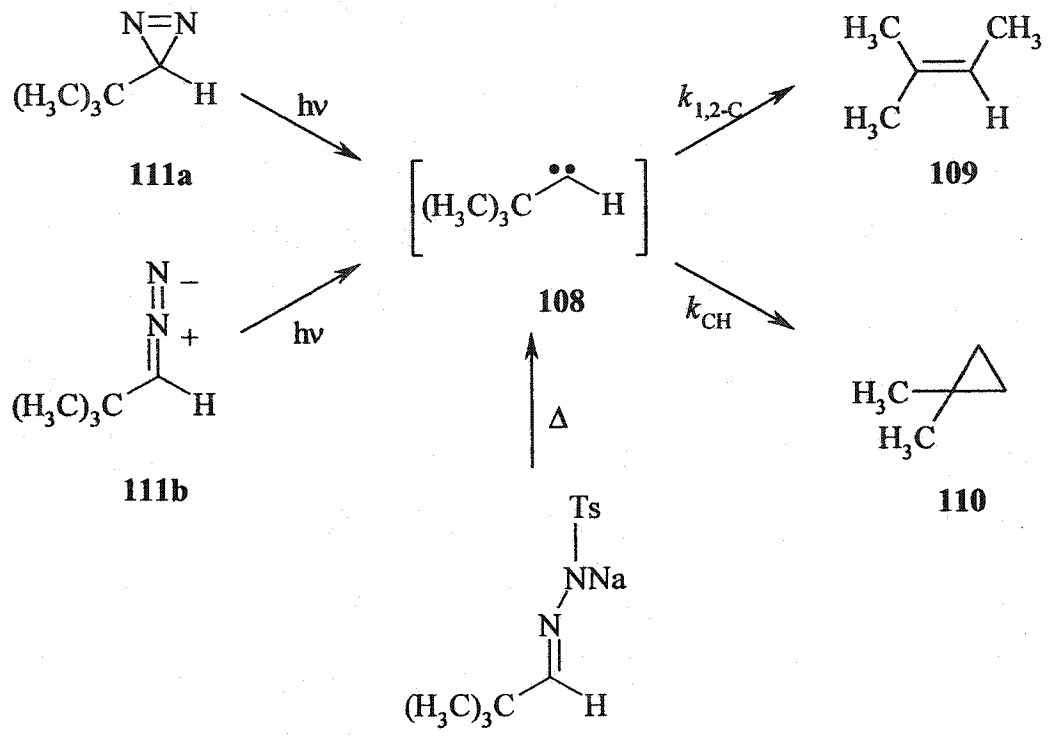

Perhaps the most elegant example that illustrates the involvement of excited states was the work of Moss and coworkers on the photolysis of 3-*tert*-butyl-3-chlorodiazirine (**113**).[168] Two types of rearrangement products were observed: **114** and **115** from [1,2]-methyl migration and CH-insertion, respectively, analogous to the photolysis of **111a** (Scheme 2.3). When the photolysis was done in the presence of 2-methyl-1-butene (**116**), an additional cyclopropane product (**117**) was also observed. As the concentration of **116** was increased, the yield of **115** decreased, such that the **117**:**115** ratio was a linear function of [**116**]. On the other hand, the yield of [1,2]-Me migration product **114** remained constant and did not vary in the presence or absence of the carbene trap. These

results indicate that CH-insertion product **115** is derived entirely from *t*-butylchlorocarbene (**118**), whereas **114** is mainly a product of excited state rearrangement from **113**^{1*}. This result clarified the flash photolysis results of Platz and coworkers who concluded that the rate constant ($k = 9.3\text{x}10^5\ s^{-1}$) for the disappearance of **118** was partitioned between $k_{1,2\text{-C}}$ and k_{CH}.[142] In fact, Moss' experiment shows that $k = 9.3\text{x}10^5\ s^{-1}$ should be assigned solely to k_{CH}.

Scheme 2.3 Photolysis of 3-*tert*-butyl-3-chlorodiazirine (113)

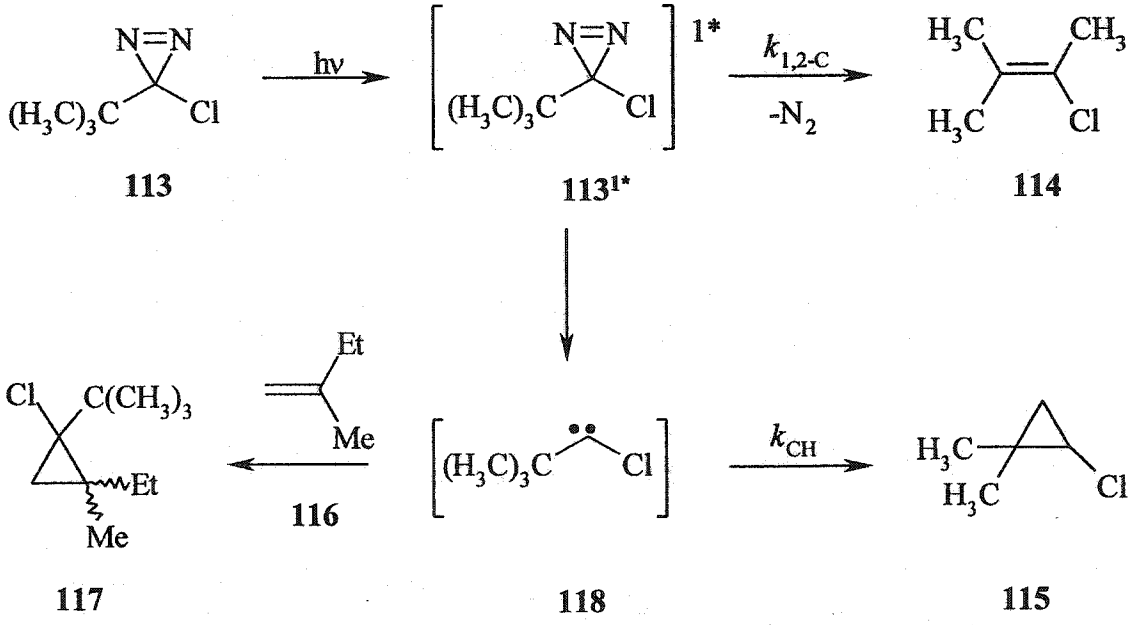

2.1.3 Photochemistry of (Trimethylsilyl)diazomethane (84)

Although there have been no kinetic studies on the rearrangements of α-silylcarbenes, the photochemistry of (trimethylsilyl)diazomethane (**84**) has been studied

in significant detail. Haszeldine, Scott and Tipping were the first to study the photolysis (>300 nm) of **84** at room temperature in the presence of neat *trans*-2-butene (**119**) in a molar ratio of 1:3.[169] The products observed included cyclopropane **120** and alkene **121** in chemical yields of 23% and 61%, respectively, as well as a polymeric residue. A second photolysis in the presence of an 18-fold excess of trimethylsilane (**122**) led to the formation of **123**, in 66% yield. Products **120** and **123** have been proposed to arise from the intermediate trimethylsilylcarbene (**124**). The stereospecificity of the reaction with *trans*-2-butene led to the proposal that **124** is a ground state singlet (**124-s**, Scheme 2.4). *Trans*-alkene **121** was proposed to arise from the thermal reaction of **124-s** with the starting material (**84**).

Scheme 2.4 Photolysis of (Trimethylsilyl)diazomethane (84) at 25°C

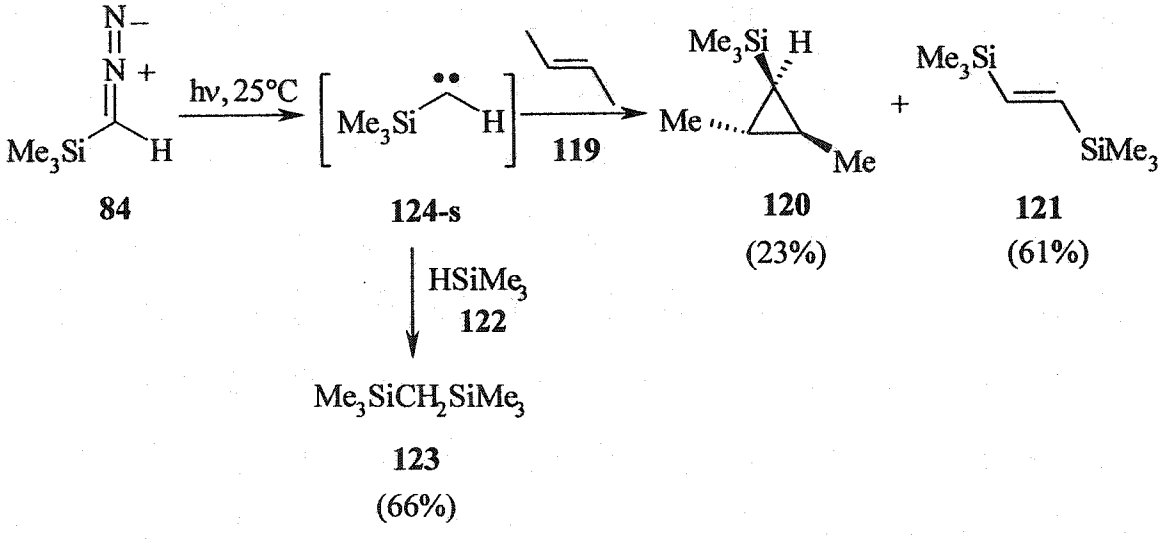

Two years later, Kreeger and Shechter examined the photolysis of **84** in isopropanol.[170] Isopropoxysilane $\mathbf{125_{iPr}}$ was identified as the sole product of the reaction,

and was proposed to arise from the trapping of 1,1,2-trimethylsilene (**83a**). No products attributed to (trimethylsilyl)carbene (**124**) were found.

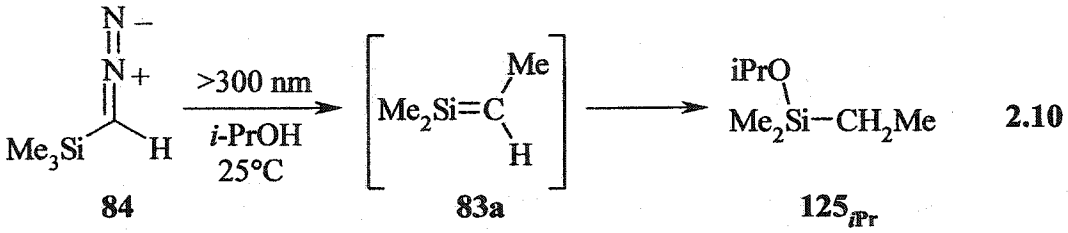

84 **83a** **125**$_{iPr}$ **2.10**

The third and fourth studies of the photolysis of this compound appeared simultaneously. Chapman, Barton and coworkers reported that the photolysis of **84** at 8 K in an argon matrix afforded a photostationary state mixture of **84** and (trimethylsilyl)diazirine (**87,** Scheme 2.5).[171] Continued photolysis of this mixture led to the formation of **83a**, which was identified on the basis of its IR spectrum and was proposed to result from the rearrangement of (trimethylsilyl)carbene (**124**). Upon warming the matrix to >45 K, *cis*- and *trans*-1,1,2,3,3,4-hexamethyl-1,3-disilacyclobutanes (***cis*-/*trans*-126**) were formed, which were proposed to arise from the dimerization of **83a**.

Scheme 2.5 Photolysis of (Trimethylsilyl)diazomethane (84) at 8 K Monitored by IR Spectroscopy

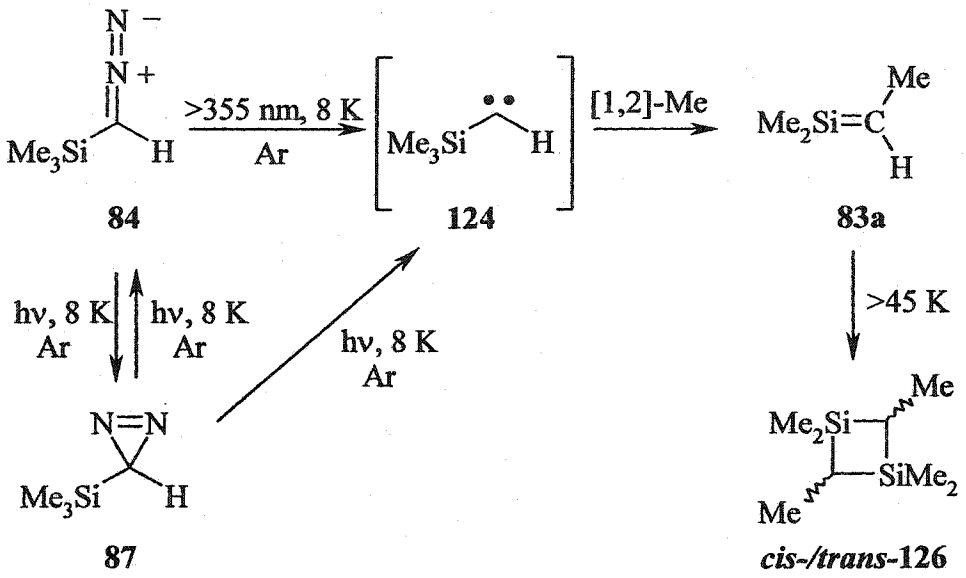

Chedekel and coworkers examined the photolysis of **84** under the same conditions and obtained similar results to those reported by Chapman, Barton and coworkers.[172] However, epr spectroscopy was also used to identify *triplet* (trimethylsilyl)carbene (**124-t**) which was produced along with (trimethylsilyl)diazirine (**87**). The triplet carbene was proposed to arise as a primary product from photolysis of **84** or by intersystem crossing (ISC) of *singlet* trimethylsilylcarbene (**124-s**), a process that competes with rearrangement to **83a** (Scheme 2.6). It was further proposed that the α-TMS group stabilizes the triplet state of the carbene relative to CH_3 due to the advantangeous overlap of the mutually perpendicular p orbitals on carbon with the vacant d orbitals of the adjacent silicon. This result is consistent with the theoretical work of Carter and coworkers, who predicted $HCSiH_3$ (**92**) to be a ground state triplet (see Table 2.1).[146]

Scheme 2.6 Photolysis of (Trimethylsilyl)diazomethane at 8 K Monitored by EPR Spectroscopy

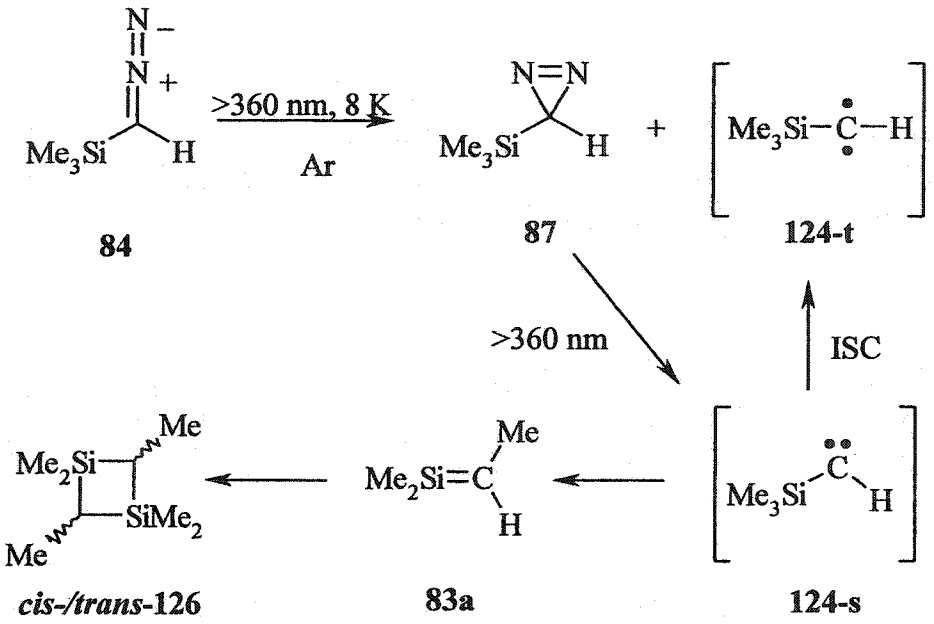

The goal of the work described in the present chapter was to examine the photochemistry of **82a, 84** and **87** at room temperature in hexane solution by nanosecond laser flash photolysis techniques. The pyridine probe technique was used to trap (trimethylsilyl)carbene (**124-s**), to determine the absolute rate constant for methyl migration in the formation of silene **83a**.

2.2 Results and Discussion

2.2.1 Steady-State Photolyses of 82a, 84 and 87

Direct irradiation of (trimethylsilyl)ketene (**82a**, 0.003 M) as a deoxygenated solution in hexane containing *t*-butyl alcohol (0.15 M) with the light from a Zn resonance lamp (214 nm) led to the formation of a single product, $\mathbf{125}_{t\mathbf{Bu}}$ (Scheme 2.7), identified by

GC coinjection with an authentic sample.[102] No other products were observed in ≥5% yield relative to the major product up to 50% conversion of the starting material. Similar results were obtained from the photolysis of **82a** (0.01 M) containing 0.26 M *t*-butyl alcohol with 300 nm light.[a]

Photolysis of (trimethylsilyl)diazirine (**87**, 0.02 M) as a deoxygenated solution in hexane containing *t*-butyl alcohol (0.3 M) with 300 nm light led to the exclusive formation of $\mathbf{125}_{t\mathbf{Bu}}$ (Scheme 2.7), up to <40% conversion of the starting material. Alkoxysilane $\mathbf{125}_{t\mathbf{Bu}}$ was again identified by GC/FID and GC/MS analyses. Photolysis to higher conversions of **87** resulted in small amounts of unidentified materials that were attributed to secondary photochemical reactions.

Scheme 2.7 Photolyses of 82a and 87 in Hexane Solution Containing *tert*-Butyl Alcohol

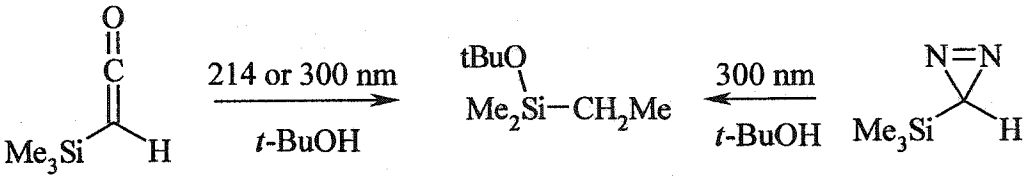

82a $\mathbf{125}_{t\mathbf{Bu}}$ **87**

Photolysis of (trimethylsilyl)diazomethane (**84**, 0.001 M) as a deoxygenated solution in hexane containing *t*-butyl alcohol (0.15 M) with 254 nm light in a Rayonet reactor also led to the exclusive formation of $\mathbf{125}_{t\mathbf{Bu}}$, as identified by comparison of its GC retention time and mass spectrum to those of the product formed in the photolysis of

[a] I would like to gratefully acknowledge Dr. Corinna Kerst for her work on the steady-state and nanosecond laser flash photolysis of (trimethylsilyl)ketene (**82a**).

82a. If the photolysis of **84** (0.05 M) is carried out in the presence of *t*-butyl alcohol (0.5 M) at 350 nm, **125**$_{tBu}$ is still the major product, but (trimethylsilyl)diazirine (**87**) is formed (ca. 10% relative to **125**$_{tBu}$) as well. Trimethylsilyldiazirine (**87**) was identified by comparing its ^{1}H NMR and UV-vis spectra with published literature data.[171] Furthermore, when **84** was photolyzed at even longer wavelengths (0.01 M, 419 nm) in the absence or *presence* of *t*-butyl alcohol (0.3 M), the major product was (trimethylsilyl)diazirine (**87**). No evidence for formation of **125**$_{tBu}$ could be obtained in the photolysis carried out in the presence of *t*-BuOH (Scheme 2.8). This photolysis was monitored by UV (Figure 2.2) and ^{1}H NMR spectroscopy.

Scheme 2.8 Photolysis of 84 at 254, 350 and 419 nm

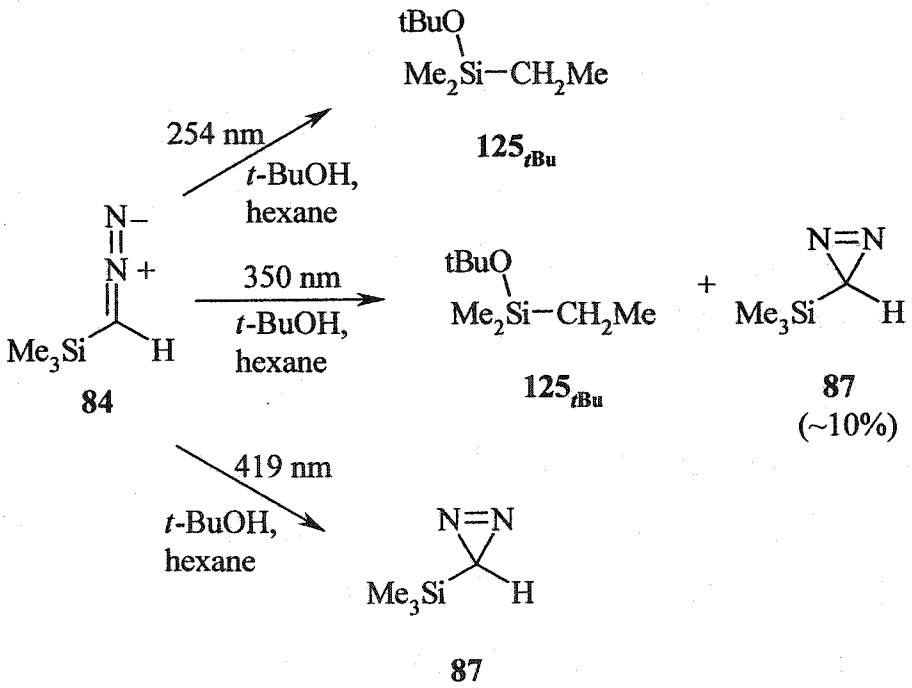

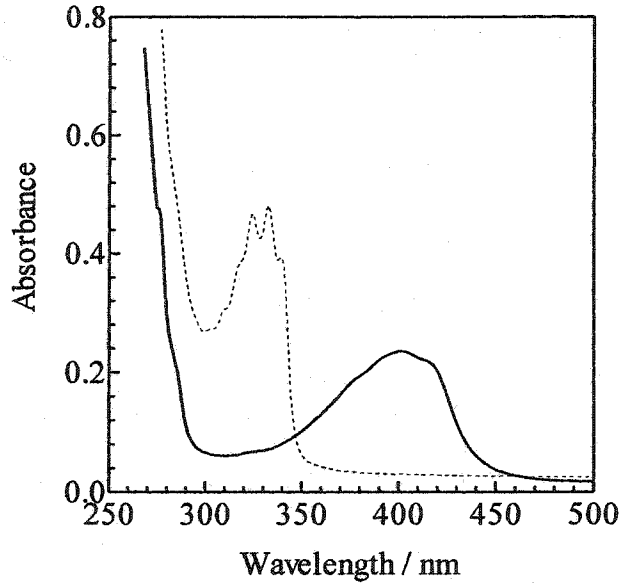

Figure 2.2 Absorption spectrum of **84** (0.01 M) in hexane (—). Absorption spectrum of the same solution after 419 nm photolysis (3.5 hours), indicating formation of **87** (------).

The photochemistry of **84** shows an interesting dependence on the wavelength of irradiation. Photolysis at 254 nm (π,π^* transition) affords only **125**$_{t\mathrm{Bu}}$, consistent with the formation of 1,1,2-trimethylsilene (**83a**). It is possible that the silene results from [1,2]-methyl migration in **124-s**, though at this stage it is impossible to rule out the involvement of the excited state of **84** as the immediate precursor to **83a** at this wavelength. Irradiation of **84** at 419 nm (n,π^* transition) leads exclusively to photoisomerization product **87**, with no evidence for the formation of products resulting from photodenitrogenation.

Most flash photolysis studies of alkyl-substituted carbenes have employed diazirines as precursors, which are intrinsically less reactive than their diazomethane

isomers.[173] Alkyldiazomethanes have also been used as precursors for room temperature studies,[174] although much less frequently.

The wavelength dependence of the photochemistry of diazo compound **84** is not unprecedented. Theoretical studies show that isomerization of unsubstituted diazirine to diazomethane is an energetically favourable pathway,[175] and there have been a number of studies that illustrate the photoisomerization of substituted derivatives experimentally.[176] For example, Seburg and McMahon examined the photolysis of diazoethane (**127**) at >399 nm in an Ar matrix at 4.5 K (Scheme 2.9).[177] The product mixture included ethene (**103**) and a "small amount of 3-methyldiazirine" (**102**). Photolysis of 3-methyldiazirine (λ=344 nm), resulted in complete conversion to ethene, with no formation of diazoethane.

Scheme 2.9 Photolysis of Diazoethane and 3-Methyldiazirine at 4.5 K

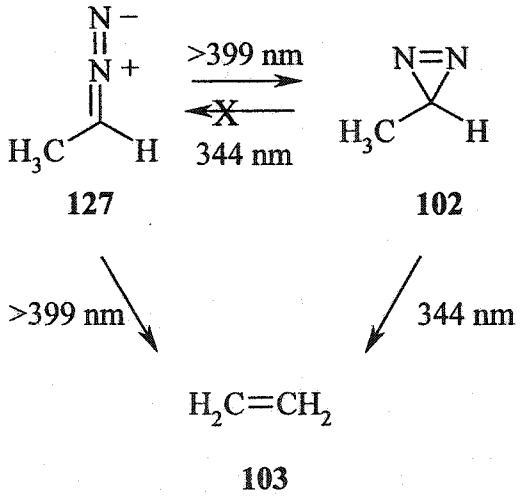

127 **102** **103**

Lowe and Parker studied the photochemical interconversion of a series of α-diazoamides,[178] an example of which is illustrated in Scheme 2.10. Irradiation of **128** in

carbon tetrachloride at λ>400 nm affords only diazirine **129**, while irradiation at 290 nm afforded lactams consistent with carbene CH insertion (**130** and **131**). Irradiation of the diazirine at 320 nm results in exclusive photoisomerization back to the diazo compound.

Scheme 2.10 Photoisomerization of an α-Diazoacetamide and Diazirine-carboxamide

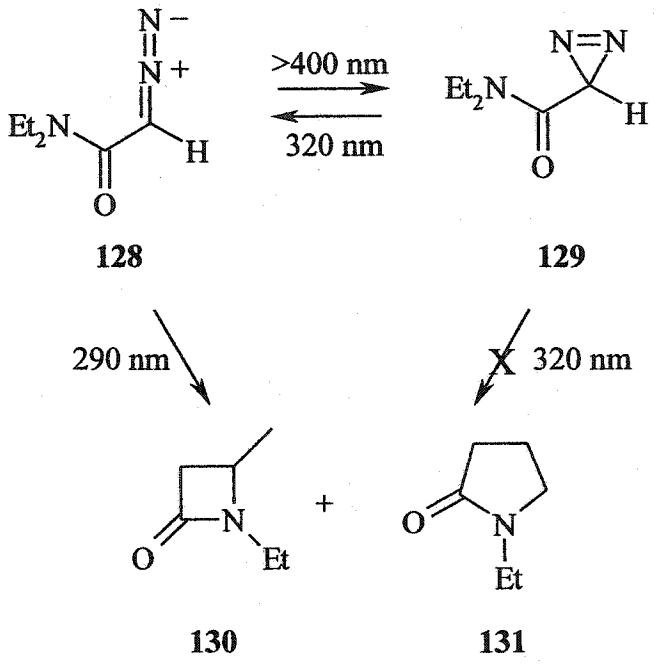

128 **129** **130** **131**

There are also cases where denitrogenation and isomerization occur upon irradiation of either isomer.[176] For example, the photolysis of 3,3-bis(1,1-difluorohexyl)diazomethane (**132a**) at 410 nm in cyclohexane solution leads to formation of the diazirine isomer (**132b**).[179] The diazirine can be converted back to the diazo compound upon irradiation at 310 nm. In both the photolysis of the diazo and diazirine isomers, alkene **133** and cyclopropane **134** are also formed, which arise from alkyl migration and CH-insertion, respectively (Scheme 2.11).

Scheme 2.11 Photolysis of 3,3-Bis(1,1-difluorohexyl)diazomethane (132a) and its Diazirine Isomer (132b)

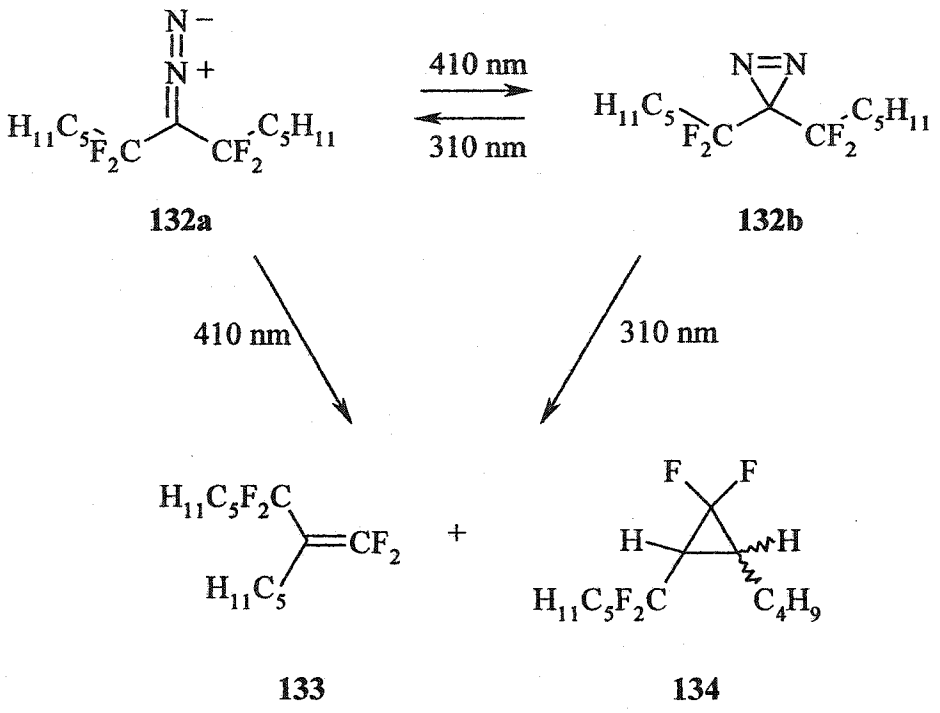

There are many other examples of photointerconversion of diazomethanes and diazirines.[176,180,181] In general, photoisomerization occurs in the S_1 state,[182] which is populated by irradiation of either isomer at wavelengths greater than 310 nm. Irradiation at shorter wavelengths results in excitation to S_2 where denitrogenation occurs to form the products.

The photointerconversion of diazirines and diazomethanes has also been demonstrated using laser flash photolysis techniques.[183] Laser flash photolysis (355 nm) of diazirines **135a,b** in isooctane solution afforded the corresponding diazomethanes **136a,b**, as detected by their transient absorption spectra (equation 2.11). The diazomethanes exhibited temperature dependent lifetimes of ca. 200 s at -25°C to 0.6 s at

room temperature. The quantum yield for diazomethane formation was determined to be on the order of Φ_{diazo}= 0.10.

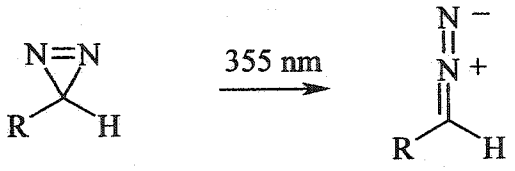

135 **136** **2.11**

a. **R** = isopropyl
b. **R** = *n*-propyl

The photochemical reactions of (trimethylsilyl)diazirine (**87**) and -diazomethane (**84**) have many similarities with their counterparts in carbon-based chemistry. The photochemistry of **84** is dependent on the wavelength of irradiation, in similar fashion to the examples cited above. Irradiation of **84** at 419 nm leads to photoisomer **87** as the major product. Irradiation of **84** or **87** at 350 or 300 nm, respectively, leads to predominantly silene formation; there is no indication that diazirine→diazomethane photoisomerization occurs in **87**.

2.2.2 Laser Flash Photolysis of 82a, 84 and 87

Laser flash photolysis of a continuously flowing, deoxygenated hexane solution of (trimethylsilyl)diazomethane (**84**, 0.001 M), using the pulses (248 nm, 90-110 mJ, ~20 ns) from a KrF excimer laser for excitation, led to the formation of transient absorptions in the 235-300 nm spectral range (Figure 2.3a). Flash photolysis of **82a** (193 nm) afforded a similar transient with a similar absorption spectrum and decay kinetics to that

obtained from **84** (Figure 2.3b). Flash photolysis of a deoxygenated hexane solution of **84** (0.04 M) employing the pulses (351 nm, 15 mJ, ~25 ns) of a XeF excimer laser led to a similar transient absorption spectrum, although the absorptions were much weaker than that observed from flash photolysis at 248 nm. Also, a shorter transient lifetime (~500 ns) was observed when **84** was photolyzed at 351 as compared to 248 nm, and the decay followed clean pseudo-first order kinetics. The spectra obtained at room temperature from the two precursors are identical to that observed by Sekiguchi and Ando in the photolysis of **84** in a 3-methylpentane glass at 77 K.[184]

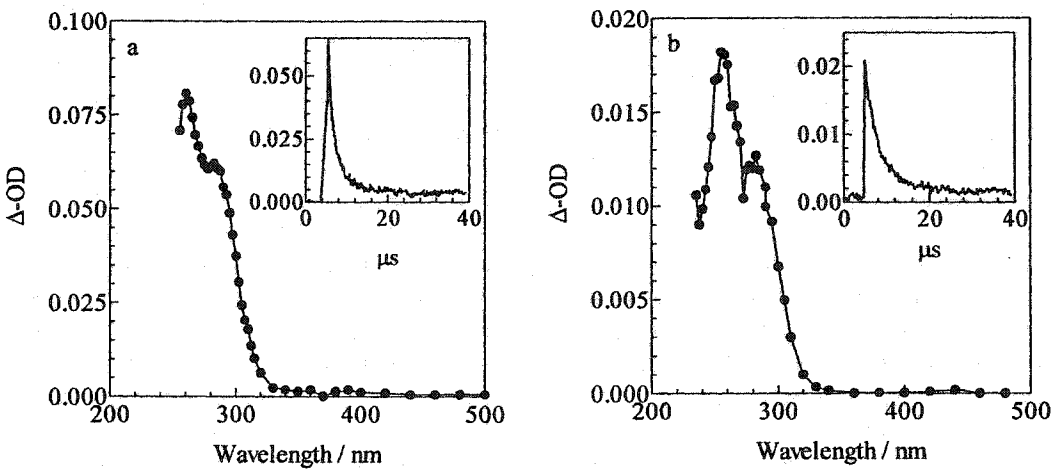

Figure 2.3 Transient UV absorption spectra from nanosecond laser flash photolysis of a) (trimethylsilyl)diazomethane (**84**) at 248 nm and b) (trimethylsilyl)ketene (**82a**) at 193 nm in deoxygenated hexane solution at 23°C. The spectra were recorded 0.1-1.0 μs after excitation. Typical decay traces recorded at a) 280 nm and b) 255 nm are shown as inserts.

Laser flash photolysis of a deoxygenated hexane solution of (trimethylsilyl)diazirine (**87**) with the pulses (337 nm, 6 mJ, 6 ns) from a nitrogen laser also led to the formation of a transient, which had a pseudo-first order lifetime of ~200 ns. The transient could only be monitored at the edge of the absorption attributed to the

silene (275-290 nm), because screening of the monitoring beam by the precursor at shorter wavelengths prevented the determination of the full transient absorption spectrum.

The transients observed from all precursors at the wavelengths studied were shortened upon addition of methanol, consistent with their assignment to silene **83a**. Plots of k_{decay} vs. methanol concentration from flash photolysis of **82a** or **84** exhibited positive curvature (Figure 2.4), indicating that the rate of decay of **83a** has a mixed-first order and second order dependence on alcohol concentration. Rate constants k_{MeOH} and k_{2MeOH} were determined by fitting the data to equation 1.23. The shorter lifetime observed when **87** was used as the precursor made it impossible to span the same range in k_{decay}, so only small amounts of methanol could be added. Therefore, k_{decay} of **83a** was shown to be a linear function of methanol concentration. However, the observed rate constant (k_{MeOH}) matched the first-order component for alcohol quenching observed when **82a** or **84** were used as precursors. The rate constants are summarized in Table 2.3.

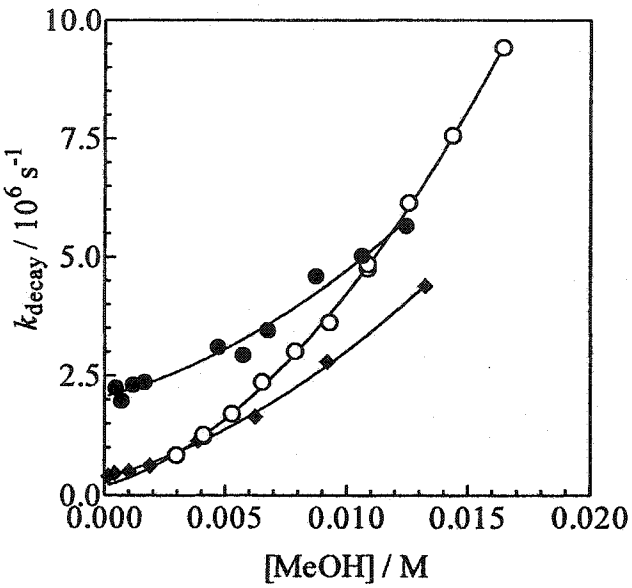

Figure 2.4. Plots of k_{decay} vs. [MeOH] for quenching of silene **83a**, from 193-nm flash photolysis of **82a** (♦), and 248- (O) or 351-nm (●) flash photolysis of **84** in deoxygenated methanolic hexane solutions at 23°C.

Table 2.3 Absolute Rate Constants for Reaction of Silene 83a with Methanol in Hexane at 23°C

Precursor	Excitation λ / nm	Monitoring λ / nm	k_{MeOH} / 10^8 M^{-1} s^{-1}	k_{2MeOH} / 10^{10} M^{-2} s^{-1}
82a	193	260	1.4±0.4	1.2±0.3
84	248	280	1.6±0.6	2.5±0.3
84	351	285	1.3±0.9	2±1
87	337	285	1.3±0.2	*a*

a. not determined; see text.

2.2.3 Laser Flash Photolysis of 82a, 84 and 87 in the Presence of Pyridine

In an effort to intercept singlet trimethylsilylcarbene (**124-s**), the flash photolysis of **82a, 84** and **87** was carried out in the presence of pyridine. Laser flash photolysis (308 nm) of a hexane solution of **82a** in the presence of 2 M pyridine led to the observation of a weak transient with an absorption maximum at 370 nm (Figure 2.5a). The growth of this signal was unresolvable from the laser pulse and had an initial decay (~1 μs) to a residual absorption that appeared to be stable over several hundred microseconds. Laser flash photolysis (308 or 337 nm) of **87** led to the observation of a similar, but weaker absorption in the 350-400 nm range, even in the presence of higher concentrations of pyridine (Figure 2.5b). Bleaching of the starting material accounts for the negative absorptions in the 300-330 nm range and also for the apparent shift in the absorption maximum compared to that obtained from flash photolysis of **82a**. The spectra derived from the photolyses of both precursors are typical of other carbene-pyridine ylides[144,155] and the absorption is assigned to the pyridine ylide of singlet trimethylsilylcarbene (**137**, Scheme 2.12). The weaker absorption of **137** that results from the photolysis of **87** as compared to **82a** is likely a result of the difference in $\phi_{carbene}$. It is possible that $\phi_{carbene}$ (**87**) < $\phi_{carbene}$ (**82a**) is due to a difference in partitioning of the excited states of the two precursors. Diazirines and diazomethanes have already been shown to form rearrangement products directly from the excited state,[165,168] resulting in a decrease in $\phi_{carbene}$.

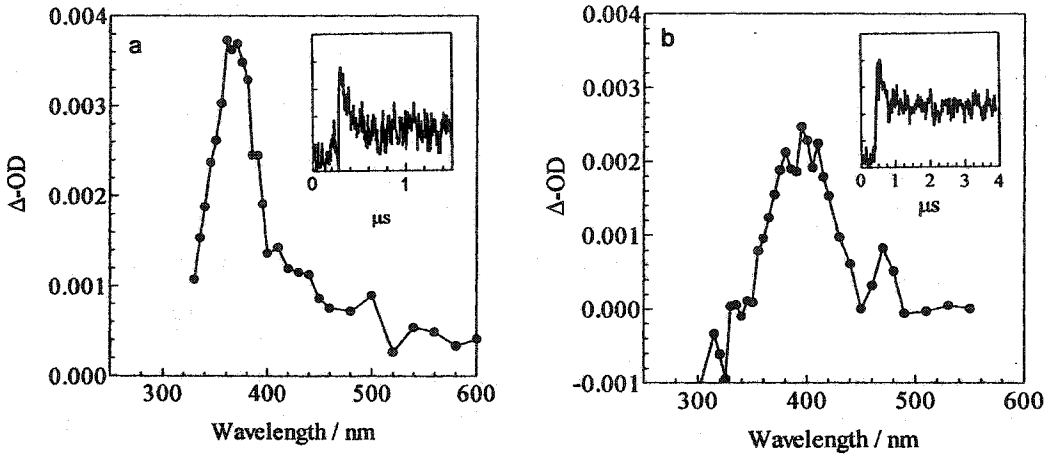

Figure 2.5. Transient UV absorption spectra from nanosecond laser flash photolysis of a) (trimethylsilyl)ketene (0.1 M, **82a**) at 308 nm in the presence of 2 M pyridine and b) (trimethylsilyl)diazirine (0.02 M, **87**) at 337 nm in the presence of 8 M pyridine at 23°C. The spectra were recorded 200-500 ns after excitation. Typical decay traces recorded at a) 370 nm and b) 390 nm are shown as inserts.

Scheme 2.12 Trapping of Singlet (Trimethylsilyl)carbene with Pyridine

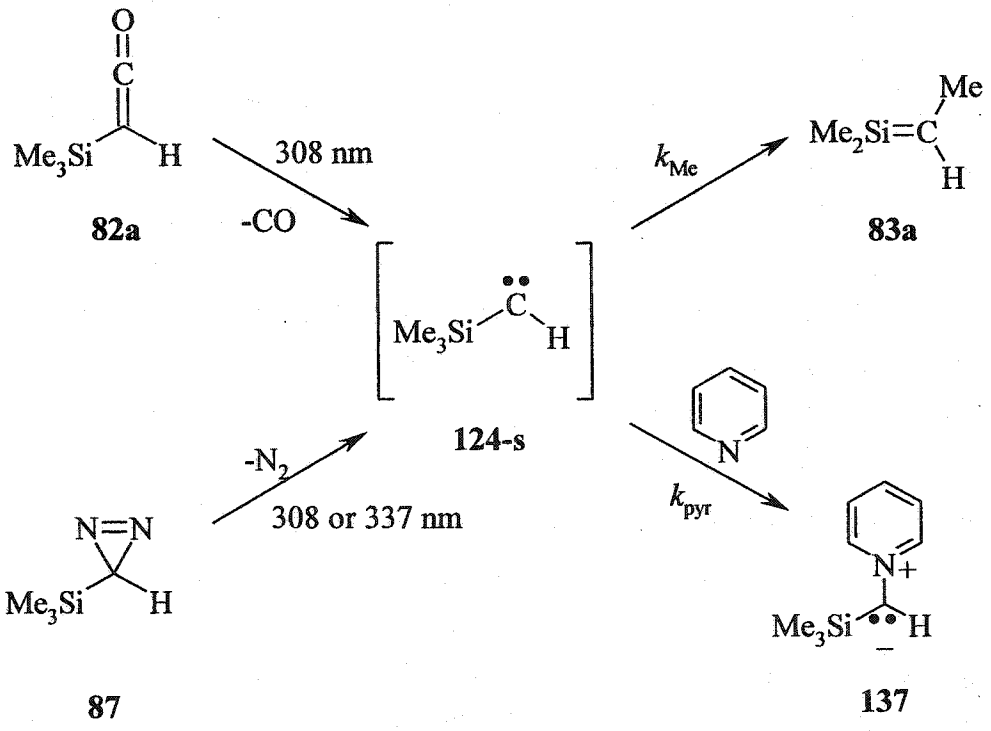

The growth of **137** was unresolvable from the laser pulse for both precursors, so it is impossible to determine $\tau_{124\text{-}s}$ from the growth kinetics of the ylide (equations 2.3 and 2.4). $(\Delta\text{-OD})_{max}$ at 370 or 390 nm from flash photolysis of **82a** or **87**, respectively, increased with increasing pyridine concentration. The observed $(\Delta\text{-OD})_{max}$ is a function of pyridine concentration, (equation 2.7)[144], where $\tau_{carbene}$ is the lifetime of carbene **124-s** and k_{PYR} is the bimolecular rate constant for reaction of **124-s** and pyridine.

Values of $(\Delta\text{-OD})_{max}$ were measured in the presence of 1-10 M pyridine using both **82a** and **87** as precursors. The maximum absorbance of the ylide ($(\Delta\text{-OD})_{pyr}$) was taken as the relatively long-lived residual absorption observed in the insets of Figure 2.5. Plots of $(\Delta\text{-OD})_{pyr}$ vs. [PYR] for both precursors are shown in Figure 2.6. Fitting the data to equation 2.7 afforded $k_{pyr}\tau_{124} = 0.33\pm0.10\ M^{-1}$ and $0.35\pm0.08\ M^{-1}$ from **82a** and **87**, respectively. The greater amount of scatter in the data from photolysis of **87** is attributed to the lower yield of the ylide as compared to that from photolysis of **82a**. The excellent agreement observed between the two precursors is strong evidence that (trimethylsilyl)carbene (**124-s**) precedes the formation of 1,1,2-trimethylsilene (**83a**) in both cases.

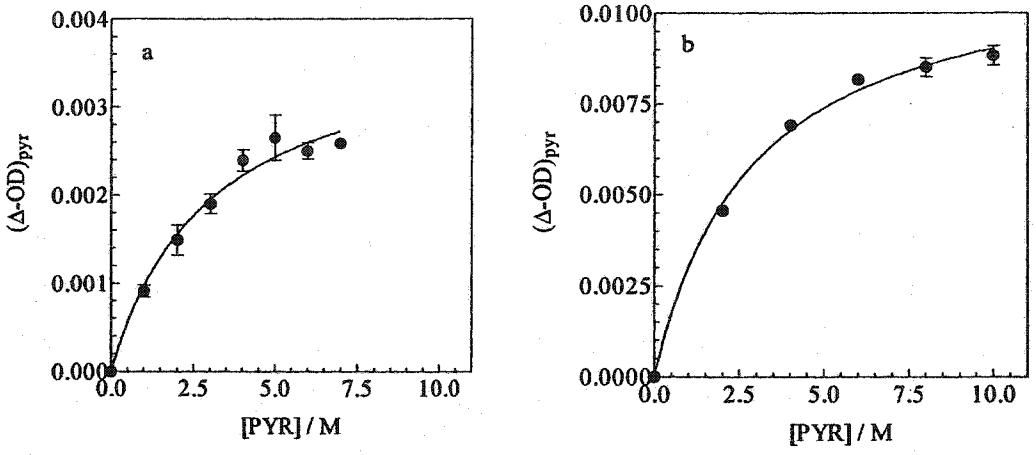

Figure 2.6 Plots of $(\Delta\text{-OD})_{pyr}$ vs. [PYR] from flash photolysis of a) **87** (337 nm) and b) **82a** (308 nm).

If k_{pyr} for reaction of **124-s** and pyridine is assumed to be the same as that for other alkyl- and dialkylcarbenes (k_{pyr} = (1-5) x 10^9 M^{-1} s^{-1}),[144,161] then the lifetime of **124-s** lies between 0.07 and 0.4 ns in deoxygenated hexane solution at 23°C. At the concentrations used for the experiments with **82a** and **84**, the bimolecular reaction between the carbene and the precursor can be neglected, especially because the formation of azine (**138**) was not observed in the product mixture of the steady-state photolysis of **87** at similar concentrations as were employed in the flash photolysis experiments (equation 2.12). Azines have been shown to be the products of the reaction between diazirines or diazomethanes and carbenes.[185] As would be expected, azines are formed when the precursor concentration is particularly high and/or the carbene is particularly long-lived. Furthermore, there were no triplet carbene-derived products (ie. products consistent with radical reactions, such as hydrogen-abstraction from the solvent) formed

in significant yields relative to the silene-derived products (ie. **124**$_{tBu}$) in the steady-state photolyses of **82a** and **87**, suggesting that intersystem crossing (k_{ISC}) is slower than silene formation (k_{Me}) under the conditions employed for this experiment. Therefore, the rate constant for methyl migration in (trimethylsilyl)carbene is estimated to be $k_{Me} \sim (8\pm6)\text{x}10^9$ s^{-1}, calculated from the midpoint of the estimated lifetime range. Considering the rate data of Table 2.2, this rate constant is among the largest of all carbene rearrangements known in the condensed phase.

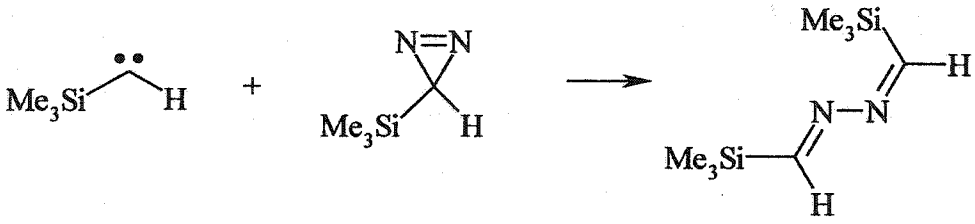

2.12

124-s **87** **138**

It is interesting to note that the calculated barriers for [1,2]-H migration in $HCCH_3$ (**90**)[162] and H_3SiCH (**92**, equation 2.13)[186] are 1.5 and 1.9 kcal/mol, respectively. The variation in the barriers to H-migration as a function of the atom of origin is minimal. The small barrier in **90** is also reflected in its value for hydrogen migration ($k_H > 2\text{x}10^9$ s^{-1}, *vide supra*).[161]

The rate constant for [1,2]-methyl migration in **124-s** is similar to those for H-migration in **90** and **92**. This is an interesting result, considering that the rate constant for methyl migration in *t*-butylcarbene (**108**) is four orders of magnitude smaller[168] than the rate constant for methyl migration in **124-s**.

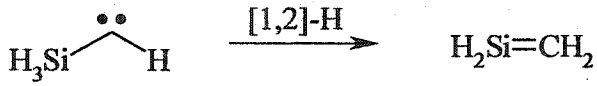

92 9a 2.13

The theoretical work of Platz and Schaeffer predict that the lowest energy pathway for hydrogen migration in ethylmethylcarbene (**139**) depends on the orthogonal position of the hydrogen relative to the rest of the molecular framework.[187] This geometry maximizes the hyperconjugative interaction between the C-H bond and the empty p orbital on the carbenic centre and facilitates the migration to form 2-butene (**140**). The calculated barrier to [1,2]-hydrogen migration is 5.2 kcal/mol (Scheme 2.13).[187]

Scheme 2.13 Hydrogen Migration in Ethylmethylcarbene (139)

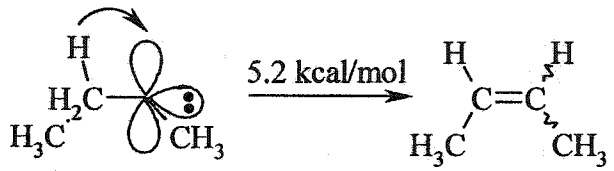

139 **140**

The barrier to the analogous carbon migration in **139** is 18 kcal/mol under the same geometrical constraints. It was proposed that carbon migrations require different geometries with barriers that are minimized when the alkyl group that is migrating is closer to the carbenic centre. It was shown that cyclobutylidene (**141**) assumes a puckered conformation, where the migrating carbon is closer to the carbene centre. This geometry results in a barrier to migration that is smaller than [1,2]-C migration in **139** by

8 kcal/mol. Further calculations also suggested that the thermodynamic stabilities of the products were of minimal importance in the migrations of both hydrogen and carbon.

Scheme 2.14 Carbon Migration in Cyclobutylidene (141)

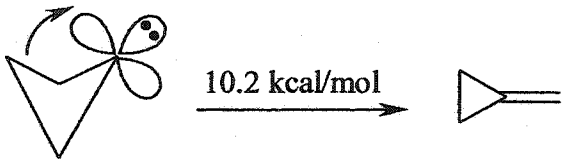

141 **142**

The results of Platz and Schaeffer suggest that the barrier to [1,2]-Me migration in **124** would be smaller than that in **108**. The bond between the silicon and carbon that is broken in the transition state between **124** and **83a** is longer and weaker than the bond that is broken in the rearrangement of **108.** The electropositive nature of silicon might also drive the migration, particularly if the reaction involves negative charge density on the migrating group in the transition state[188,189] and positive charge density at silicon.

Although flash photolysis of **84** at 351 nm led to the formation of silene **83a**, no transients ascribable to **124-s** could be detected when flash photolysis was carried out in neat pyridine. This result is a good indication that the silene must be formed by an alternative mechanism, at least upon long-wavelength excitation. Most likely this alternate pathway is direct rearrangement and nitrogen extrusion in the excited state of **84**. It has been shown through a number of examples that the excited states of diazo and diazirine compounds can lead directly to products that appear to be derived from carbene intermediates (section 2.1.2).[160,167,174,190-192] A similar photolysis could not be carried out

at 248 nm to probe for the intermediacy of **124-s** due to the absorption of pyridine at this wavelength. In comparison to the previous photolysis of **84** by Chedekel and coworkers,[172] no evidence for the formation of triplet (trimethylsilyl)carbene (**124-t**) has been found with either 248- or 351-nm light. Either the triplet is not formed or it is not detectable under the experimental conditions employed. It is also conceivable that [1,2]-Me migration is significantly slower at 8 K such that intersystem crossing competes with or is faster than methyl migration (ie. $k_{Me} \leq k_{ISC}$ at 8 K).

2.3 Summary

It has been shown that the photolysis of (trimethylsilyl)ketene and diazirine in the condensed phase leads mainly to the formation of 1,1,2-trimethylsilene. Though there are examples in carbon-based chemistry of photoisomerization of diazirines to diazomethanes, there is no evidence for this type of reaction in the case of **87**. Photolysis of the ketene (**82a**) at 308 nm and the diazirine (**87**) at 308 or 337 nm leads to the formation of singlet (trimethylsilyl)carbene (**124-s**) which is one of the immediate precursors to the silene (**83a**). The rate constant for methyl migration (k_{Me}) in **124-s** was found to be $(8\pm6)\times10^{9}$ s^{-1}.

Photolysis of (trimethylsilyl)diazomethane (**84**) at 248 and 351 nm also led to the formation of **83a**, though no evidence for a carbene intermediate could be obtained. The fact that no ylide is formed when the flash photolysis of **84** is carried out in pyridine at 351 nm is intriguing, especially because steady-state results show that the silene is indeed formed at this wavelength. This is an excellent example of exclusive excited state reactivity, which is rare in carbene chemistry. Furthermore, irradiation of **84** at 419 nm exclusively leads to photoisomerization product **87**, with selectivity that is also relatively unique in the area of diazirine–diazo interconversions.

Chapter 3

A Kinetic Investigation of Silenes Derived from α–Silylketenes and –diazomethanes

3.1 Background

The research that has been done by N. Wiberg and coworkers on 1,1-dimethyl-2,2-bis(trimethylsilyl)silene (**11a**) was an important contribution to silene chemistry.[30,123,124,193] His work involved the first measurement of kinetic data for the reactions of transient silenes, which made it an essential contribution to the development of our current understanding of silene reactivity. However, Wiberg's studies yielded only *relative* kinetic data for the addition of various silenophiles to **11a**, and the first *absolute* rate constants for many other silenes were not reported until many years later.[126]

There were two initial goals of the work described in this chapter. Firstly, because there is now a large library of *absolute* kinetic data for other silenes,[25] the determination of absolute rate constants for reaction of **11a** with some of the reagents previously employed by Wiberg would link the more recent studies on silene kinetics and substituent effects with the original investigation. Secondly, the rate constant for methanol addition to **11a** might be added to the 1,1-dimethyl-2-substituted silene series (Figure 1.7) to test the hypothesis that **11a** should be extremely reactive due to its substitution pattern on the double bond. The initial challenge was to generate **11a**

photochemically in fluid solution at ambient temperatures under conditions where it could be detected directly.

The NLFP technique, which we were certain would be required in order to detect **11a** directly and monitor its kinetic behaviour, requires a precursor from which the silene can be generated photochemically. Two α-silylcarbene precursors, (pentamethyldisilanyl)(trimethylsilyl)diazomethane **88a** and the analogous ketene **88b** were proposed as likely candidates for this purpose (equation 3.1).

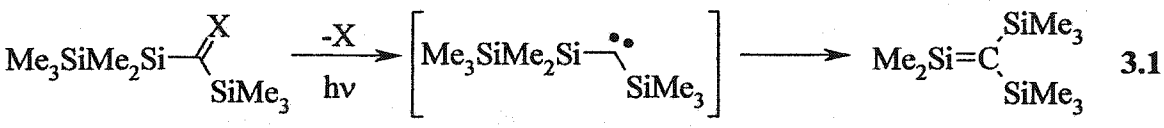

88 **143** **11a** **3.1**

a. X = N_2
b. X = CO

A previous report suggested that **88a** would be a suitable precursor. Sekiguchi and Ando reported that photolysis of (pentamethyldisilanyl)(trimethylsilyl)diazomethane (**88a**) at 77 K in a 3-methylpentane glass led to a product exhibiting a UV absorption spectrum with a maximum absorption at 278 nm. The photolysis was repeated at room temperature in the presence of *t*-butyl alcohol. The course of the reaction was monitored by ^{1}H NMR, showing that alkoxysilane $\mathbf{144_{Bu}}$ was the only detectable product under these conditions. Its formation was attributed to the trapping of **11a** by the alcohol. Consequently, the absorption at 278 nm in the 77 K matrix was assigned to **11a** (equation 3.2).[184] No previous studies have been done on the photochemistry of **88b**.

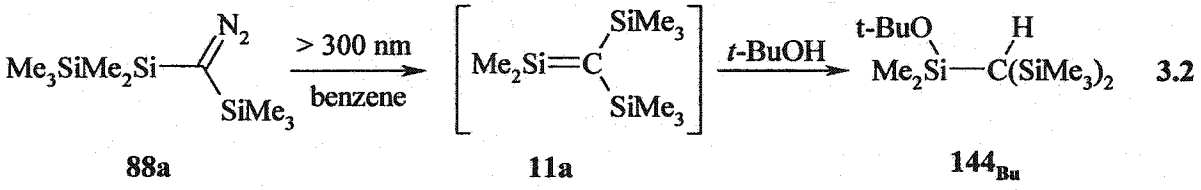

88a **11a** **144$_{Bu}$** **3.2**

3.2 Results and Discussion

3.2.1 Synthesis of (Pentamethyldisilanyl)(trimethylsilyl)diazomethane (88a)

The synthesis of **88a** was accomplished following the procedure of Seyferth and coworkers for the synthesis of bis(trimethylsilyl)diazomethane.[194] (Trimethylsilyl)diazomethane (**84**) was treated with *n*-butyllithium in hexane solution at -78°C (equation 3.3). A yellow precipitate formed almost immediately. The reaction mixture was allowed to stir at this temperature for three hours. Pentamethylchlorodisilane[195] was then added dropwise, and the mixture was allowed to stir overnight while warming to room temperature. The resulting solution was bright orange and this was concentrated by rotatory evaporation. The residue was bulb-to-bulb distilled following three freeze-pump-thaw cycles and then fractionally distilled to obtain **88a**. The product was further purified (>98%) by semi-preparative gas chromatography (yield: 20% after purification).

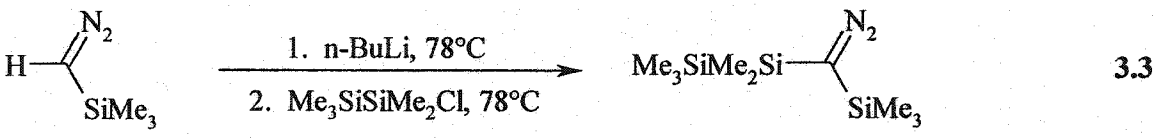

84 **88a** **3.3**

Our collaborators Professor Tom Tidwell and Annette Allen at the University of Toronto synthesized ketene **88b**.

3.2.2 Direct Detection of 1,1-Dimethyl-2,2-bis(trimethylsilyl)silene by Laser Flash Photolysis of 88a and 88b

Laser flash photolysis of a continuously flowing, deoxygenated solution of (pentamethyldisilanyl)(trimethylsilyl)diazomethane (**88a**, $4x10^{-4}$ M) in deoxygenated hexane with the pulses from a Kr/F_2 excimer laser (248 nm, 90-100 mJ, ~20 ns), led to the formation of readily detectable transient absorptions in the 270-330 nm spectral range (Figure 3.1a). The transient decay kinetics varied, depending on the observation wavelength. Transients monitored at 310 nm decayed with mixed first- and second-order kinetics and with a pseudo-first order lifetime of >15 μs. Those monitored at 280 nm consisted of a short-lived, major component (τ ~500 ns) superimposed on a long-lived component that decayed with similar kinetics to those of the transient at 310 nm. The lifetime of the 280-nm transient was sensitive to the presence of oxygen. The rate constant for reaction with oxygen was determined to be $k_{O2} \sim 7 \times 10^8$ M^{-1} s^{-1}, as determined by three measurements of k_{decay} under nitrogen-saturated (0 M oxygen), oxygen-saturated (0.015 M oxygen) and air-saturated (0.003 M oxygen) conditions.[196] The 310-nm transient was not sensitive to the presence of oxygen. Addition of 0.01 M methanol affected the lifetimes at both 280 and 310 nm; the former was shortened to <30 ns, while the decay of the latter was changed to clean pseudo-first order kinetics and a lifetime of ~10 μs. The transient spectrum recorded 1-1.2 μs after the laser pulse (i.e.

after the 280-nm species completely decayed), is shown in Figure 3.1b. Under both sets of conditions, negative absorptions were observed at monitoring wavelengths less than 265 nm due to irreversible bleaching of the precursor. Thus, both spectra of Figure 3.1 are skewed, so that the apparent absorption maxima are red-shifted from the actual values; this is particularly true in the case of Figure 3.1a.

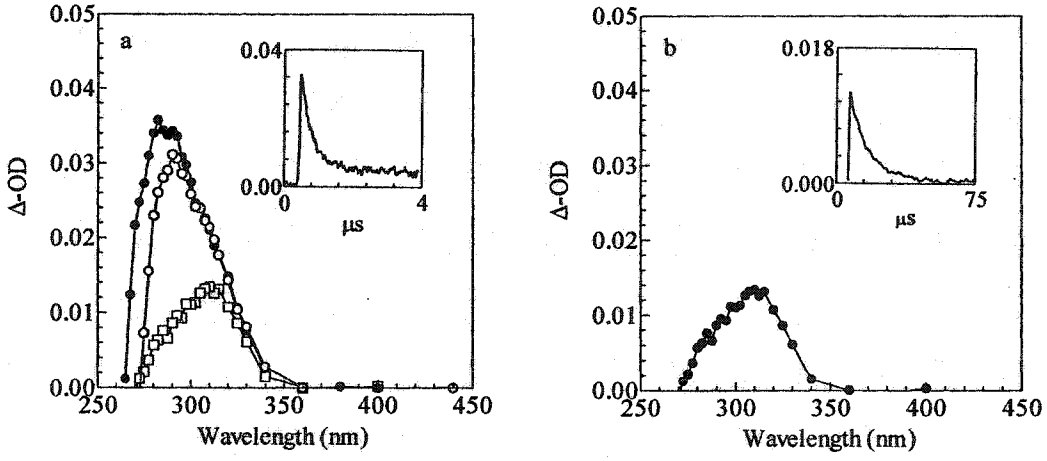

Figure 3.1. Transient UV absorption spectra from 248-nm laser flash photolysis of **88a** in deoxygenated hexane solution at 24°C. a) The transient UV spectrum in the absence of methanol recorded at 80-100 ns (●), 150-200 ns (○) and 1.4-1.8 μs (□) after the laser pulse. The insert shows a typical decay trace recorded at monitoring wavelength of 280 nm. b) The transient UV spectrum in the presence of 0.01 M methanol, recorded 1-1.2 μs after the laser pulse. The insert shows a typical decay trace recorded at a monitoring wavelength of 310 nm.

Similarly, laser flash photolysis of a continuously flowing solution of (pentamethyldisilanyl)(trimethylsilyl)ketene (**88b**, 6×10^{-5} M) in deoxygenated hexane with the pulses from an Ar/F_2 excimer laser (193 nm, 5-7 mJ, ~20 ns), led to the observation of readily detectable transient absorptions in the 230-330 nm spectral range (Figure 3.2). As was observed in the flash photolysis of **88a**, these decayed with varying

kinetics, depending on the observation wavelength. Transient absorptions monitored at 310 nm decayed with similar kinetics to the transient monitored at 310 nm in the flash photolysis of **88a**. Transients recorded at 260 nm decayed with clean pseudo-first order kinetics as in the experiments with **88a**, but with a longer lifetime (2 - 3 μs). Monitoring at 250 nm resulted in the observation of two overlapping pseudo-first order decays. One decay resulted in a lifetime of ca. 3 μs, while the second decay was <1 μs. This short-lived transient was not observed in the flash photolysis of the diazo compound because bleaching of the diazomethane precursor made it impossible to examine the short-wavelength region of the spectrum. The kinetic behaviour or identification of this transient was not pursued further, however, it is possible that the absorption at 250 nm could be the third silene produced in the photolysis of **88b** (see section 3.2.3). Alternatively, it could be due to traces of oxygen in the solvent that absorb at 193 nm.[139]

As in the experiments with **88a**, the lifetimes of both the short- and long-lived transients were shortened upon addition of methanol to the solutions of **88a** or **b**. Plots of k_{decay} versus methanol concentration are shown for the 280-nm transients from both **88a** and **88b** (Figure 3.3a). The data were analyzed according to equation 1.26, where k_0 is the pseudo-first-order rate constant for transient decay in the absence of methanol and k_{MeOH} is the second-order rate constant for reaction of the species with methanol. In the case of the long-lived species monitored at 310 nm from flash photolysis of **88a**, plots of k_{decay} versus [MeOH] are curved, as shown in Figure 3.3b. These data were thus fit to the quadratic expression of equation 1.23, where k_{2MeOH} is the third-order rate constant for quenching of the silene. The data set derived from flash photolysis of **88b** does not span

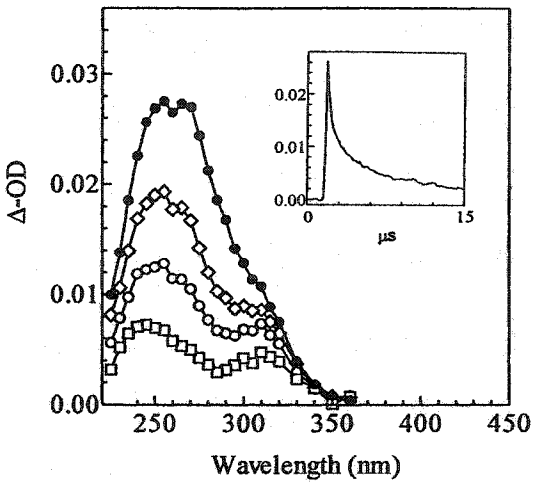

Figure 3.2 Transient UV absorption spectra from 193-nm laser flash photolysis of ketene **88b** in deoxygenated hexane solution at 24°C, recorded 0.1-0.3 (●), 1.0-2.0 (◇), 3-5 (○), and 11.0-13.0 (□) μs after the laser pulse. The insert shows a typical decay trace recorded at 280 nm.

the same concentration range as that obtained from the photolysis of **88a** due to screening effects at higher concentrations of methanol. Table 3.1 lists the second- and third-order rate constants obtained from these experiments; the agreement between the data obtained with the two precursors is excellent.

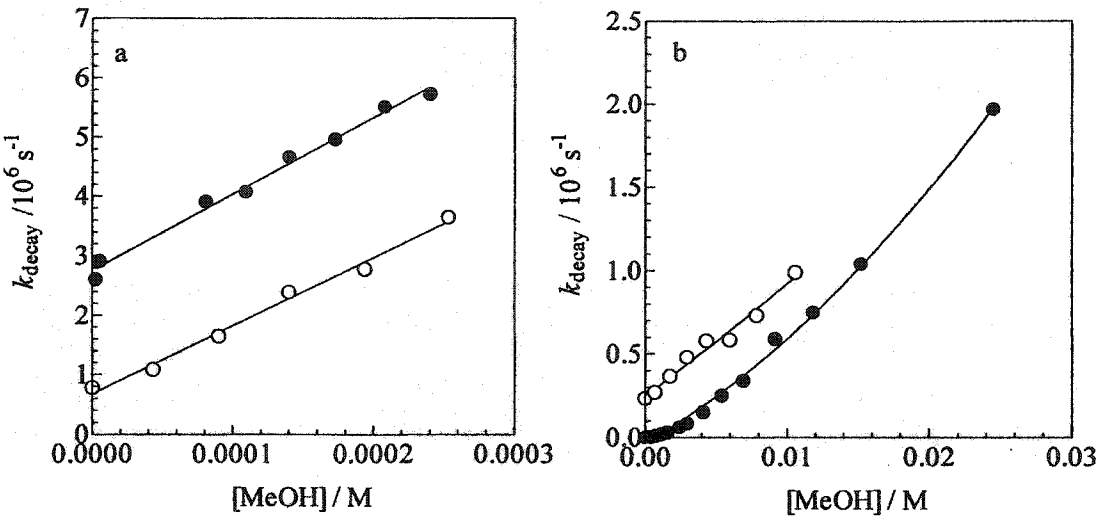

Figure 3.3 Plots of k_{decay} vs. [MeOH] for quenching of silenes from laser flash photolysis of **88a** (●) and **88b** (○) in deoxygenated hexane in 24°C monitored at (a) 280 nm and (b) 310 nm.

Table 3.1 Absolute Rate Constants for Reaction of Transient Silenes with Methanol in Hexane at 23°C Derived from Photolysis of 88a and 88b[a]

Precursor	**88a**		**88b**		
Transient λ / nm	280	310	255	280	310
Lifetime / μs	0.50 ± 0.10	15 ± 2	3 ± 1	3 ± 1	15 ± 2
k_{MeOH} / 10^9 M^{-1} s^{-1}	13 ± 2	0.049 ± 0.008	12 ± 2	14 ± 2	0.06 ± 0.01
k_{2MeOH} / 10^9 M^{-2} s^{-1}	*b*	1.3 ± 0.6	*b*	*b*	0.4 ± 0.2

a. errors reported as ±2σ
b. shows linear dependence on [MeOH], see equation 1.26.

There are some interesting differences between the transient spectra and kinetics derived from photolysis of **88a,b**, even though the results from steady-state experiments indicate the two precursors give rise to similar products, via similar transient silenes (*vide infra*). First, flash photolysis of **88a** gave rise to more strongly absorbing transients as compared to **88b**, a trend that is consistent with the behaviour of other homologous α-silylketenes and diazomethanes that have been studied.[102] For example, the absorption of 1,1,2-trimethylsilene (**83a**) was much stronger when (trimethylsilyl)diazomethane (**84**, equation 1.31) was used as the precursor as compared to (trimethylsilyl)ketene (**82a**, equation 1.30). This difference in signal strengths from the two precursors is due, at least in part, to the difference in laser intensities: the KrF emission (248 nm) is 3-6 times more intense than the ArF emission (193 nm) with the laser employed for our experiments. The second significant difference is the shorter lifetime that the 280-nm transient exhibits when it is generated from **88a** as compared to **88b**. This difference may be due to reaction of the 280-nm transient with the diazomethane precursor, as silenes have been shown to react with substituted diazomethanes via [2+3]-cycloaddition.[30] In the experiments with **88b**, the precursor concentration was lower and therefore reaction with the silene, if it occurs, is insignificant relative to other processes.

The shorter-lived, more reactive species (λ_{max} ~ 260 nm; Figure 3.2) is assigned to silene **11a**. Its prominence in the transient spectrum as compared to the second transient is consistent with it being the major product in the photolysis of **88a,b** (see section 3.2.3), assuming that the extinction coefficients of the silenes are similar. Furthermore, the spectrum matches that observed by Sekiguchi and Ando in a 3-methylpentane glass at 77

K, who found that **11a** was the only product of the photolysis. Their conclusion was supported by the observation of $\mathbf{144_{Bu}}$ by ^{1}H NMR as the sole product in the presence of *t*-butyl alcohol.[184] However, our results clearly indicate that at least one other transient product is formed as well. It seems possible that other silenes could potentially result from photolysis of **88a** and **88b**, if a methyl group were to migrate in the rearrangement of carbene **143** or in the excited state of **88a** and/or **b**.

This type of competitive migration between substituents on the carbene centre has been observed in the photolysis of (1-phenylsilacyclobutyl)(trimethylsilyl)diazomethane (**49**, Scheme 1.2)[99] and pentamethyldisilanylketene (**82c**).[102] The photolysis of a methanolic hexane solution of **82c** led to the formation of two isomeric methoxysilanes **145** and **146** in a 9:1 product ratio.[102] These products are those of methanol trapping of the silenes formed by trimethylsilyl and methyl migration, respectively, in carbene **147** (Scheme 3.1). If a statistical correction is made for the migratory aptitudes of the two groups, the trimethylsilyl group migration is 18 times faster than that of methyl migration. We thus decided to re-examine the steady-state photolysis of **88a** in order to help assign the 310-nm transient species observed in the flash photolysis experiments.

Scheme 3.1 **Silene Trapping in the Photolysis of (Pentamethyldisilanyl)ketene (82c)**

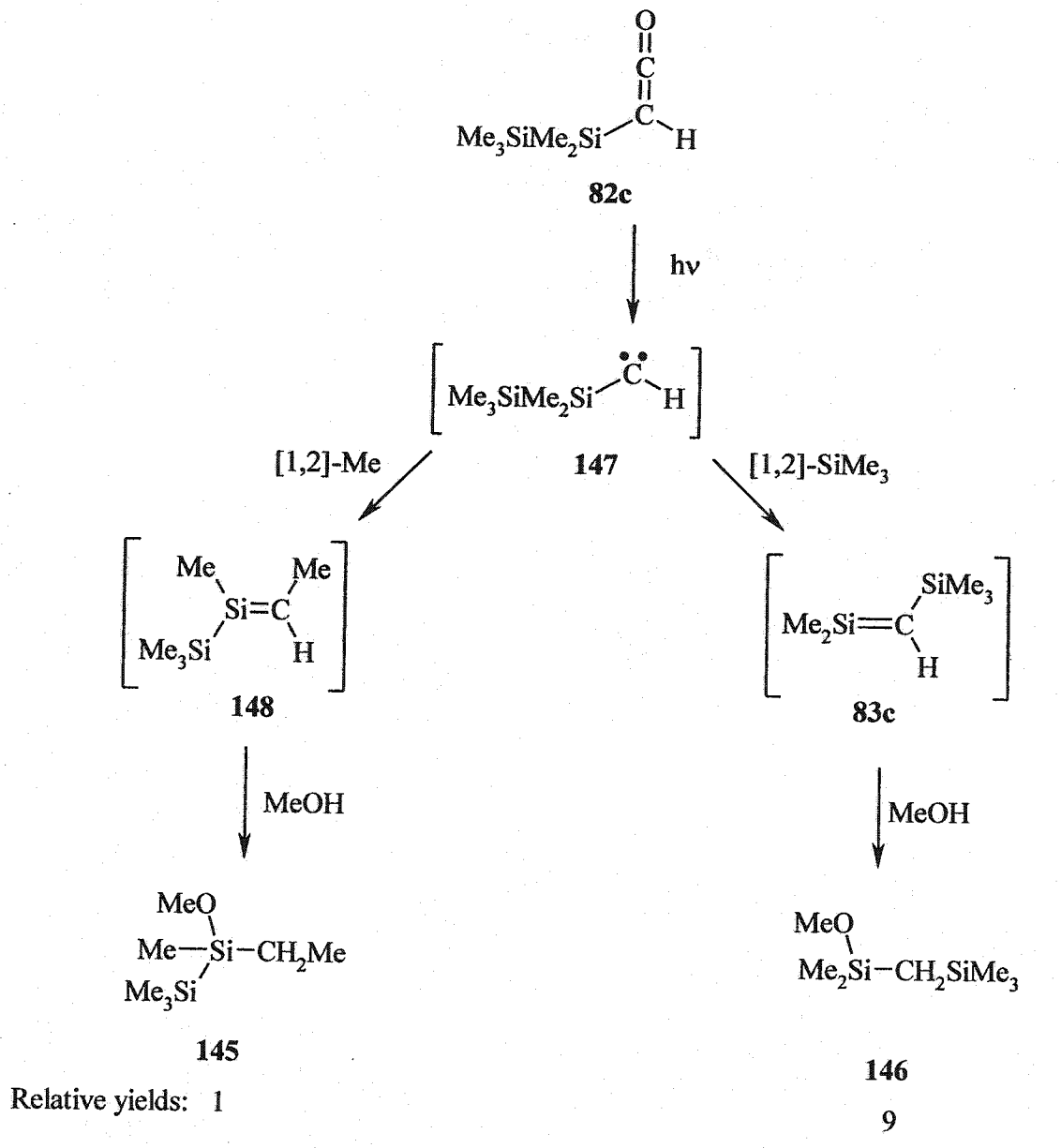

3.2.3 Steady-State Photolysis of 88a and 88b in Hexane Solution

Direct irradiation (254 nm) of **88a** as a deoxygenated solution (0.024 M) in hexane containing methanol (0.15 M), led to the formation of four products in a ratio of 79.6:8.7:7.9:4.5, as determined by ^{1}H NMR of the crude reaction mixture. No other products could be detected by this method between 5 and 90% conversion of the starting material. All four products were also detected by GC/MS, but only two were detected on two other capillary columns in GC/ FID analyses. The dominant peaks in the ^{1}H NMR spectrum and the mass spectrum of the major component are consistent with its assignment to methoxysilane $\mathbf{144_{Me}}$. The mass spectra of the three minor products indicate that they are isomers of the major product. Direct irradiation of a deoxygenated solution (0.002 M) of **88b** in hexane containing methanol (0.2 M) with the light from a Zn resonance lamp (214 nm) led to the formation of the same four products in similar relative yields.

Conclusive identification of the three minor isomers is more difficult. In an attempt to isolate the three minor products from the photolysate, a preparative scale photolysis of **88a** was carried out (250 mg in 25 mL in the presence of 0.2 M methanol) to ca. 95% conversion of the starting material. Semi-preparative gas chromatography was used to isolate two different mixtures of the four products that were then analyzed by ^{1}H NMR spectroscopy. The minor products were tentatively identified as $\mathbf{149_{Me}}$, $\mathbf{150_{Me}}$ and $\mathbf{151_{Me}}$ (equation 3.4) on the basis of their mass (Figure 3.4a-d) and 500 MHz ^{1}H NMR spectra (Figure 3.5a,b). The assignment of the absolute stereochemistry in $\mathbf{149_{Me}}$ and $\mathbf{150_{Me}}$ is arbitrary. Evidence for the formation of isomers $\mathbf{149_{Me}}$-$\mathbf{151_{Me}}$ relies on the

observation of three additional methoxy singlets at δ 3.405, 3.412, and 3.429 ppm and in the three sets of doublets at δ 0.978, 1.105 and 1.043 ppm (J ~ 9 Hz). Comparison of the two spectra leads to the conclusion that the 3.429, 3.412 and 3.405 ppm peaks correspond to the doublets at 1.105, 0.978 and 1.043 ppm, respectively. The SiCH region of the spectrum (0.2 – 0.5 ppm) was exceptionally complex. However, a one-proton quartet attributed to one of the minor isomers could be picked out in the spectrum of the mixture that had been enriched in the minor products (Figure 3.5b).

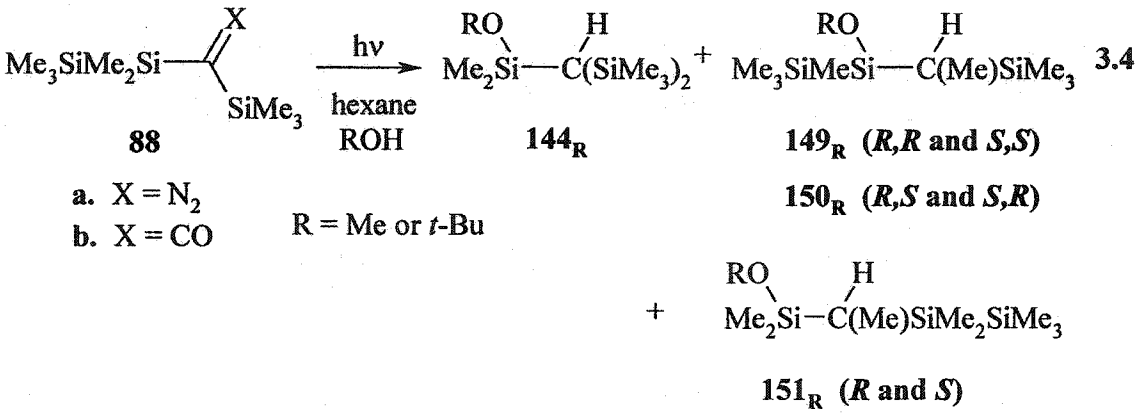

88

a. X = N_2

b. X = CO

R = Me or *t*-Bu

144$_R$

149$_R$ (***R,R*** **and** ***S,S***)

150$_R$ (***R,S*** **and** ***S,R***)

151$_R$ (***R*** **and** ***S***)

3.4

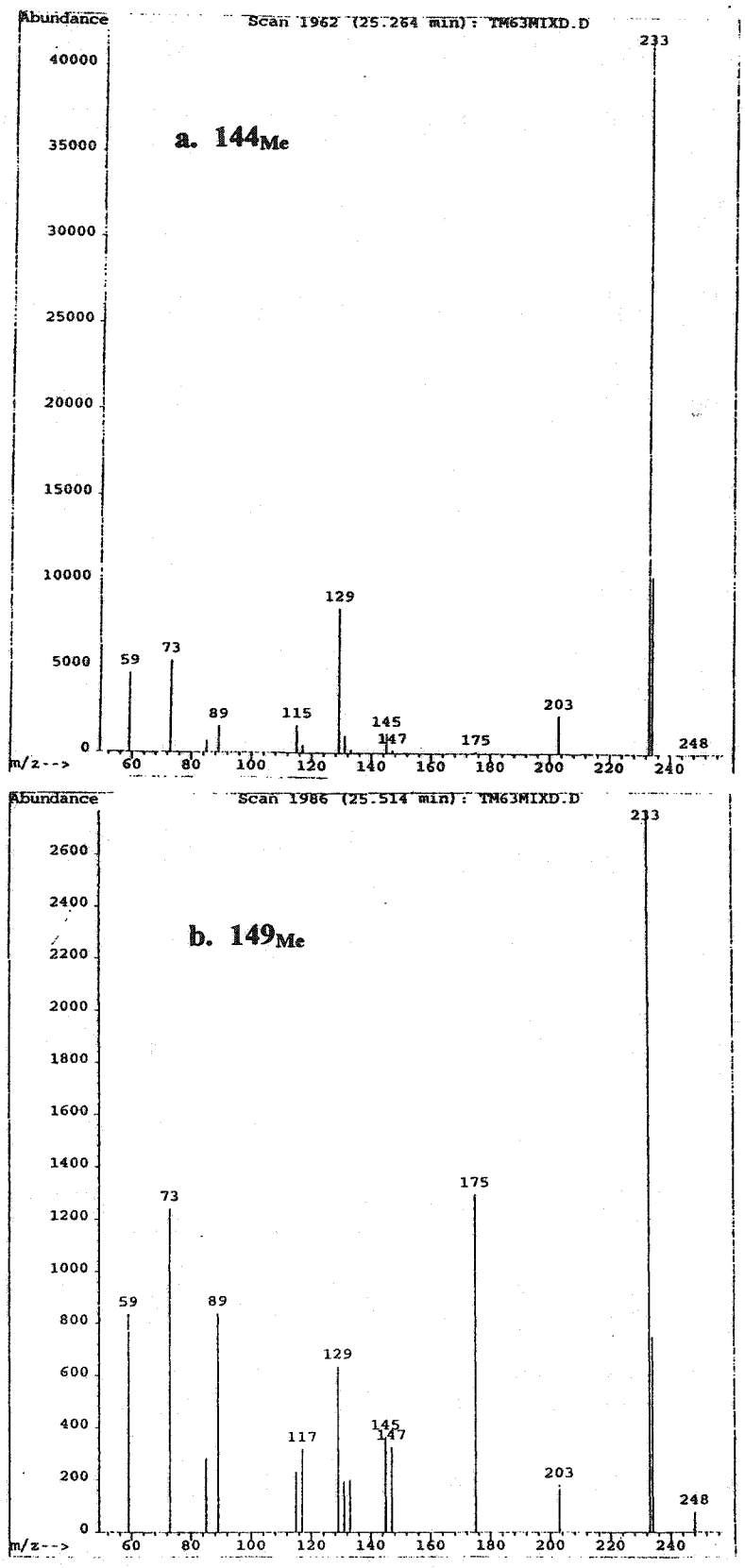

Figure 3.4 Mass spectra of methoxysilane isomers a) 144_{Me} and b) 149_{Me}.

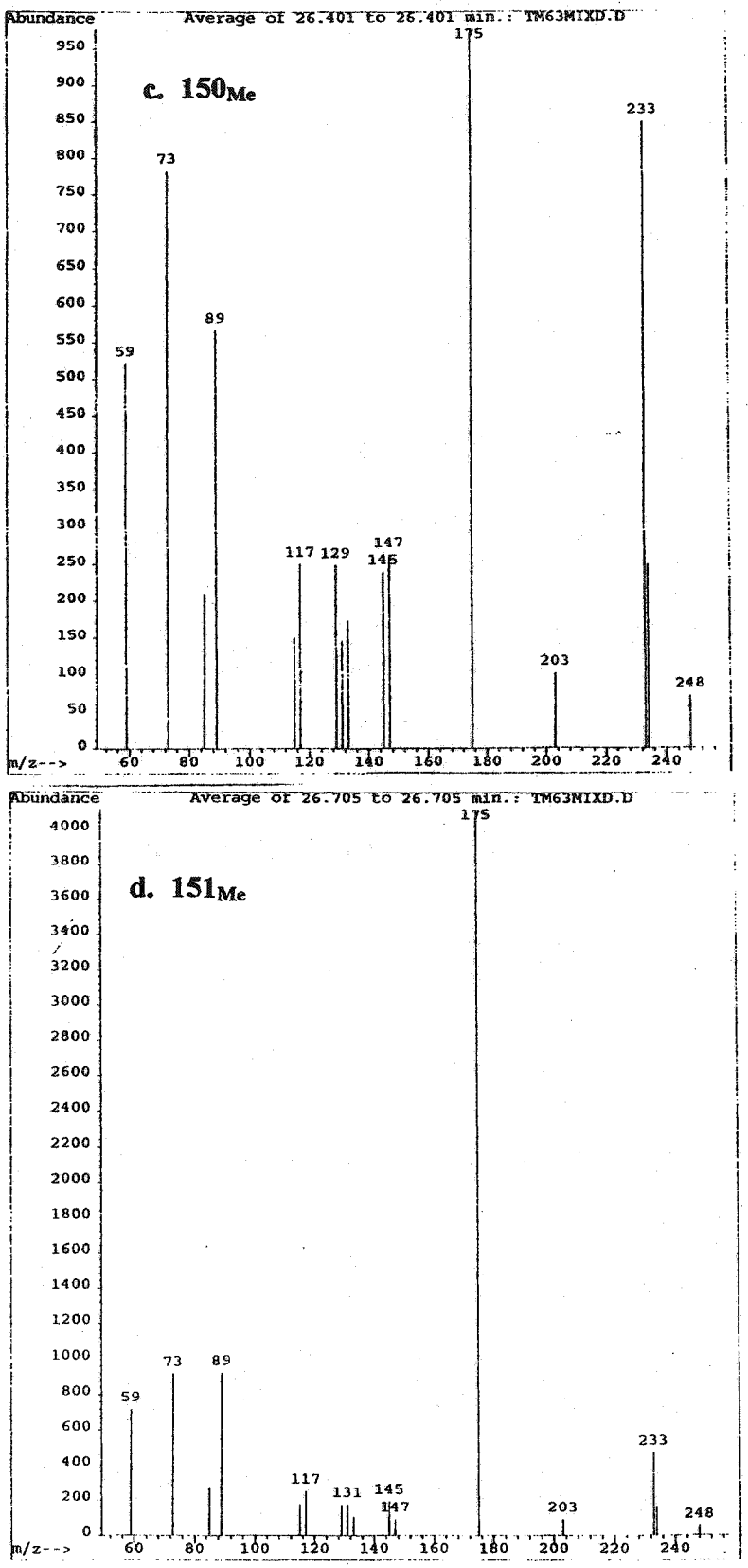

Figure 3.4 Mass spectra of methoxysilane isomers c) 150_{Me} d) 151_{Me}.

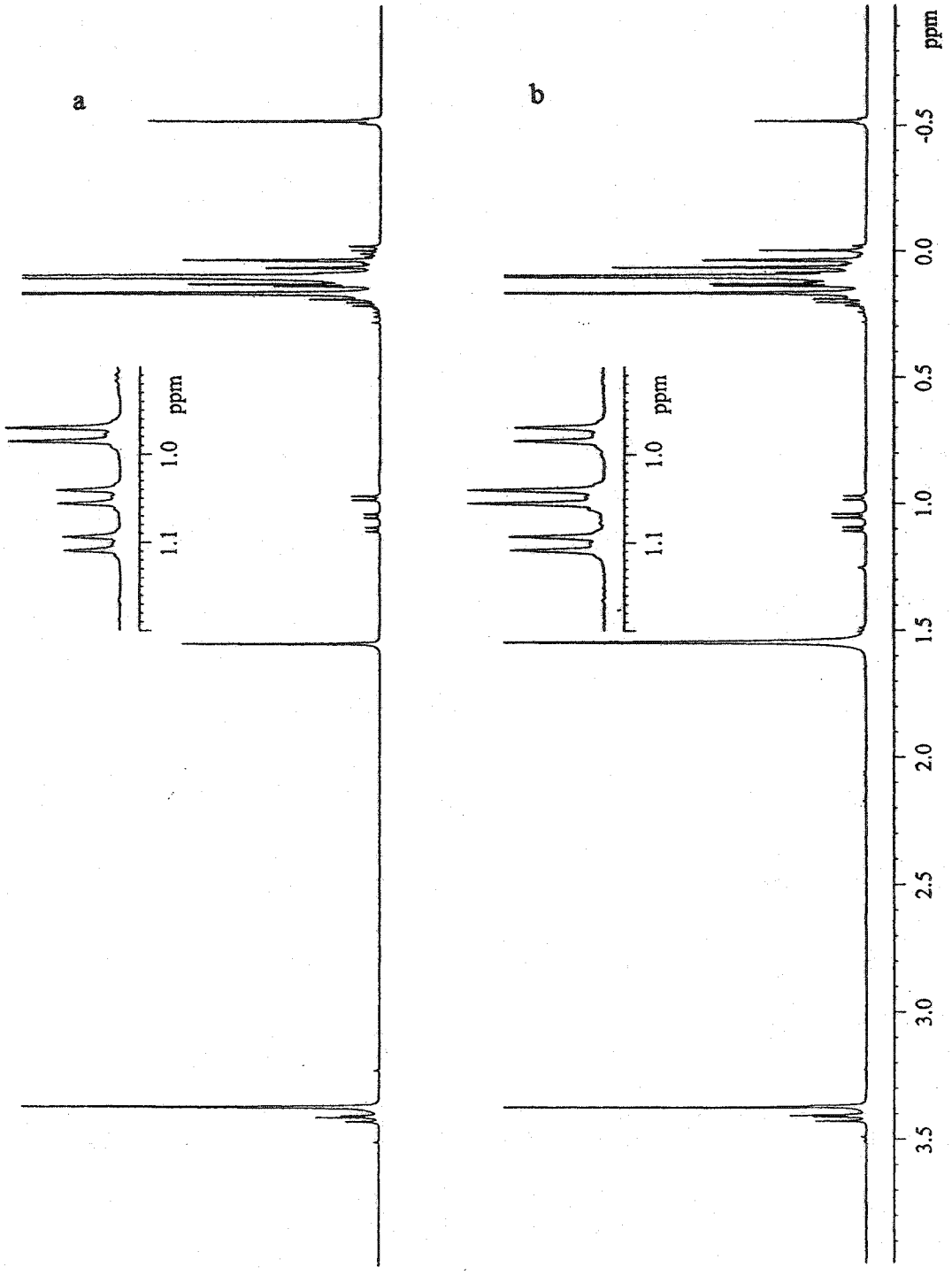

Figure 3.5 a) ^{1}H NMR spectrum of the product mixture from the photolysis of **88a** (0.01 M) in the presence of methanol (0.2 M) purified by semi-preparative gas chromatography. b) ^{1}H NMR spectrum of the same photolysis mixture, enriched in isomers $\mathbf{149_{Me}}$ – $\mathbf{151_{Me}}$ as compared to $\mathbf{144_{Me}}$ by semi-preparative gas chromatography.

The product yields determined from the ^{1}H NMR spectrum of the crude photolysis mixture compared favourably with the yields determined by GC/MS analysis. Thus, the mass spectra of the various products were tentatively matched with the resonances of the ^{1}H NMR spectra. Table 3.2 lists the retention times from the GC/MS analysis (Figure 3.4), accompanied by their corresponding integrations. The product formed in 8.7 % yield (8.9% by NMR) was assigned to $\mathbf{151_{Me}}$ on the basis of its stronger $M^{+\bullet}$-73 peak compared to those in the mass spectra of the other three products.

Table 3.2 GC/MS and ^{1}H NMR Yields for Methoxysilanes $\mathbf{144_{Me}}$, $\mathbf{149_{Me}}$-$\mathbf{151_{Me}}$

Ret. Time / min.	GC/MS Yield / %	NMR Yield / %	δ / ppm (s, OCH_3)	δ / ppm (d, CH-Me)	Tentative Assignment
25.273	79.6	77.8	3.371	N/A	$\mathbf{144_{Me}}$
25.510	7.9	7.6	3.429	1.105	$\mathbf{149_{Me}}$
26.421	4.5	5.8	3.412	0.978	$\mathbf{150_{Me}}$
26.714	8.7	8.9	3.405	1.043	$\mathbf{151_{Me}}$

While four distinct products could be detected readily from the photolysis of **88a** in the presence of methanol, detecting the analogous four products when *t*-butyl alcohol was used as the trap was far more difficult. The ^{1}H NMR spectrum of the photolysis mixture of **88a** (0.024 M) in the presence of *t*-BuOH (0.15 M) in cyclohexane-d_{12} consisted of prominent resonances assignable to $\mathbf{144_{Bu}}$, and numerous weak, poorly

resolved resonances in the 0 – 1 ppm region. However, when this same reaction mixture was analyzed by GC/MS, three isomeric products were observed in a ratio of 83.5:8.5:8.0. These were identified as **144$_{Bu}$**, **149$_{Bu}$** and **150$_{Bu}$** on the basis of their identical molecular weights and the fact that the mass spectra of the two minor isomers were similar to one another. Presumably the fourth isomer (**151$_{Bu}$**) coeluted with **144$_{Bu}$**.

Alkoxysilanes **144$_{Me}$** and **144$_{Bu}$** are the products of alcohol trapping of silene **11a**, which formally results from [1,2]-migration of the trimethylsilyl group in silylcarbene **143** (Scheme 3.2). The three minor products are proposed to result from trapping of *E*- and/or *Z*-1,2-dimethyl-1,2-bis(trimethylsilyl)silene (***E/Z*-152**) and 1,1,2-trimethyl-2-pentamethyldisilanylsilene (**153**), formed by [1,2]-migration of any of the methyl groups at the β-position of carbene **143**, respectively. Although these isomers have not been previously reported, their observation is not surprising. The photolysis of pentamethyldisilanylketene (**82c**) in the presence of methanol led to the formation of isomeric methoxysilanes **146** and **145** in a 9:1 product ratio (Scheme 3.1).[102] If the relative yields of the four products formed are statistically corrected for the number of methyl groups, the relative migratory aptitudes are 30:2.25:1 for the β-trimethylsilyl group, the -$SiMe_2$- methyl groups and the -$SiMe_3$ methyl groups, respectively.

Scheme 3.2 **Silene Trapping in the Photolysis of (Pentamethyldisilanyl)-(trimethylsilyl)diazomethane (88a) and –ketene (88b)**

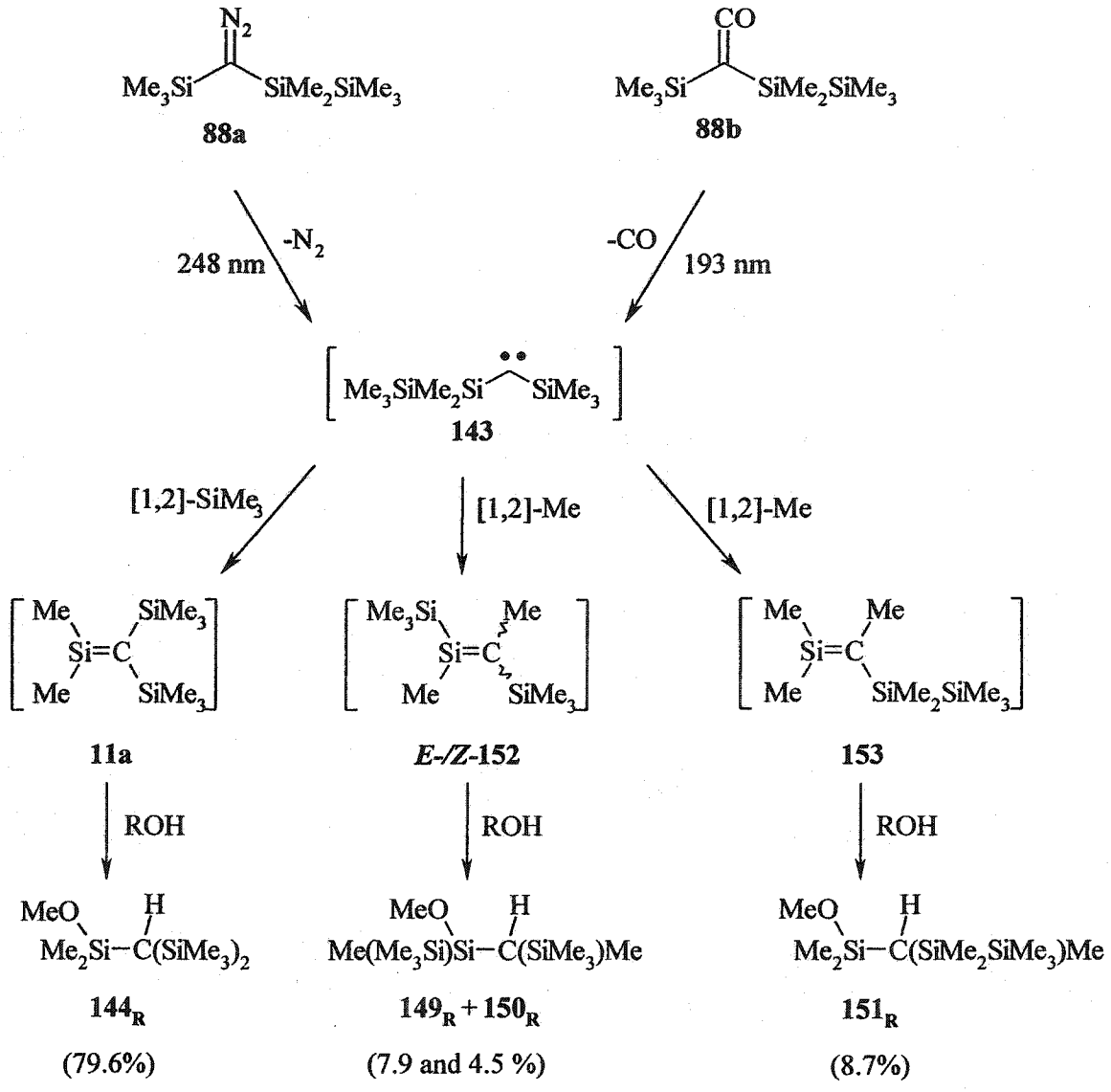

3.2.4 The Effect of Silicon Substituents on the Rate Constants for Methanol Addition to Silenes

Product studies indicate the formation of three minor silene addition products that could potentially be assigned to the transient absorption at 310 nm. A systematic review of the effects that groups at silicon have on the kinetic behaviour and absorption spectra of silenes is necessary in order to assess which silene (***E*-/*Z*-152** or **153**) could be responsible for the 310-nm absorption. A number of trimethylsilyl-substituted silenes, along with their absorption maxima and k_{MeOH} values, are summarized in Table 3.3. The value of k_{MeOH} determined for **11a** (1.3×10^{10} M^{-1} s^{-1}) is consistent with those reported previously for 1,1-dimethylsilene (**7a**, $k_{MeOH} = 4.9 \times 10^9$ M^{-1} s^{-1})[138] and 1,1-dimethyl-2-trimethylsilylsilene (**83c**, $k_{MeOH} = 8.5 \times 10^9$ M^{-1} s^{-1}).[102] If one of the methyl groups of **7a** is replaced with a trimethylsilyl group, as in 1-methyl-1-trimethylsilylsilene (**81h**, $k_{MeOH} = 1.8 \times 10^8$ M^{-1} s^{-1}), the reactivity is reduced ~25-fold. The same 25-fold decrease can be applied to k_{MeOH} for 1,1,2-trimethyl-2-trimethylsilylsilene (**83b**, $k_{MeOH} = 1.8 \times 10^9$ M^{-1} s^{-1}) to estimate k_{MeOH} for ***E*/*Z*-152**. This treatment leads to a predicted value of $k_{MeOH} \sim 7 \times 10^7$ M^{-1} s^{-1}, which is very close to k_{MeOH} for the transient at 310 nm. Similarly, the 30-nm red-shift in λ_{max} for **81h** compared to **7a** leads one to expect $\lambda_{max} \sim 310$ nm for ***E*/*Z*-152**, since **83b** has $\lambda_{max} = 280$ nm.

Table 3.3 Absolute Rate Constants for Reaction of TMS-Substituted Silenes with Methanol in Hexane Solution at 23°C

No.	Silene	λ_{max} / nm	k_{MeOH} / 10^9 M^{-1} s^{-1}	Ref.
81h	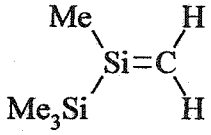	285	0.18±0.2	104
7a	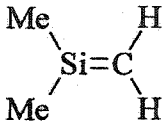	255	4.9±0.3	138
83c	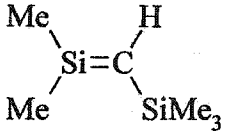	270	8.5±0.6	102
11a	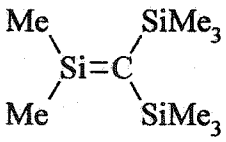	260	13±2	*a*
83a	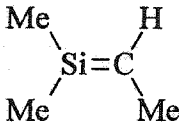	260	0.18±0.04	102
83b	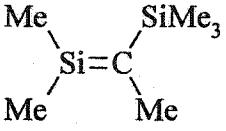	280	1.8±0.1	102
***E/Z*-152**	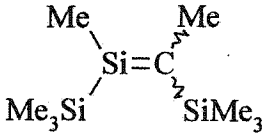	310*	0.07[b] 0.049±0.008	*a*
153	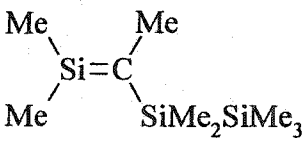	310*	0.07[b]	*a*

a. this work. *b*. predicted values based on established trends (see text).

Although these trends seem to support the assignment of the 310-nm transient to ***E/Z*-152**, it is not possible to rule out that the 310-nm species might be attributed to **153**. The pentamethyldisilanyl group has been shown to be a hyperconjugative π-donor in arenes and alkenes.[197-199] The data of Table 3.4 include absorption maxima and ionization potentials of ethylene (**103**), benzene (**154**), pentamethylvinyldisilane (**21**) and pentamethylphenyldisilane (**23**). The red-shift in the absorption maximum of **21** compared to that of ethylene illustrates that a disilyl group attached to the double bond can donate electron density via hyperconjugation.[200] This trend would lead one to predict that the absorption maximum of **153** should be significantly red-shifted and k_{MeOH} should be smaller compared to 1,1,2-trimethylsilene (**83a**; λ_{max} = 260 nm; $k_{MeOH} = 1.8 \times 10^8$ M^{-1} s^{-1}). A similar red-shift is observed in **21** relative to benzene, and the lower ionization potential supports the electron releasing ability of the disilyl group. Unfortunately, the σ_{R° value for the $-SiMe_2SiMe_3$ group is unknown, so there is no way of predicting its effect on the kinetics of silenes by interpolating k_{MeOH} from Figure 1.7. Futhermore, the extinction coefficients for ***E/Z*-152** and **153** are unknown, so it is impossible to predict which silene is responsible for the absorption at 310 nm on the basis of product yields.

Table 3.4 Absorption Maxima and Ionization Potentials for Ethylene (103), Benzene (154), Pentamethylvinyldisilane (21) and Pentamethylphenyldisilane (23)

No.	Compound	λ_{max} / nm	E_{IP} / eV
103	$H_2C{=}CH_2$	<140 [a]	10.5 [b]
21	$H_2C{=}CHSiMe_2SiMe_3$	223 [c]	8.56 [d]
154	C_6H_6	200 [e]	9.24 [f]
23	$C_6H_5SiMe_2SiMe_3$	231 [g]	8.35 [h]

a. Ref. 201. *b*. Ref. 202. *c*. Ref. 11. *d*. Ref. 203. *e*. Ref. 204. *f*. Ref. 205. *g*. Ref. 206. *h*. Ref. 200.

3.2.5 Comparison of k_{MeOH} of 11a to Those of Other 1,1-Dimethylsilenes

The rate constant for the addition of methanol to Wiberg's transient silene (**11a**) indicates that it is the most electrophilic silene studied to date.[117] As shown in the preceeding section, its reactivity can be rationalized by comparing its value for k_{MeOH} with those of **7a** and **83c**. In this section we examine how well k_{MeOH} fits with those of other carbon-substituted 1,1-dimethylsilenes that have been reported (recall Figure 1.7).[102] The original work showed a linear relationship between log k_{MeOH} and σ_{R° (ρ_{R° = +8.0±2.2; r^2 = 0.909). Addition of k_{MeOH} for **11a** to the plot (Figure 3.6a), does not improve this correlation, but accentuates the curvature that appears to be defined by the more reactive members of the series. Such curvature is expected as reactivity approaches

the diffusion-controlled limit.[207] Diffusional effects are expected to truncate the reactivity of any derivatives exhibiting absolute rate constants above $k_{MeOH} \sim 5x10^9$ M^{-1} s^{-1}, so it becomes particularly important to account for the effect of diffusion if the data for **11a** are going to be added to the plot.

For very fast reactions, the steps of equation 3.5 must be considered, where k_{diff} and k_{-diff} are diffusion of the silene and methanol together and apart, respectively. Once the two species are in the solvent cage, unimolecular reaction occurs (k_r) to yield the reaction products.

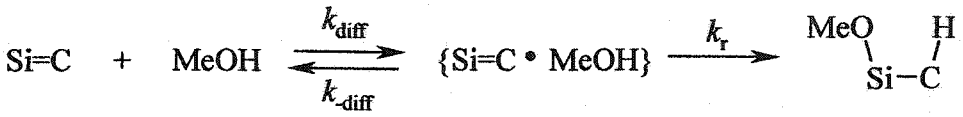

3.5

Using the steady-state approximation for the solvent cage species, the rate expression becomes that of equation 3.6. Substitution of this expression into equation 3.7 for the experimentally observable rate constant (k_{MeOH}), results in equation 3.8, where k_{corr} is the rate constant for methanol addition to a silene that has been corrected for the effects of diffusion. By rearranging equation 3.8, equation 3.9 is obtained, relating the experimentally determined rate constant for methanol addition (k_{MeOH}) to k_{corr}.

$$\nu = \frac{k_{diff} \bullet k_r}{k_{-diff} + k_r} [Si{=}C] [MeOH] \qquad \textbf{3.6}$$

$$\nu = k_{MeOH} [Si{=}C] [MeOH] \qquad \textbf{3.7}$$

$$\frac{1}{k_{MeOH}} = \frac{1}{k_{diff}} + \frac{k_{-diff}}{k_{diff} \bullet k_r} = \frac{1}{k_{diff}} + \frac{1}{k_{corr}} \qquad \textbf{3.8}$$

$$k_{corr} = \frac{k_{diff} \bullet k_{MeOH}}{k_{diff} - k_{MeOH}} \qquad \textbf{3.9}$$

The value of $k_{diff} = 2.4 \times 10^{10}$ M^{-1} s^{-1} in hexane at 25°C, is obtained from the standard Debye equation (equation 3.10),[208] using the published viscosity value for η at 25°C.[209]

$$k_{diff} = \frac{8RT}{3000\eta} \qquad \textbf{3.10}$$

When equation 3.9 is applied to all the observed rate constants of Figure 3.6a, the linear correlation is improved significantly (Figure 3.6b, $r^2 = 0.937$), yielding $\rho_{R^\circ} = +8.1 \pm 1.6$. The large positive ρ_{R° reinforces what theory predicts[103]: that π–donors at carbon decrease the reactivity of silenes towards nucleophiles, a trend that is fully consistent with the kinetic stability of Brook's silene **29**.[67,69]

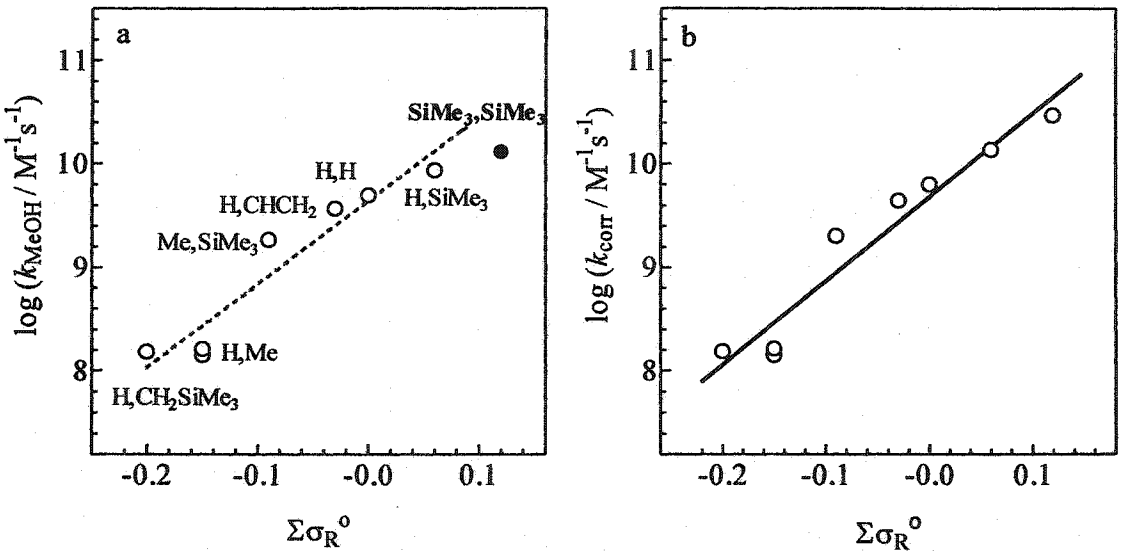

Figure 3.6 a) Rate constants for reaction of C-substituted 1,1-dimethylsilenes with methanol in hexane at 24°C vs. the resonance substituent parameter ($\Sigma\sigma_{R^o}$), showing the original correlation with **11a** added to the plot. b) Corrected rate constants (k_{corr}, see equation 3.9) versus the resonance substituent parameter $\Sigma\sigma_{R^o}$.

The addition of **11a** to the substituent plots of Figure 3.6 supports the validity of the linear free energy relationship approach to rationalizing silene reactivity. Ultimately, it can be concluded that the stable analogue of **11a**, Wiberg's silene **60**, is kinetically stable to dimerization solely due to the steric stabilization afforded by the –SiMe(*t*-Bu)$_2$ substituent.[137,210]

3.2.6 Comparison of Absolute and Relative Reactivities of Various Nucleophiles with Wiberg's Transient Silene

Rate constants were also measured for addition of a number of other nucleophiles to **11a** and ***E/Z*-152(153)**, such as acetic acid (AcOH), isopropanol (*i*-PrOH), cyclohexanol (*c*-HxOH), *tert*-buylamine (*t*-$BuNH_2$) and *tert*-butyl alcohol (*t*-BuOH). All plots of $k_{decay} - k_0$ vs. [Nu] for **11a** were linear, as shown in Figure 3.7a. Rate constants were calculated by least-squares analysis of data (6-10 points) that spanned at least a factor of five in k_{decay}. In contrast, all plots of $k_{decay} - k_0$ vs. [Nu] for ***E/Z*-152(153)** were curved, as shown in Figure 3.7b. The exception to this is acetic acid (not shown in Figure 3.7b), which shows a linear relationship. This is consistent with the kinetic behaviour of other silenes with acidic nucleophiles.[83] Rate constants were calculated by non-linear least squares fitting of the data (15-20 points) to equation 1.23. Table 3.5 lists the absolute rate constants obtained from these experiments, along with the relative rate data of Wiberg that were determined in diethyl ether at 100°C. The absolute data determined in hexane at 25°C have been calibrated to *t*-BuOH for comparison to the relative data of Wiberg.

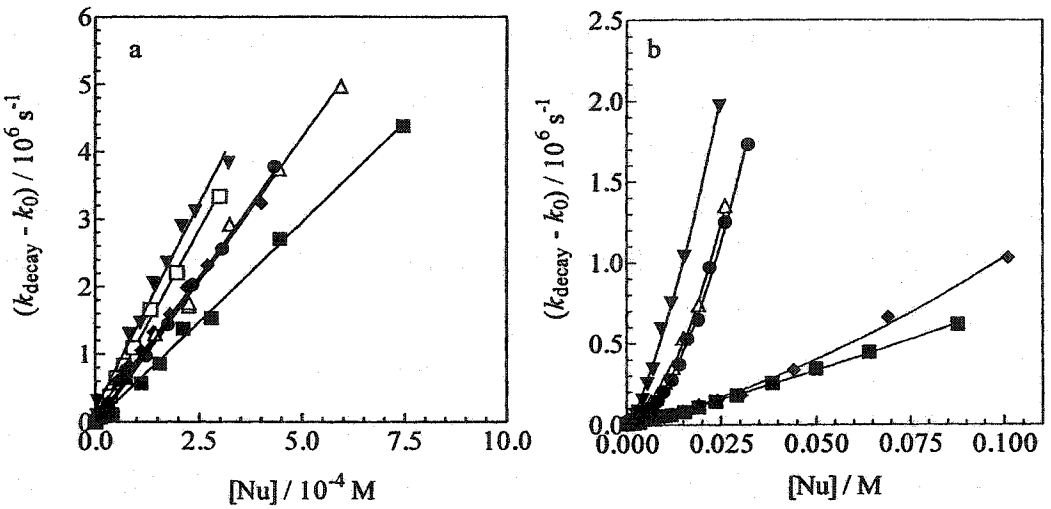

Figure 3.7 Plots of $k_{decay} - k_0$ vs. [Nu] for the addition of acetic acid (□), methanol (▼), isopropanol (●), cyclohexanol (△), *t*-butylamine (◆) and *t*-butyl alcohol (■) to a) **11a,** monitored at 280 nm and b) ***E/Z*-152(153),** monitored at 310 nm in hexane solution at 24°C.

Table 3.5 **Absolute Rate Constants (k_{Nu}) in Hexane Solution at 25°C for 11a and *E/Z*-152(153) and Relative Rate Constants (k_{rel}; relative to *t*-BuOH) in Diethyl Ether at 100°C for reaction of 11a with Nucleophiles**

	11a		*E-/Z*-153(154)	
Nu	Wiberg k_{rel} [a]	k_{Nu} [b] / 10^9 M^{-1} s^{-1}	k_{Nu} [b] / 10^7 M^{-1} s^{-1}	k_{2Nu} [b] / 10^7 M^{-2} s^{-1}
	(k_{Nu} / $k_{t\text{-BuOH}}$)	(k_{Nu} / $k_{t\text{-BuOH}}$)	(k_{Nu} / $k_{t\text{-BuOH}}$)	
MeOH	10,500	13±2	4.9±0.8	130±20
	(3.1)	(2.2±0.2)	(7.8±1.9)	
AcOH	8,500	12±4	620±40	*c*
	(2.5)	(2.0±0.4)	(984±10)	
i-PrOH	5000	8.3±0.3	1.0±0.4	140±20
	(1.5)	(1.4±0.3)	(1.6±0.3)	
c-HxOH	380	8.4±0.3	0.85±0.30	160±10
	(0.11)	(1.4±0.3)	(1.3±0.2)	
t-BuNH$_2$	5,500	8.0±0.4	0.60±0.08	4.4±0.8
	(1.6)	(1.3±0.3)	(0.9±0.2)	
t-BuOH	3,400	5.9±0.2	0.63±0.06	1.1±0.3
	(1)	(1)	(1)	

a. Ref. 30. Obtained from product ratios in competition experiments between the nucleophile and 2,3-dimethyl-butadiene in diethyl ether at 100°C. *b*. In hexane at 24°C. c. Linear dependence of k_{decay} on [AcOH].

The rate ratios measured by Wiberg in diethyl ether at 100°C generally agree quite well with the corresponding absolute rate ratios calculated from the data obtained in hexane at 24°C. The only significant discrepancy is in the relative rate constants for cyclohexanol quenching, where that from the direct measurement is ca.10 times higher than that reported by Wiberg et al. on the basis of product studies. A secondary measurement of the absolute rate ratio was carried out using steady-state competition experiments, in which a 0.3 M solution of **88a** in hexane containing 1.4 M each of *t*-BuOH and *c*-HxOH was photolyzed with 254-nm light. This gave rise to two major products which were tentatively identified as $\mathbf{144_{Bu}}$ and $\mathbf{144_{cHx}}$ by GC/MS, in the ratio $\mathbf{144_{cHx}}$:$\mathbf{144_{Bu}}$ = 1.9±0.3. The $\mathbf{144_{cHx}}$:$\mathbf{144_{Bu}}$ ratio agrees within experimental error with the value calculated from the absolute rate constants ($k_{MeOH}/k_{t\text{-}BuOH}$ = 1.4±0.3).

The good agreement between the relative rate data of Wiberg (in diethyl ether at 100°C) and the absolute data of this work (in hexane at 25°C) is somewhat surprising, considering the differences in solvent and temperature between the two sets of experiments. Ether solvents are known to reduce the reactivity of transient silenes considerably, and also alter their relative reactivities toward nucleophilic reagents.[211] In fact, this may be the explanation for the poor agreement between the two sets of data for cyclohexanol quenching of **11a**. In order to investigate the effect of ether solvents and temperature on the reactivity of **11a** in more detail, the Arrhenius parameters for reaction with methanol in hexane solution and the spectroscopic behaviour and reactivity in THF solution were studied.

3.2.7 Temperature Dependence of the Addition of Methanol to 11a

Absolute rate constants for the reaction of **11a** with MeOH were determined at several temperatures between 0 and 60°C by flash photolysis of **88a** in hexane solution. The quenching plots were linear at each temperature over a 10-fold span in k_{decay} and the rate constants are summarized in Table 3.6. The resulting Arrhenius plot is shown in Figure 3.8. The Arrhenius plot for diffusion in hexane is also included in the plot, calculated using the standard Debye equation (equation 3.10) and values of η from published temperature-viscosity data.[209]

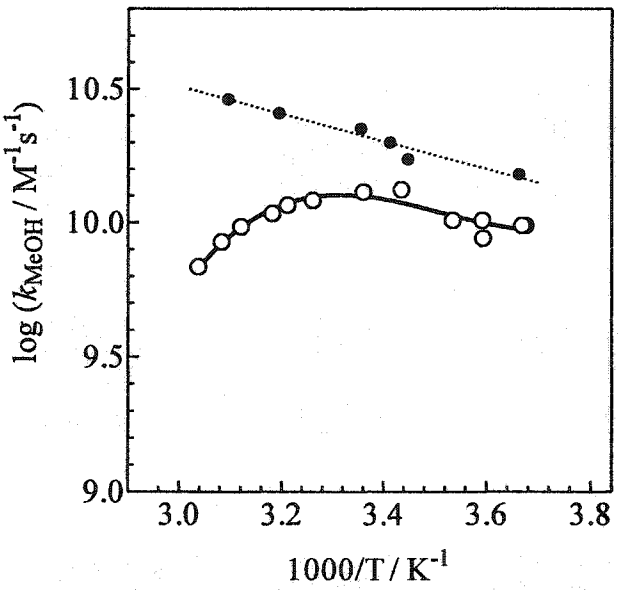

Figure 3.8 Arrhenius plot for the addition of methanol to **11a** in hexane solution (○). The dashed line (●) is the Arrhenius plot for diffusion in hexane solution.

Table 3.6 **Rate Constants for Methanol Addition (k_{MeOH}) to 11a in Hexane Solution at Various Temperatures**

Temperature / °C	k_{MeOH} / 10^9 M^{-1} s^{-1}
-0.4	9.7±0.3
-0.9	9.8±0.4
5.2	8.7±0.3
5.4	10.0±0.4
9.8	10.2±0.3
18.1	13.1±0.2
24.6	13.0±0.2
33.7	12.1±0.2
38.4	11.0±0.4
41.3	10.8±0.3
47.4	9.7±0.4
51.3	8.5±0.4
56.2	6.8±0.4

The rate constants for the addition of methanol to silene **11a** exhibit a pronounced non-linear dependence on temperature, consistent with the two-step mechanism for silene-alcohol additions discussed earlier (section 1.3.2.2). The apex of the bell (24°C) represents the point where $k_{-C} \sim k_H$ and therefore $k_H/(k_{-C} + k_H) = 0.5$.[102] Hence, k_{MeOH} =

½k_C at this temperature. Using k_{MeOH} = (1.3±0.2)x10^{10} M^{-1} s^{-1}, the value of k_C is calculated to be (2.6±0.4)x10^{10} M^{-1} s^{-1}, which is identical to the rate constant for diffusion in hexane at this temperature (k_{diff} = 2.4 x10^{10} M^{-1} s^{-1}). From these calculations, it can be concluded that complexation between methanol and **11a** is fully diffusion-controlled (ie. $k_C = k_{diff}$).

The rate constant for addition of MeOD to **11a** (k_{MeOD} = (1.2±0.3)x10^{10} M^{-1} s^{-1}) led to k_H/k_D = 1.0±0.1 in hexane at 24°C. The negligible isotope effect suggests that proton transfer is not rate-limiting for **11a**, as it is for the addition of methanol to many other silenes.[25] The bell shaped plot and the discussion of negative activation energies of chapter 1 (Figures 1.4 and 1.5) holds for silenes that do not react at the diffusion-controlled limit (ie. $k_C < k_{diff}$). However, the effects of diffusion play a significant role in the reaction of **11a**. Another way to interpret the temperature dependence shown in Figure 3.8 is to consider the rate determining step to be diffusion itself (k_{diff}), and the apex of the bell is the point where the rate constant for diffusion apart of **11a** and MeOH is equal to the rate constant for reaction within the solvent cage ($k_{-diff} \sim k_r$, equation 3.5).

At temperatures greater than 24°C, the overall activation energy is negative, indicating that k_{-diff} is larger than k_r in this temperature range. The pronounced curvature in this part of the plot suggests that there is a large entropic barrier ($\Delta S^{\neq}$) to reaction within the solvent cage. It is possible that the mechanism for methanol addition to silene **11a** within the solvent cage could be different from the stepwise process shown in Scheme 1.5, but the effects of diffusion make it difficult to discern any differences from the standard mechanism.

3.2.8 Nanosecond Laser Flash Photolysis of 88a in THF Solution at 24°C

Laser flash photolysis of **88a** in deoxygenated THF led to a transient absorption spectrum that was somewhat different from that in hexane solution (Figure 3.1). Like the spectrum in hexane, irreversible bleaching of the precursor does not allow monitoring of the absorption spectrum at wavelengths lower than 270 nm. Due to this limitation, any spectral shifts in THF as compared to hexane are masked. Unfortunately, flash photolysis of the ketene at 193 nm is not viable because THF has a significant absorption at the excitation wavelength.[212] The observed transients thus cannot be clearly defined into separate bands, but monitoring the absorption at 290 nm and 320 nm gave rise to different decay kinetics. Transient decays obtained at 290 nm exhibited mixed first- and second-order kinetics and a first-order lifetime of ~30 μs (Figure 3.9a). On the other hand, monitoring at 320 nm resulted in decay kinetics that were clean pseudo-first order and exhibited a lifetime of ~5 μs (Figure 3.9b). The trend in alcohol quenching was similar to that observed in hexane: the rate of decay of the long-wavelength silene showed a quadratic dependence on methanol concentration, while the shorter-wavelength silene showed a linear dependence (Figure 3.10). The values for k_{MeOH} observed for the two silenes are significantly smaller in THF than in hexane solution at ambient temperature (Table 3.7).

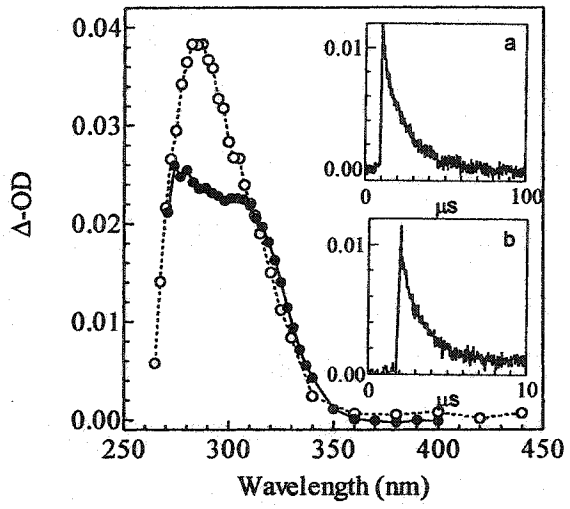

Figure 3.9 Transient UV absorption spectra from 248-nm laser flash photolysis of **88a** in deoxygenated THF solution (–•–) at 24°C, recorded 2-3 μs after the laser pulse. The inserts show typical decay traces recorded at a) 290 nm and b) 320 nm. The second spectrum (--o--) is that in hexane solution from Figure 3.1a, recorded 80-100 ns after the laser pulse.

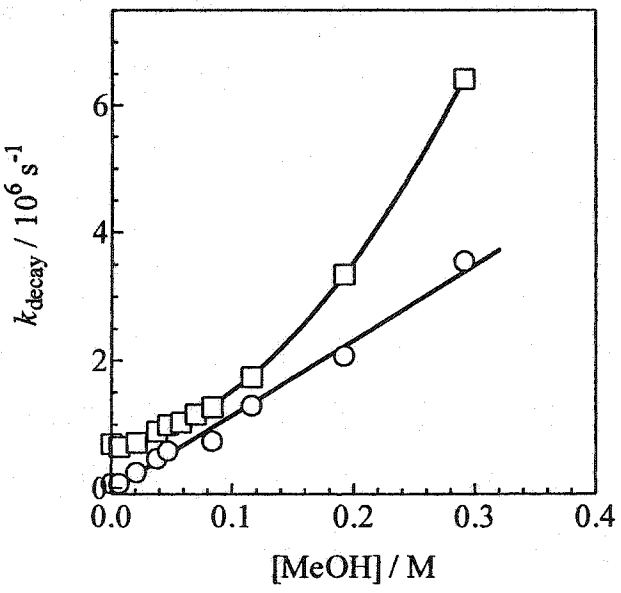

Figure 3.10 Plots of k_{decay} vs. [MeOH] for quenching of silenes absorbing at 290 nm (○) and 320 nm (□) from flash photolysis of **88a** in deoxygenated THF solution at 24°C.

Table 3.7 Absolute Rate Constants for the Addition of Methanol to Silenes 11a and *E/Z*-152(153) in Hexane and THF Solution at 24°C from Flash Photolysis of 88a

	Hexane		THF	
Transient λ / nm	280	310	290	320
Lifetime / μs	0.50 ± 0.10	15 ± 2	20 ± 2	5 ± 0.5
k_{MeOH} / 10^8 M^{-1} s^{-1}	130 ± 20	0.49 ± 0.08	0.118 ± 0.008	0.026 ± 0.004
k_{2MeOH} / 10^8 M^{-2} s^{-1}	*a*	13 ± 6	*a*	0.59 ± 0.04

a. linear correlation with [MeOH].

Recall that the transient absorption spectra determined in hexane from flash photolysis of **88b** exhibited two silenes with absorption maxima that were relatively well resolved from each other (Figure 3.2). Although this was less obvious in the flash photolysis of **88a**, **11a** could be quenched preferentially so that the spectrum of only ***E/Z*-152(153)** could be obtained (Figure 3.1b). The spectrum of Figure 3.9 does not show two separate absorption bands for the two silenes. However, the difference in the decay kinetics measured at 290 and 320 nm support the presence of two transients. In hexane, differences in maximum absorbance of the two silenes were crudely reflected in the product yields: $\mathbf{144_{Me}}$ was the major product of the photolysis and **11a** dominated the absorbance spectrum in the flash photolysis of **88a** and **88b** in hexane. The spectrum of Figure 3.9 and the decay traces of Figures 3.9a and b show that the absorbances of the two silenes are similar at the two monitoring wavelengths. In order to assign the two

silenes at 290 and 320 nm to silenes **11a** or ***E/Z*-152(153)**, our group examined the effect of THF on the UV absorption spectra and rate constants for methanol addition to two other silenes that differ significantly in electrophilicity: 1,1-diphenylsilene (**31a**) and 1,1-bis(4-trifluoromethylphenyl)silene (**31f**).[211]

At room temperature in hexane or THF, 1,1-diphenylsilene (**31a**) exhibits a relatively sharp absorption band centred at 325 nm. However, at 1.5°C, the absorption spectrum is broadened dramatically and the maximum is shifted to 350 nm. The shift in absorption is a strong indication that the silene exists mainly as its THF complex at that temperature. In contrast, at 55°C, the absorption spectrum almost exactly matches that observed in hexane at room temperature, indicating that there is less solvent complexation. The more electrophilic **31f** also has an absorption maximum at 325 nm in hexane, but in THF the spectrum is red-shifted to 375 nm at 1.5 and 25°C. At 55°C in THF, the absorption shifts back to 325 nm.[211] The transient absorption spectra indicate that the more electrophilic silene is complexing with THF, even at room temperature.

The observed trends for **31a** and **f** predict that the absorption maximum for the more electrophilic silene **11a** should be shifted to longer wavelengths in THF as compared to its maximum in hexane (λ_{max}=260 nm, as determined from flash photolysis of **88a**). Because the true absorption maximum cannot be observed in Figure 3.9 due to bleaching of the precursor, it is possible that the absorption monitored at 290 or 320 nm could be attributed to **11a**, since both monitoring wavelengths are longer than 260 nm. On the other hand, the less electrophilic silene is predicted to exhibit little or no shift in

absorption maximum in THF, which supports the tentative assignment of the 320-nm absorption to ***E/Z*-152(153).**

This tentative assignment can be supported by considering the differences in absolute rate constants for the addition of methanol in THF and hexane solutions. The rate constant for methanol addition to **31a** in THF is ~2.5 times smaller than k_{MeOH} in hexane at 24°C. The effect is even more dramatic for **31f**, where k_{MeOH} is 24 times smaller in THF as compared to hexane.[211] The observed rate constant for methanol addition (k_{MeOH}) will decrease if the silene concentration is reduced. If THF adds to the silene to form a silene–THF complex, the effective concentration of free silene available to react with methanol decreases (Scheme 3.3). If assumptions are made that the THF complex exists in rapid equilibrium with the free silene (K_{solv}) and THF does not affect any other part of the mechanism (ie. k_C, k_{-C}, and k_H are the same in THF as they are in hexane), then a new expression for k_{MeOH} can be derived using the steady-state approximation for the methanol-silene complex (equation 3.11).

Scheme 3.3 The Reaction of 1,1-Diarylsilenes with Methanol in the Presence of THF

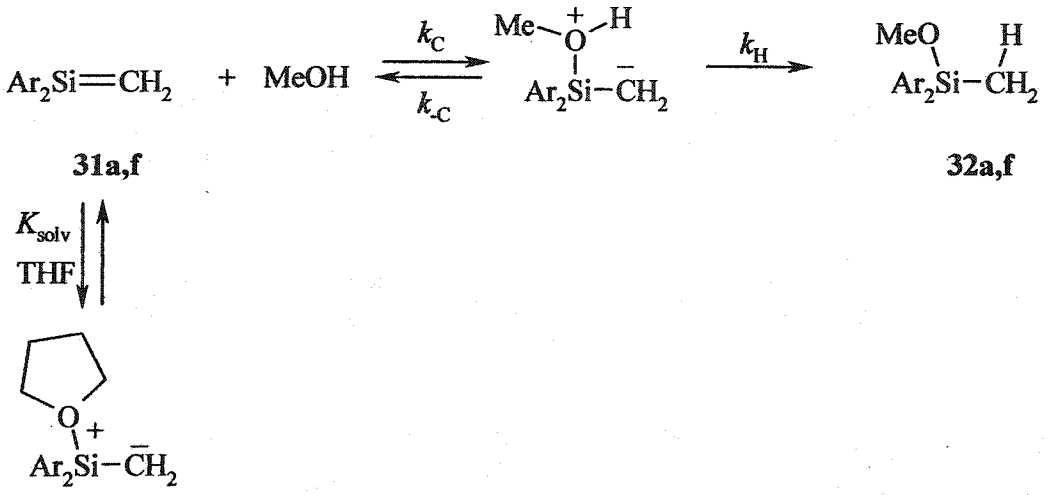

$$k_{MeOH} = \frac{1}{1 + K_{solv}[THF]} \bullet k_C \bullet \frac{k_H}{k_{-C} + k_H} \qquad 3.11$$

As the electrophilicity of the silene increases, so does the magnitude of its solvent effect. The equilibrium constant, K_{solv}, will therefore be larger for more electrophilic silenes (ie. **31f**) and a more substantial decrease will be observed in THF as compared to hexane. The larger rate constant ratio for **31f** (k_{MeOH} (hexane) / k_{MeOH} (THF) ~ 24) as compared to that for **31a** (hexane) / k_{MeOH} (THF) ~ 2.5) illustrates this point. This general treatment illustrates that an ether solvent will affect the more electrophilic silene more substantially.

The k_{MeOH} (hexane)/k_{MeOH} (THF) ratio observed for the 290- and 320-nm transients in the photolysis of **88a** are ~1300 and ~19, respectively. These rate ratios suggest that the 290-nm transient is **11a**, because its k_{MeOH} value is most significantly

affected in the presence of THF. The large ratio is consistent with the potent electrophilicity observed for **11a** in hexane. Silenes ***E/Z*-152(153)** are less electrophilic and therefore it is expected that the solvent effect would be smaller. Therefore the 320-nm transient is assigned to ***E/Z*-152(153)**.

The rate constants for the addition of nucleophiles to **11a** that were studied in hexane were also studied in THF for comparison to Wiberg's relative rate data (Table 3.8). The correlation is poor between the ratios of the absolute rate constants determined in THF at 24°C and the relative rate data for nucleophilic addition to **11a** determined by Wiberg in diethyl ether at 100°C. This is an interesting observation, considering the absolute rate data in hexane correlated well with Wiberg's relative data (Table 3.5). The poor correlation may be due to the fact that **11a** exists primarily as its THF complex at room temperature, whereas K_{solv} at 100°C in ether favours free, uncomplexed silene, so that the relative rates approach those of the uncomplexed form observed in hexane. To test this hypothesis, the effect of higher temperatures on the flash photolysis of **88a** in THF was investigated.

Table 3.8 **Absolute Rate Constants (k_{Nu}) of 11a and *E/Z*-152(153) from Flash Photolysis of 88a in THF and Relative Rate Constants for Reaction of 11a with Nucleophiles (Nu)**

	11a		*E/Z*-152(153)	
Nu	Wiberg k_{rel} [a] (k_{Nu} / $k_{t\text{-BuOH}}$)	k_{Nu} [b] / 10^6 M^{-1} s^{-1} (k_{Nu} / $k_{t\text{-BuOH}}$)	k_{Nu} [b] / 10^6 M^{-1} s^{-1} (k_{Nu} / $k_{t\text{-BuOH}}$)	k_{2Nu} [b] / 10^6 M^{-2} s^{-1}
MeOH	10,500 (3.1)	11.8±0.8 (24±2)	2.6±0.8	59±4
AcOH	8,500 (2.5)	32±2 (65±2)	54±3	linear
i-PrOH	5000 (1.5)	2.1±0.2 (4.3±0.2)	*c*	*c*
c-HxOH	380 (0.11)	2.6±0.2 (5.2±0.2)	*c*	*c*
t-BuNH$_2$	5,500 (1.6)	*c*	*c*	*c*
t-BuOH	3,400 (1)	0.49±0.04 (1)	0.30±0.01	0.45±0.01

a. from Ref. 30. Obtained from product ratios in competition experiments between the nucleophile and 2,3-dimethyl-butadiene in diethyl ether at 100°C. *b*. in THF at 24°C. *c*. not measured.

3.2.9 Nanosecond Laser Flash Photolysis of 88a in THF Solution at 55°C

Flash photolysis (248 nm) of **88a** at 55°C resulted in a similar transient absorption spectrum to that recorded at 24°C (Figure 3.11). However, the decay kinetics at 290 nm were significantly different. The absorption at 290 nm showed a two-component decay (insert of Figure 3.11), in contrast to the decay at this wavelength at room temperature. At the edge of the absorption (330 nm), mixed first- and second-order decay kinetics were observed. The irreversible bleaching of the precursor in the 230-270 nm spectral region masked significant shifts in absorption. Furthermore, the two-component decay of the 290-nm absorption made it impossible to assign the two transients conclusively. It has already been outlined earlier that silene electrophilicity and temperature play key roles in solvatochromatic shifts,[211] so specifically assigning the two components observed at 290 nm would be speculative at best. A clean source of **11a** that produces no side products with significant extinction coefficients in the 270-350 nm range is essential for sorting out which of these overlapping transients is that of Wiberg's transient silene (see Chapter 5).

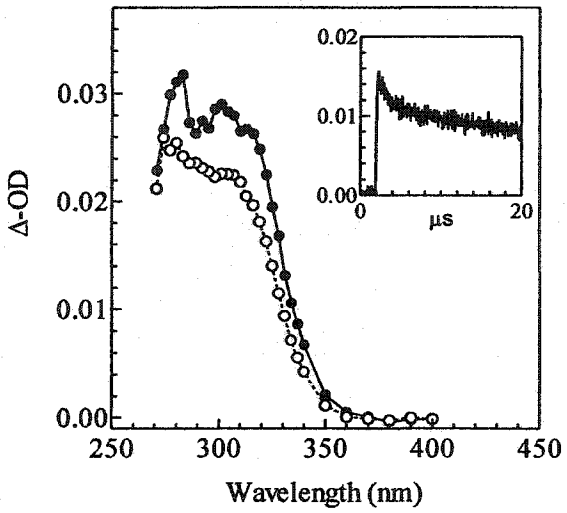

Figure 3.11 Transient UV absorption spectrum from 248-nm laser flash photolysis of **88a** in deoxygenated THF solution at 55°C (–•–), recorded 2-3 μs after the laser pulse. The insert show shows a decay trace recorded at 290 nm. The second spectrum (--o--) is that in THF solution from Figure 3.8a, recorded at 24°C.

3.3 Summary

Photolysis of (pentamethyl)(trimethylsilyl)diazomethane (**88a**) and the analogous ketene (**88b**) results in the formation of four isomeric silenes, in contrast with the original report of Ando and Sekiguchi. The major product of the photolysis is indeed Wiberg's transient silene **11a**, which is the most electrophilic silene in hexane solution studied to date. The absolute rate constant for methanol addition to **11a** correlates well with the substituent effect studies that have been carried out previously on other transient 1,1-dimethylsilenes. Furthermore, the rate constant ratios determined in hexane at 24°C for other nucleophiles compare favourably to the relative rate data determined by Wiberg in diethyl ether at 100°C.

The bell-shaped Arrhenius dependence over the temperature range studied reflects the stepwise reaction of **11a** with methanol, a mechanism that has been supported by several other studies on silene reactivity.[84]

The reactivity of the silenes is reduced when the photolysis of **88a** is carried out in THF due to complexation by the solvent and an overall reduction in the concentration of free silene available for product formation. Bleaching of the precursor made it impossible to quantitate the expected shift in the absorption spectrum of **11a** in THF relative to hexane. This difficulty was accentuated at higher temperatures where two-component decays were observed, making it more challenging to assign the transients conclusively. The rate constants for the addition of nucleophiles to **11a** in THF at 25°C do not even show the same trends as the relative rate data determined in diethyl ether at 100°C. In fact, the largest rate constant observed at room temperature is that for acetic

acid. Had Wiberg done his original study at room temperature, it is entirely possible that he might have proposed a different mechanism for the addition of nucleophiles to silenes.

Chapter 4

Absolute Rate Constants and Arrhenius Parameters for the Head-to-Tail Dimerizations of 1,1-Diphenylsilene and 1,1-Diphenylgermene

4.1 Background

To this point, the focus of this thesis has been on the kinetics and mechanisms of nucleophilic addition to silenes. In the absence of nucleophiles, silenes dimerize in head-to-tail or head-to-head fashion (section 1.3.1). This chapter focuses on the kinetics and mechanism of the head-to-tail dimerization of 1,1-diphenylsilene. For comparative purposes, the head-to-tail dimerization of 1,1-diphenylgermene was also investigated.

The mechanisms of the head-to-tail dimerization of silenes and germenes have not been investigated experimentally. However, the head-to-tail dimerization of the parent molecule (**9a**) has been studied using *ab initio* methods by four different groups and three possible dimerization mechanisms have been proposed (*vide infra*). In the case of the parent germene $H_2Ge{=}CH_2$ (**9b**), only one theoretical study has been reported.[22]

Damrauer and coworkers were the first to examine the dimerization of silene (**9a**) theoretically. They illustrated qualitatively that head-to-tail dimerization was a lower energy process than the head-to-head reaction.[213] In a later study, Ahlrichs and Heinzmann used ab initio methods (RHF/6-31G*) to calculate that the head-to-tail dimerization was exothermic by approximately 76 kcal/mol. The calculated transition

state was found to be 14 kcal/mol higher in energy than the starting materials.[214] This barrier is exceptionally high compared to later values obtained using higher levels of theory (*vide infra*), but is not unexpected considering that the molecular symmetry was constrained to C_{2h} along the entire reaction path and the σ bonds forming were restricted to bond angles of 90°.

In 1992, Seidl, Grev and Schaefer proposed that dimerization of **9a** proceeds through a C_{2h}-symmetric transition state ([π2s+π2s]) in a single step (6-31G*/DZ+d CCSD)(equation 4.1).[215] Kudin and coworkers also predicted a concerted mechanism for dimerization of **9b** (B3LYP / 6-311G(d,p)) and located a transition state with a structure very similar to that of Seidl et al. for **9a**.[22] The relative enthalpies determined for both systems are outlined in equation 4.1.

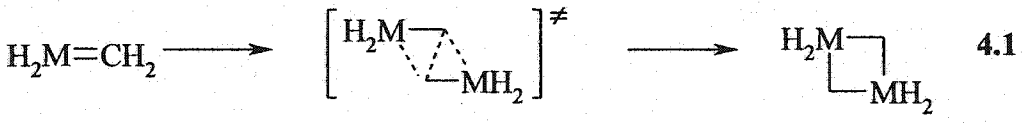

4.1

9		**155**
a = Si 0 kcal/mol	5.2 kcal/mol	-79.1 kcal/mol
b = Ge 0 kcal/mol	3.6 kcal/mol	-65.3 kcal/mol

Soon after, Bernardi, Robb and coworkers reported the results of calculations (CAS-SCF / 3-21G* or DZ+d) that support an alternative mechanism. Their results indicate that dimerization of **9a** first involves the formation of the anti 1,4-(1,3-disila)butanediyl biradical **156** (Equation 4.2),[216,217] lying 16 kcal/mol lower in energy than the starting silene. Bond rotation and ring closure in the second step leads to the

head-to-tail dimer (**155a**). The transition state for the coupling of **156** is 1.9 kcal/mol higher than the enthalpy of **156**, but it is still lower in energy than the starting material.

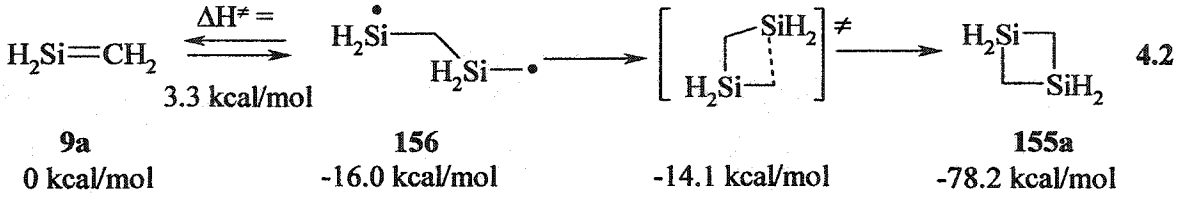

4.2

The same research group later proposed a different stepwise dimerization mechanism for **9a** from calculations carried out at a higher level of theory than that in their previous study (CAS-PT2/6-311G* // CAS-SCF/6-31G*).).[218] They showed that 1,4-(2,3-disila)butanediyl biradical **157** corresponds to a local energy minimum and is formed with a negligible activation barrier (equation 4.3). This biradical then undergoes a [1,2]-silyl sigmatropic shift to form **155a**, or ring closes to form head-to-head dimer **158**.

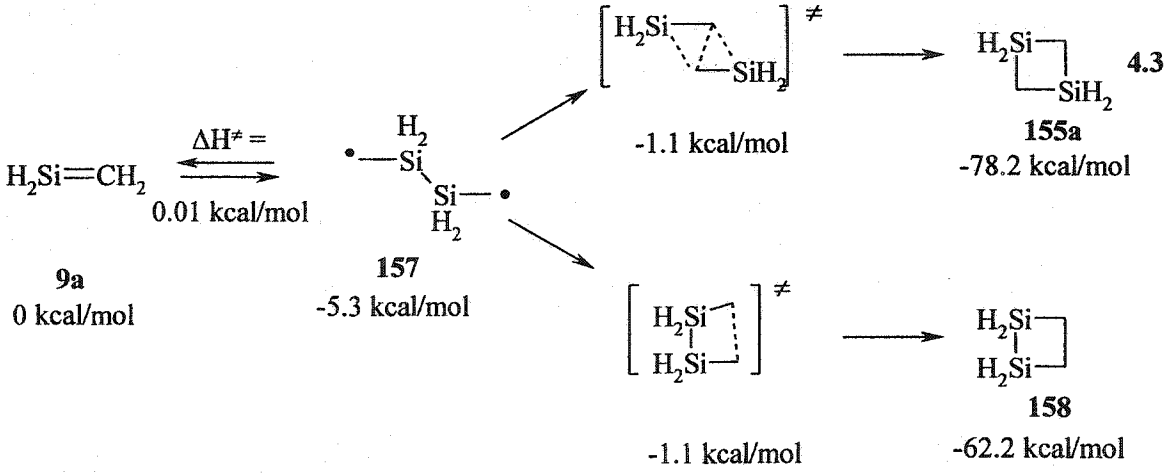

4.3

Photolysis of methanolic hexane solutions of **30a,b** at room temperature lead to the clean formation of the corresponding methoxysilane adducts (**32a,b**, equation 1.11).

In the absence of nucleophiles, the photolysis of **30a,b** leads to the formation of head-to-tail dimers 1,1,3,3-tetraphenyl-1,3-dimetallacyclobutanes (**33a,b**), as determined by X-ray crystallography.[91]

Laser flash photolysis (248 nm) of **30a** and **b** (Figure 4.1) has been used extensively to study the nucleophilic addition reactions of 1,1-diphenylmetallaenes.[59,90,127,128,135] Diphenylgermene (**31b**) decays with second order kinetics in dry hexane such that the rate constant for dimerization can be determined (*vide infra*). On the other hand, diphenylsilene (**31a**) decays with mixed-first and second order decays in dry hexane, which can be attributed to competing dimerization and reaction with trace hydroxylic impurities in the solvent. Given this, rate constants (k_{dim}) can be extracted from these decays and the Arrhenius parameters for dimerization can be determined.

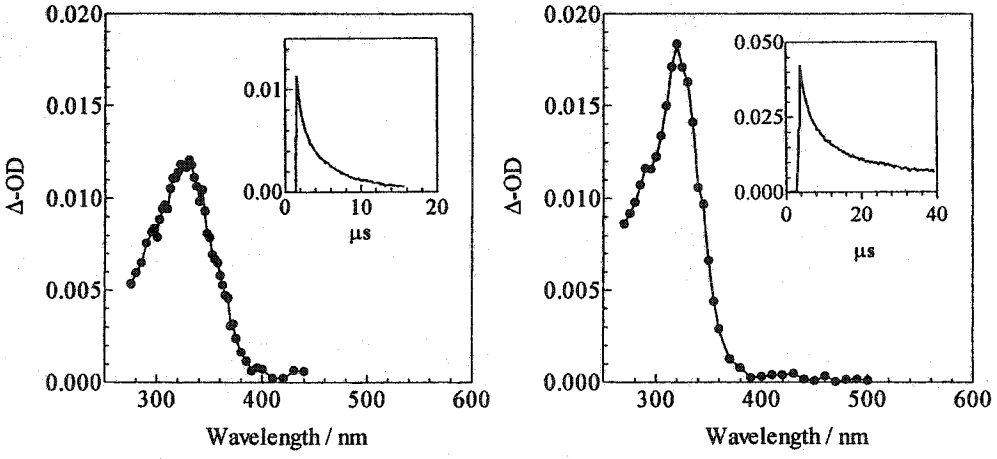

Figure 4.1 Transient absorption spectra obtained after 248-nm laser flash photolysis of (a) **30a** and (b) **30b** in hexane solution. Inserts show typical decay traces at 325 nm.

Bimolecular rate constants for the reaction of metallaenes with nucleophiles have been determined by monitoring the change in concentration of the metallaene ($[M]_t$) as a function of time (equation 4.4), where $[M]_0$ is the concentration of metallaene immediately following the laser pulse. The term k_d is the sum of the pseudo-first order rate constants for decay in the absence (k_0) and presence or a nucleophile (k_{Nu}). The technique of laser flash photolysis relies on measuring the change in concentration by monitoring the change in UV absorbance at a given wavelength. Under pseudo-first order conditions, it is not necessary to know the concentration of the metallaene explicitly, and the absorbance can be monitored directly to measure bimolecular rate constants (equation 4.5).[207] However, the bimolecular rate constant for reaction of a metallaene with itself is strictly a second-order process (equation 4.6) and so it is essential to know the concentration of the reacting species explicitly in order to extract the absolute rate constant from the data. If the concentration is to be monitored by UV absorption, then the extinction coefficients at the monitoring wavelength must first be determined.

$$[M]_t = [M]_0 \exp(k_d t) \qquad \textbf{4.4}$$

$$\Delta OD_t = \Delta OD_0 \exp(k_d t) \qquad \textbf{4.5}$$

$$\frac{1}{[M]_t} = \frac{1}{[M]_0} + 2k_{dim}t \qquad \textbf{4.6}$$

The primary goals of this chapter were to determine the extinction coefficients of 1,1-diphenylsilene and 1,1-diphenylgermene (**30a,b**), and determine absolute rate

constants and Arrhenius parameters for their dimerization in hexane solution. Efforts have also been made to determine the mechanism for dimerization by examining the photochemistry of **33a,b**.

4.2 Results and Discussion

4.2.1 Determination of Extinction Coefficients for 31a and b

The measurement of extinction coefficients (ε) for stable species is relatively straightforward, but it is more involved for transient species. A number of different techniques have been employed in the past, particularly for triplet ketones.[219] Conlin, Scaiano and coworkers employed the so-called "laser dose method"[220,221] for the determination of the extinction coefficient of silene **55** (Scheme 1.3) at 330 nm.[106] This was the method that was used for the determination of $\varepsilon_{31a,b}$.

The "laser dose" method involves the use of an actinometer that forms a transient species with a known quantum yield (Φ) and extinction coefficient at a given wavelength. Benzophenone has been shown to work well as an actinometer.[107,219] The irradiation of benzophenone (**159**) affords the corresponding triplet state (**159**^{3*}, λ_{max} = 525 nm, $\varepsilon_{159^{3*}}$ = 6250 ± 940 M^{-1} cm^{-1}) with a quantum yield of unity (Φ_{159} = 1.0) (equation 4.7).[222]

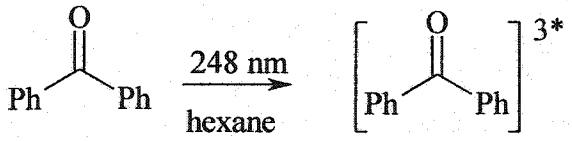

159 **159**^{3*} **4.7**

The extinction coefficients of **31a** and **b** were determined by flash photolysis of optically matched, nitrogen saturated hexane solutions of **30a**, **30b** and **159** at 248 nm. The maximum absorbances of **31a,b** (λ_{max} = 325 nm) and **159**^{3*} (λ_{max} = 525 nm) were determined as a function of laser intensity, using a series of neutral density filters to vary the laser dose (Figure 4.2).

The ratio of the slopes of the lines for **31a,b** relative to that for **159**^{3*} ($S_{M=C}$ /S_{159}) gives the ratio of the extinction coefficients ($\varepsilon_{M=C}$ /ε_{159}) multiplied by the ratio of the quantum yields for formation of the two species (equation 4.8).[221] Substituting the known values for $\Phi_{31a,b}$ (0.21±0.02[223] and 0.22±0.02,[91] respectively) into this equation affords the values for $\varepsilon_{M=C}$ at 325 nm shown in Table 4.1. Two sets of experiments were carried out, and the results were averaged to yield $\varepsilon_{325\ nm}$ = 8900 ± 1800 L·mol^{-1}·cm^{-1} and $\varepsilon_{325\ nm}$ = 11 400 ± 2700 L·mol^{-1}·cm^{-1} for **31a** and **b**, respectively. These results should be compared to ε_{250nm} = 7680 M^{-1} s^{-1} for 1,1-diphenylethylene, the corresponding carbon-based analogue.[204] It should be noted that only the linear portions of the plots for **159**^{3*} were used for these calculations. The deviation from linearity at higher laser intensities is the result of decomposition of **159**, as shown by the change in the static absorption spectrum after repeated exposure to the laser beam.

$$\frac{\varepsilon_{M=C} \bullet \Phi_{M=C}}{\varepsilon_{159} \bullet \Phi_{159}} = \frac{S_{M=C}}{S_{159}} \qquad \textbf{4.8}$$

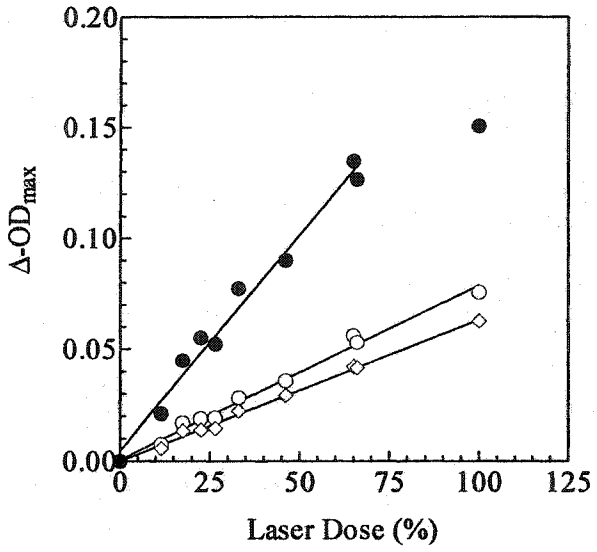

Figure 4.2 Maximum absorbances of **31a** (◇), **31b** (○) and **159**^{3*}(●) vs. laser dose.

4.2.2 Determination of Absolute Rate Constants for Dimerization of 31a and b

Nanosecond laser flash photolysis of continuously flowing, nitrogen-saturated solutions of **30a** and **b** in dry hexane or isooctane allows for the direct detection of the corresponding diphenylmetallaene **31a** and **b** as transient absorptions at λ_{max} = 325 nm.[84] The decay of **31a** (Figure 4.3a) did not fit well to the standard expression for second order kinetics, so the rate constant for dimerization could not be determined directly from equation 4.6. Rather, the decay was modelled as mixed pseudo-first and second order kinetics, according to equation 4.9. Substituting [M] of equation 4.9 for absorbance (ΔOD) results in the expression in equation 4.10. Nonlinear least-squares fitting of

$\Delta OD_t/\Delta OD_0$ vs. time data (Figure 4.3a) to equation 4.10 led to the calculation of k_{dim}, where l is the path length of the cell (3mm), ε is the extinction coefficient of **31a** at 325 nm and k_1 is the pseudo-first order component of the decay, which presumably arises from reaction with hydroxylic impurities present in the solvent. Typically, fitting the data to equation 4.10 resulted in $k_1 \sim 10^4\ s^{-1}$.

$$\frac{[M]_t}{[M]_0} = \frac{k_1 \exp(-k_1 t)}{k_1 + 2k_{dim}[M]_0(1-\exp(-k_1 t)} \qquad \textbf{4.9}$$

$$\frac{\Delta OD_t}{\Delta OD_0} = \frac{k_1 \exp(-k_1 t)}{k_1 + 2k_{dim}(\Delta OD_0/l\varepsilon)(1-\exp(-k_1 t)} \qquad \textbf{4.10}$$

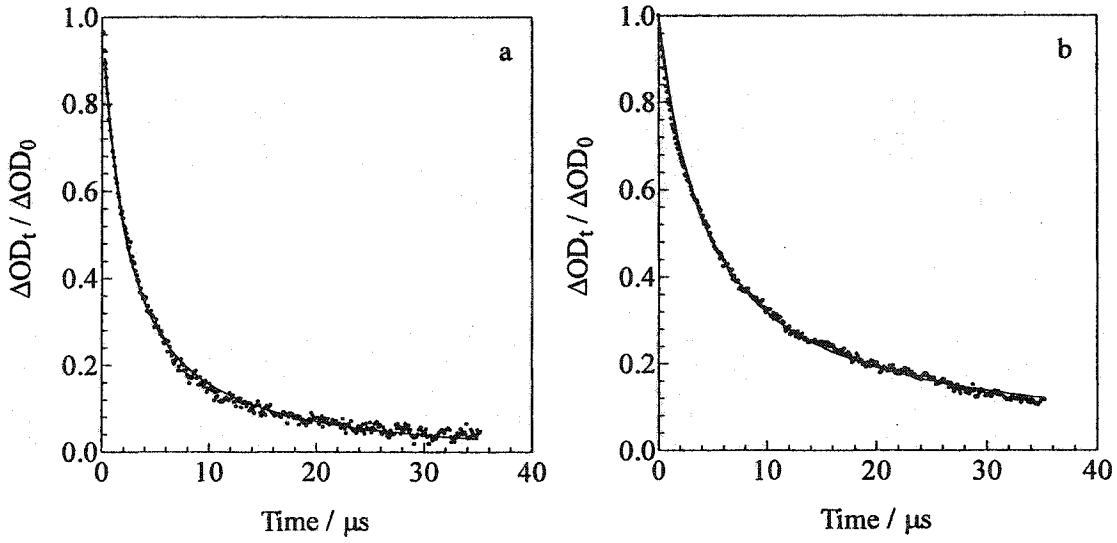

Figure 4.3 Plots of $\Delta OD_t/\Delta OD_0$ vs. time for the decay of (a) **31a** and (b) **31b** in hexane solution at 24°C.

The decay of 1,1-diphenylgermene (**31b**) did not fit well to the standard expression for second order kinetics either. A plot of $1/\Delta OD$ vs. time deviated substantially from the linear relationship expected for clean second-order decays. The inset of Figure 4.1b and Figure 4.3b show that **31b** decays to a residual absorption that presumably arises from a minor photoproduct that appears to be stable over the time window observed. Therefore, the second-order decays were more appropriately plotted as $\Delta OD_t/\Delta OD_0$ vs. time (Figure 4.3b) and fit to equation 4.11 to correct for the residual absorption. Table 4.1 lists the values of $2k_{dim} / \varepsilon_{31a,b}$ obtained from these analyses, the extinction coefficients, and the absolute rate constants for dimerization (k_{dim}) of **31a,b**.

$$\frac{\Delta OD_t}{\Delta OD_0} = \frac{\Delta OD_\infty}{\Delta OD_0} + \frac{1}{1+2k_{dim}(\Delta OD_0/l\varepsilon)t} \qquad \textbf{4.11}$$

Table 4.1 Rate Ratios ($2k_{dim}/\varepsilon_{31a,b}$), Extinction Coefficients (ε) and Rate Constants for Dimerization (k_{dim}) of 1,1-Diphenylsilene (31a) and 1,1-Diphenylgermene (31b) in Hexane Solution at 24°C

Metallaene	$Ph_2Si{=}CH_2$ (**31a**)	$Ph_2Ge{=}CH_2$ (**31b**)
$2k_{dim} / \varepsilon_{31a,b} / 10^6\ s^{-1}$	2.45 ± 0.34^a	1.56 ± 0.42^b
$\varepsilon_{325\ nm} / M^{-1}\ cm^{-1}$	8900 ± 1800	$11\,400 \pm 2700$
$k_{dim} / 10^{10}\ M^{-1}\ s^{-1}$	1.1 ± 0.3	0.90 ± 0.32

a. average of 4 determinations. Errors are reported as the standard deviations from the mean values corresponding to confidence intervals of 85%. *b.* average of 7 determinations. Errors are reported as the standard deviations from the mean values corresponding to confidence intervals of 95%.

The similar absolute reactivities for dimerization of **31a** and **b** are quite interesting, considering the substantial differences in their reactivity towards nucleophiles (Table 1.3). For example, **31a** reacts at close to the diffusion-controlled rate with methanol in hexane ($k_{MeOH} = 1.5x10^9\ M^{-1}\ s^{-1}$), via a stepwise mechanism that is overall first-order in alcohol concentration (*vide supra*).[82] On the other hand, germene **31b** reacts by a pathway that is strictly second order in methanol concentration. The first order pathway is too slow to be detected and so only an upper limit for its rate constant could be determined ($k_{MeOH} < 3x10^5\ M^{-1}\ s^{-1}$).[90] To address the kinetic variation in nucleophilic addition and dimerization of metallaenes, the thermochemistry of simpler derivatives was examined. Experimental heats of formation ($\Delta H_f°$) of the species involved in the dimerization of 1,1-dimethylsilene (**7a**) and its reaction with water are summarized in equation 4.12.[87,108,209,224] The $\Delta H_f°$ values can be used to calculate the heats of dimerization (ΔH_{dim}), and hydration (ΔH_{hyd}, Table 4.2).

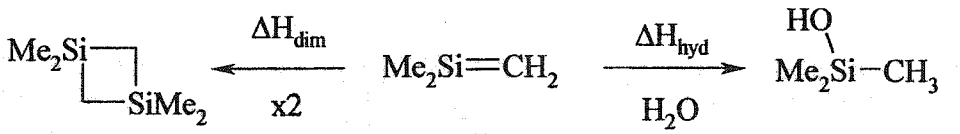

4.12

	8a	**7a**		**160**
$\Delta H_f°$ / kcal mol^{-1}	-51.6	9	-56	-119

The experimental values of ΔH_{dim} and ΔH_{hyd} for 1,1-dimethylsilene (**7a**) compare favourably with the results of high level theoretical calculations for the parent silene (**9a**, Table 4.2).[218] Experimentally determined heats of formation on the corresponding germanium compounds are not available. However, ΔH_{dim} and ΔH_{hyd} have both been

calculated for germene (**9b**, Table 4.2).[22,225] The data suggest that the dimerizations of **9a** and **9b** are similarly exothermic, which is reflected in the similar rate constants for dimerization of **31a** and **b**. On the other hand, the calculated heats of hydration for **9a** and **9b** reveal that the addition of water to **9b** is significantly less exothermic than water addition to **9a**. This difference is reflected in the absolute reactivities for **31a** and **b** with alcohols.

Table 4.2 Heats of Dimerization (ΔH_{dim}) and Hydration (ΔH_{hyd}) for 1,1-Dimethylsilene (7a), Silene (9a) and Germene (9b)

	$Me_2Si{=}CH_2$ (**7a**)	$H_2Si{=}CH_2$ (**9a**)	$H_2Ge{=}CH_2$ (**9b**)
ΔH_{dim} / kcal mol^{-1}	-69.6[a]	-77.2[b]	-75.3[d]
ΔH_{hyd} / kcal mol^{-1}	-70.0[a]	-77[c]	-61.7[e]

a. calculated from heats of formation, see equation 4.12. *b*. Ref. 218. Note: This value has been calculated by other groups.[87,214,215,217] However the value given in the table represents the value calculated at the highest level of theory reported (CASPT2/6-311G**//CASSCF/6-31G*) *c*. Ref. 226. *d*. Ref. 22. *e*. Ref. 225.

4.2.3 Arrhenius Parameters for Dimerizations of 31a and b

Rate constants for dimerization of **31a** and **b** were determined over the 0 – 60°C temperature range, using the same procedures outlined in section 4.2.2 for the room temperature experiments. Plots of log k_{dim} vs. 1000/T are shown in Figure 4.4. The resulting Arrhenius parameters, calculated by linear least squares analysis of the data according to the Arrhenius equation (equation 4.13), are summarized in Table 4.3.

$$\ln k_{dim} = \ln A - (E_a/RT) \qquad \textbf{4.13}$$

The dotted line is the Arrhenius plot for diffusion in hexane solution. The plot was calculated from the standard Debye equation (equation 3.10), where the values of η were obtained from published temperature-viscosity data.[209] The Arrhenius parameters for diffusion in hexane are $E_a = 2.4\pm0.3$ kcal/mol and log $(A / M^{-1} s^{-1}) = 12.0\pm0.2$.

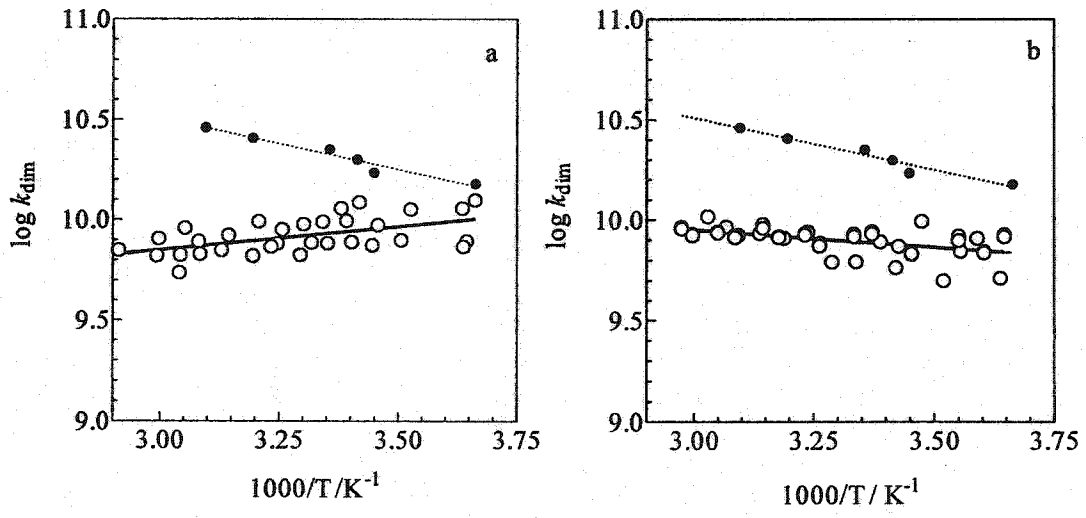

Figure 4.4 Arrhenius plots for the dimerization (O) of (a) **31a** and (b) **31b** in hexane solution over the 0-60°C temperature range. The dotted line corresponds to the Arrhenius plot for diffusion in hexane, calculated using the modified Debye equation and published viscosity data (•).

Table 4.3 Rate Constants and Arrhenius Parameters for Dimerization of 31a and b in Hexane Solution[a]

Metallaene	$Ph_2Si{=}CH_2$ (**31a**)	$Ph_2Ge{=}CH_2$ (**31b**)
$k_{dim}^{25°C}$ / 10^{10} M^{-1} s^{-1} [b]	0.9 ± 0.6	0.8 ± 0.3
E_a / kcal mol^{-1}	-1.0 ± 0.6	+0.8 ± 0.4
Log (A / M^{-1} s^{-1})	9.2 ± 0.4	10.4 ± 0.4
$\Delta H^{\neq}$ / kcal mol^{-1}	-1.6 ± 0.3	+0.2 ± 0.4
$\Delta S^{\neq}_{300\,K}$ / cal mol^{-1} K^{-1}	-18 ± 2	-13 ± 2

a. Errors are reported as ±2σ, corresponding to confidence intervals of 94-95%
b. Interpolated from the Arrhenius parameters.

The measured activation energies are nearly zero for both metallaenes, a trend that is consistent with what has been observed in other studies on the dimerization of silenes (section 1.3).[106,110,114] The preexponential factors are associated with entropies of activation of $\Delta S^{\neq}_{\mathbf{31a}}$ = -18±2 cal/mol K^{-1} and $\Delta S^{\neq}_{\mathbf{31b}}$ = -13±2 cal/mol K^{-1} at 300 K. The mechanistic implications of the Arrhenius parameters for **31a** and **b** are intriguing, considering the three mechanisms for silene dimerization that have been proposed on the basis of various theoretical calculations.[215,216,218]

One of the possible stepwise mechanisms for the dimerization of **31a** is shown in equation 4.14. The expression for k_{dim}, assuming the steady-state approximation holds for the biradical, is given in equation 4.15.

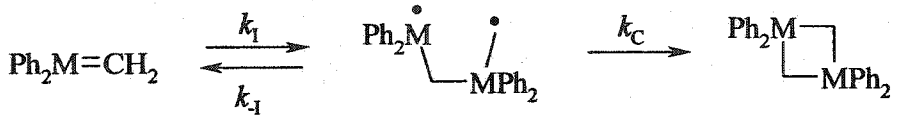

4.14

31 **161** **33**

a. M = Si

b. M = Ge

$$k_{dim} = k_1 \bullet \frac{k_{-1}}{k_{-1} + k_C} \qquad 4.15$$

This mechanism will result in a bell-shaped Arrhenius plot for k_{dim} if biradical (**161**) formation is reversible and the reaction is strongly exothermic overall. This type of temperature dependence is similar to that for the reaction of silenes with alcohols (Figure 1.5). Biradical cleavage to form the metallaene must occur faster than ring closure ($k_{-1} > k_C$) to yield the negative activation energy that would be observed at high temperatures. Biradical coupling must be the favoured step at lower temperatures ($k_{-1} < k_C$), in order to yield a positive activation energy. The slope of the plot is zero at the point where $k_{-1} = k_C$. If the dimerizations of **31a** and **b** are indeed stepwise according to the mechanism of equation 4.14, then k_{-1} must be similar to k_C over the 0 - 60°C temperature range. The slightly negative activation barrier observed in the case of **31a** indicates that if this is the mechanism, k_{-1} must be somewhat larger than k_C, while the opposite must be true for **31b**.

In order to further assess the mechanistic possibility that **161** is an intermediate on the potential energy surface of the head-to-tail dimerization of metallaenes, it is necessary to get independent information on the kinetic behaviour of biradicals **161a** and **b**. Dimers **33a,b** seemed to be reasonable photochemical precursors to the biradicals, since previous

photolyses of 1,3-dimetallacyclobutanes have led to products consistent with the formation of biradical intermediates (*vide infra*).[227,228]

4.2.4 Photochemistry of 1,1,3,3-Tetraphenyl-1,3-Dimetallacyclobutanes (33a and b)

Steady-state photolysis of **33a** and **b** in the presence of methanol led to the formation of methanol adducts **32a,b** (equation 4.16) with quantum yields of Φ_{31a} = 0.007 ± 0.0003 and Φ_{31b} = 0.11 ± 0.02).[91] Whereas the quantum yields for formation of **31a** and **b** are identical within experimental error from the photolyses of **30a** and **b**, they are significantly different when **33a** and **b** are used as the precursors.

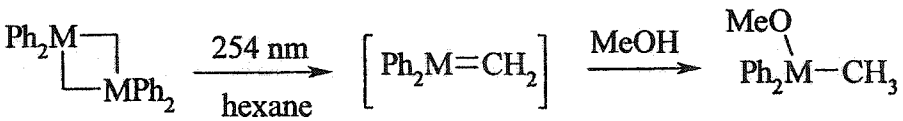

4.16

33 **31** **32**

a. M = Si
b. M = Ge

Φ_{31a} = 0.007±0.0003

Φ_{31b} = 0.11±0.02

The relative reactivities of **33a,b** towards photoinduced cycloreversion are also reflected in the results of flash photolysis (248 nm) experiments with the two compounds. The 325-nm absorption of **31a** cannot be detected in flash photolysis of **33a**. Instead, a very broad transient absorption was observed 40-60 ns after the laser pulse (Figure 4.5a), as well as fluorescence emission at 340 nm from the excited state of **33a**. The decay of the 510-nm transient is only slightly longer than the laser pulse (τ ~75 ns). Assigning this transient conclusively is impossible due to its short lifetime and faster time-resolved techniques are necessary. However, at this time, we can only speculate that this

absorption might be due to singlet 1,4-biradical **161a**. The short lifetime of the biradical is not surprising, as non-conjugated, carbon-based singlet biradicals require ultrafast time-resolved techniques to detect them directly.[229] For example, tetramethylene ($\bullet CH_2CH_2CH_2CH_2\bullet$), the simplest carbon-based 1,4-singlet biradical, has a lifetime of 840±50 fs.[230] The absorption maximum at 510 nm is quite different from the absorption of other aryl-substituted monoradicals ($\lambda_{max} \sim 330$ nm).[4,231] The long-wavelength absorption might be due to hyperconjugative stabilization of the silyl radical centre by the β-silyl group, because silicon groups are well known to stabilize electron deficient centres at the β-position, particularly carbocations.[232] Figure 4.5a shows that 500-700 ns after the laser pulse of the same experiment, a weak absorption at 325 nm is observed. This is tentatively assigned to **31a**, although further characterization of this transient by kinetic measurements was not pursued. The spectrum obtained upon flash photolysis of **33b** (Figure 4.5b) is shown for comparison.[91] The detection of **31b** (325 nm) is consistent with the higher quantum yield for metallaene formation.

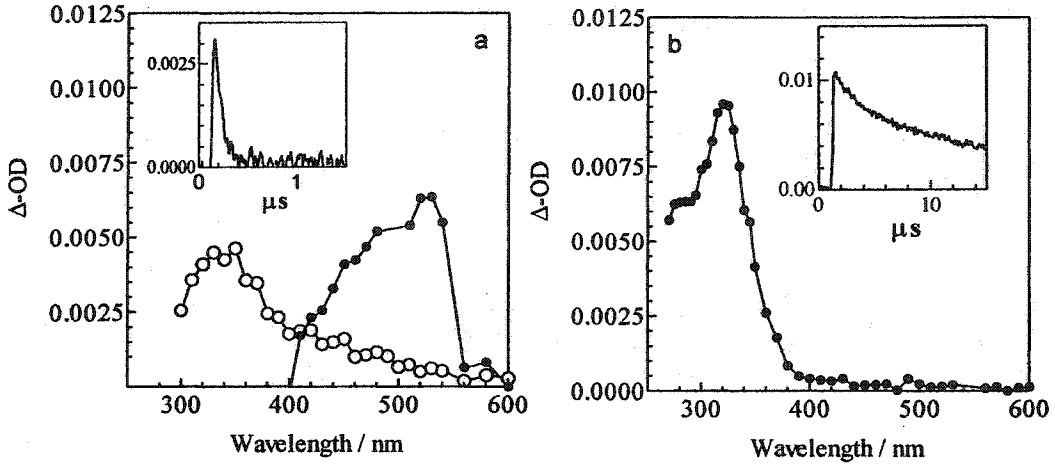

Figure 4.5 a) Transient absorption spectrum obtained by flash photolysis (248 nm) of **33a** in deoxygenated hexane at 24°C, recorded 40-60 ns (•) and 500-700 ns (o) after the laser pulse. The insert shows a typical decay trace monitored at 510 nm. b) Transient absorption spectrum obtained after flash photolysis (248 nm) of **33b** in deoxygenated hexane at 24°C. The insert shows a typical decay trace monitored at 325 nm.[91]

Assuming that photocycloreversion proceeds via 1,4-biradical **161**, the quantum yields indicate that there is a considerable quantitative difference in the mechanism for metallaene formation between **33a** and **b**. If the biradical is indeed part of the mechanism for both the dimerization of 1,1-diphenylsilene and 1,1-diphenylgermene (equation 4.14), there must be considerable differences between the rate constants for β-scission (k_{-1}) and ring closing (k_C).

Consider the mechanism of Scheme 4.1. The quantum yield for metallaene formation (Φ_{31}, equation 4.17) is given by the product of the state efficiency for biradical formation (ϕ_{161}) from the excited state of the precursor and the efficiency factor for biradical cleavage to form the metallaene (ϕ_{31}). The higher quantum yield for metallaene

formation from **33b** relative to **33a** must be due to more efficient cleavage of the M-C bond in the excited state of **33b** and/or the biradical **161b** must undergo β-scission more efficiently than **161a**.

$$\Phi_{31} = \phi_{161} \bullet \phi_{31} \qquad 4.17$$

Scheme 4.1 The Photochemistry of 33a and b

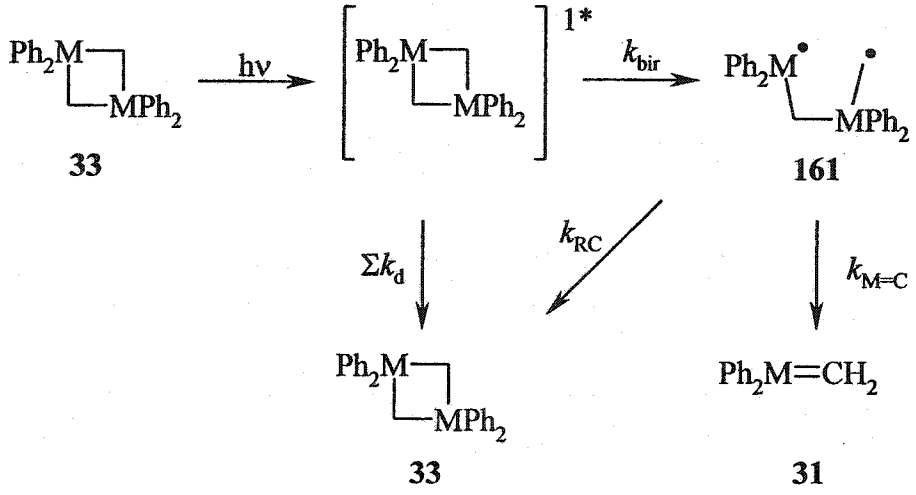

The state efficiency for biradical formation (ϕ_{161}, equation 4.18) is dependent on the ratio of the rate constant for biradical formation (k_{bir}) from the excited state precursor to the sum of the rate constants for biradical formation and all the photophysical decay processes available to 33^{1*} (Σk_d, equation 4.19), including internal conversion (k_{IC}), fluorescence (k_f) and intersystem crossing (k_{ISC}).[196] Similiarly, the state efficiency for metallaene formation (equation 4.20) is given by the ratio of the two pathways available to **161**, involving the rate constant for biradical cleavage to form the metallaene ($k_{M=C}$) and the rate constant for ring closing (k_{RC}) to form the starting material.

$$\phi_{161} = \frac{k_{bir}}{k_{bir} + \Sigma k_d} = k_{bir} \cdot \tau_s \qquad \textbf{4.18}$$

$$\Sigma k_d = k_{IC} + k_f + k_{ISC} \qquad \textbf{4.19}$$

$$\phi_{31} = \frac{k_{M=C}}{k_{M=C} + k_{RC}} \qquad \textbf{4.20}$$

It is not possible to determine the values of the individual state efficiencies ϕ_{161} and ϕ_{31} in the present cases. The determination of ϕ_{161} requires that each one of the decay pathways available to the excited state be measured separately, which would be exceedingly difficult to measure for this system. However, one general indication of the value for ϕ_{161} is provided by the fluorescence properties of **33a,b**. The singlet lifetime (τ_s) can be substituted for ($\Sigma k_d + k_{bir}$) in equation 4.18, and it might be possible to attribute variations in τ_s to differences in ϕ_{161} that ultimately contribute to the difference in Φ_{31} for the two precursors. It would also be advantageous to compare τ_s for **30a,b** to those of **33a,b**, because these two precursors have higher Φ_{31} values compared to their dimetallacyclobutane analogues. Therefore, the fluorescence spectra and singlet lifetimes of **30a,b** and **33a,b** have been determined and are the subjects of section 4.2.4.1.

The determination of ϕ_{31} requires that the biradical have an alternative form of reactivity that can be measured and compared to metallaene formation. One way this might be accomplished is to study the photochemistry of derivatives of **33a** and **b** that have substituents at carbon (Scheme 4.2). For example, photolysis of ***trans*-162** in the presence of methanol might lead to ***cis*-162**, which can be attributed to ring closing of

biradical **163**. The formation of alkoxysilane **164** would indicate biradical cleavage to form the silene (**165**). The product ratio of ***cis*-162:165** might be related to k_{RC} : $k_{M=C}$. Previous studies on the photolysis of ***cis***- and ***trans*-162** are the subjects of section 4.2.4.2.

Scheme 4.2 Photolysis of *Trans*-1,1,3,3-Tetraphenyl-2,4-Bis(neopentyl)-1,3-disilacyclobutanes

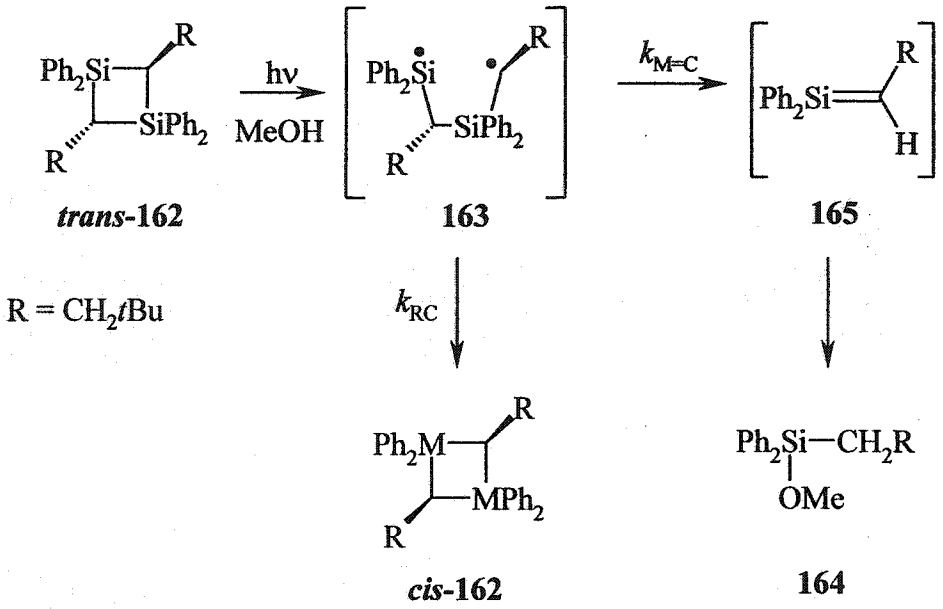

4.2.4.1 Fluorescence Emission Spectroscopy of 33a,b and 30a,b

Fluorescence emission spectra were measured for **33a,b** and **30a,b** in argon-saturated isooctane solution (Figure 4.6a-d). The emission maxima (λ_{em}) are summarized in Table 4.4. The spectra of **30a** and **33a** show maxima at 285 nm in both cases. However, **33a** also shows a broad, weak emission at longer wavelengths that may be

attributable to intramolecular excimer emission.[233] The emission properties of **30b** and **33b** are considerably different from those of their silicon analogues. The emission of **30b** is red-shifted compared to **30a**, which might be due to a larger change in geometry upon excitation. The emission spectrum of **33b** bears little resemblance to any of the other metallaene precursors.

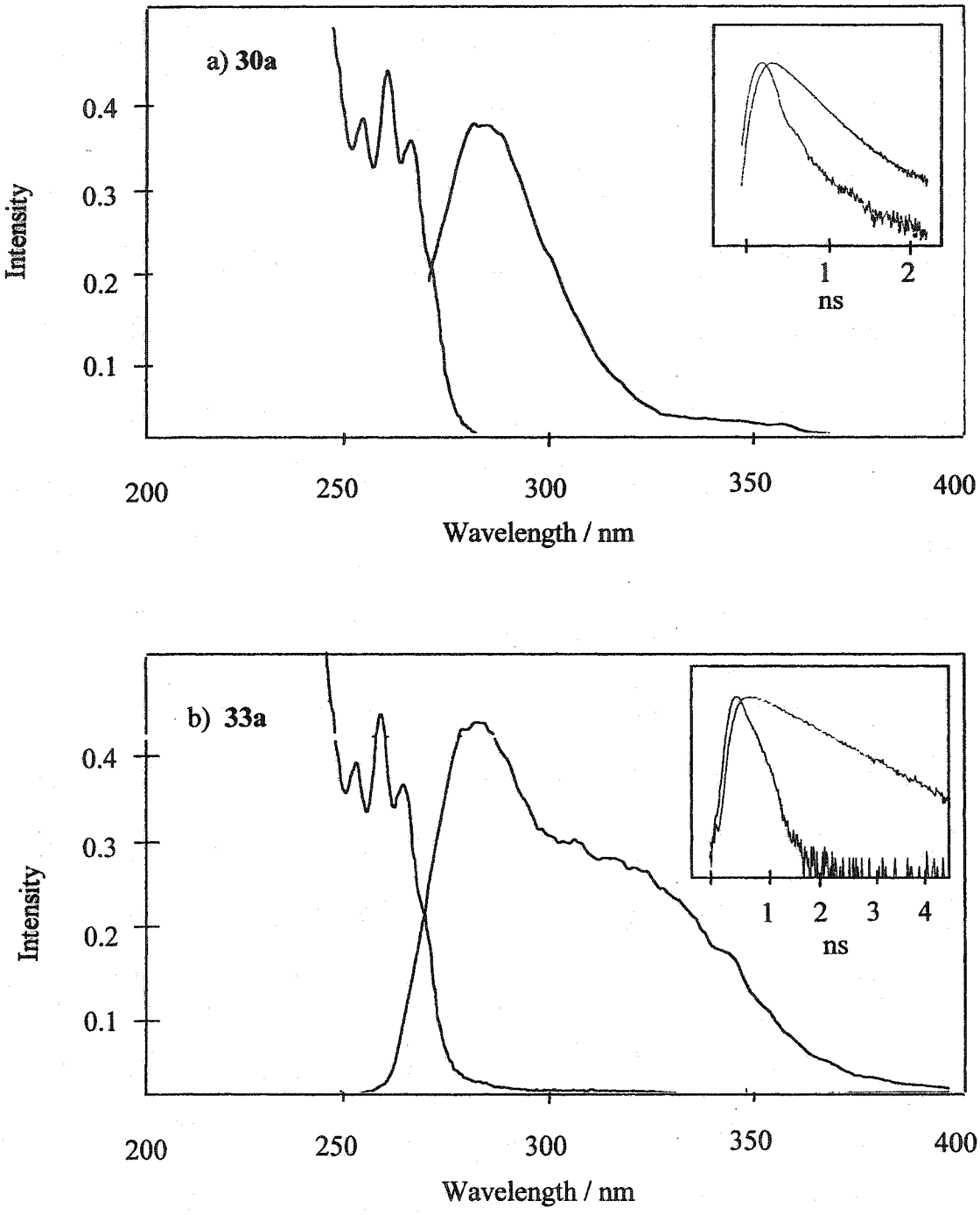

Figure 4.6 Absorption and emission spectra of a) **30a**, and b) **33a** in argon-saturated, isooctane solution. Inserts show fluorescence decays at 285 nm.

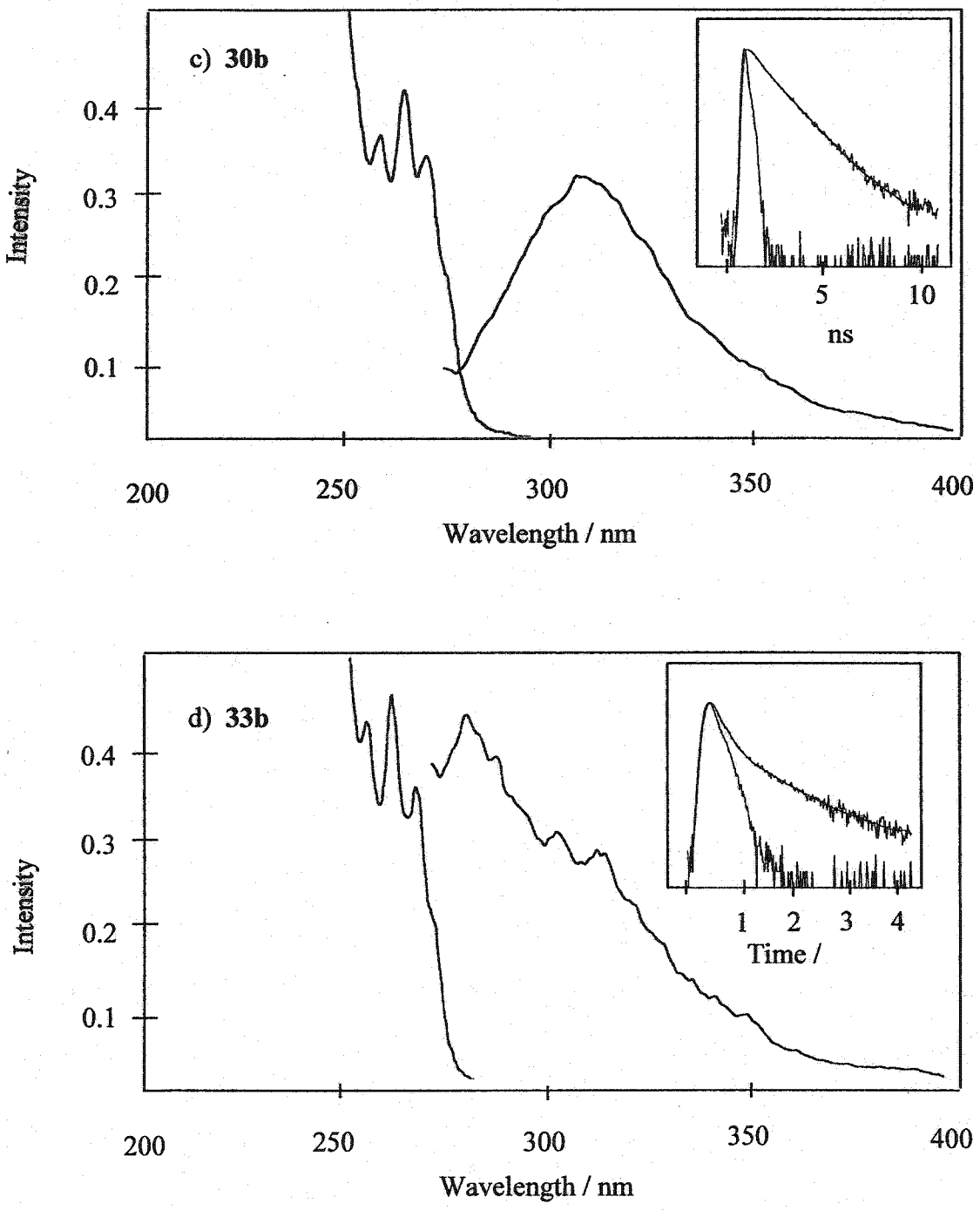

Figure 4.6 Absorption and emission spectra of c) **30b**, and d) **33b** in argon-saturated, isooctane solution. Inserts show fluorescence decays at 310 and 290 nm, respectively.

Table 4.4 Emission Maxima and Singlet Lifetimes of 30a,b and 33a,b

Precursor	λ_{em} / nm	τ_s / ns	χ^2
30a	285	2.6±0.1[b]	1.052
33a	285[a]	7.5±0.1[c]	1.193
30b	310	3.0±0.2, 12.8±0.1[d]	1.041
33b	290	1.8±0.1[e]	1.077

a. There is an additional broad, less intense band superimposed on this emission (see Figure 4.6b. *b*. Matches τ_s reported previously.[223] *c*. τ_s was found to be the same when monitored at 290 or 325 nm. *d*. Two-component decay observed with pre-exponential values of 0.28 and 0.18, respectively. *e*. There are at least two components to the fluorescence decay; the reported τ_s is for the major component.

Singlet lifetimes were determined by time-correlated single photon counting and are summarized in Table 4.4. The decays observed for **30a** and **33a** fit acceptably to a single exponential and did not vary as a function of monitoring wavelength. The longer lifetime observed for **33a** suggests that the second silicon atom slows down the ring cleavage reaction (k_{bir}) in comparison to the analogous reaction in **30a**, and therefore reduces ϕ_{31a}. The longer lifetime is also due to the equilibration between the reactive excited singlet state with an intramolecular excimer that is less reactive to ring cleavage and whose formation is supported by the broad, long-wavelength emission of Figure 4.6b. Furthermore, biradical cleavage ($k_{M=C}$) to form **31a** from **30a** is thermodynamically favoured over biradical cleavage from photolysis of **33a**, as the former yields one molecule of silene and one molecule of ethylene, while the latter yields two molecules of

31a. This suggests that $k_{M=C}$ from **30a** is likely to be greater than $k_{M=C}$ from **33a**. Therefore, the difference in Φ_{31a} for **30a** and **33a** must be due to a reduction in both ϕ_{31a} and ϕ_{161}.

The fluorescence decays observed in the germanium derivatives are difficult to interpret. The fluorescence decay of **30b** fit to two-exponentials, with both components contributing roughly equally to the overall decay. Two-component decays were also observed with **33b**, with one species dominating (see Table 4.4). Unfortunately, the fluorescence data obtained for the germanium analogues do not provide any reliable details as to how **161** behaves as a function of heteroatom.

4.2.4.2 Photolysis of 1,1,3,3-Tetraphenyl-2,4-dineopentyl-1,3-disilacyclobutane

There is one report in the literature that gives information about $k_{M=C}$ and k_{RC} for 1,3-disila-1,4-butanediyl radicals related to **161a**. Jones and coworkers reported the photolysis of *cis*- and *trans*-1,1,3,3-tetraphenyl-2,4-dineopentyl-1,3-disilacyclobutane (**162**).[227] In the photolysis of pure ***trans*-162**, a mixture of ***trans*-** and ***cis*-162** was obtained in a ratio of 70:30. Continued photolysis of this mixture led to the formation of alkene isomers ***E*-** and ***Z*-166**. The three products were attributed to initial Si-C bond cleavage to form biradical **163**, followed by bond rotation and reclosing to form ***cis*-162**, or abstraction of hydrogen to form the disproportionation product ***E*-166** (equation 4.21). The formation of the *Z*-isomer was attributed to secondary photolysis of ***E*-166**.

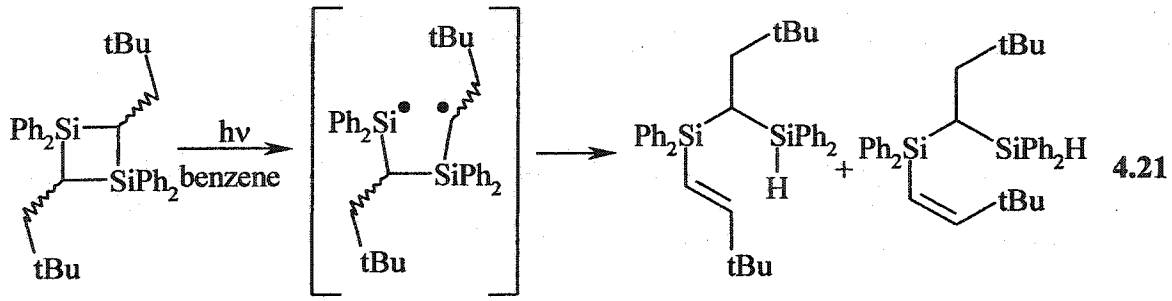

***trans*-162** (70%)
***cis*-162** (30%)

163

***E*-166**

***Z*-166**

Photolysis of a mixture of ***trans*-** and ***cis*-162** in the presence of methanol led to the formation of ***E*-** and ***Z*-166**, as well as methoxysilane **164**. Products were identified after 97% conversion of ***cis*-** and ***trans*-162**. The formation of the products was explained by the initial formation of biradical **163** (Scheme 4.3) that could either cleave to form the silene (**165**) to give **164** or undergo bond rotation and ring closing to give the corresponding diastereomer.

Scheme 4.3 Photolysis of 1,1,3,3-Tetraphenyl-2,4-dineopentyl-1,3-disilacyclobutane in the Presence of Methanol (162)

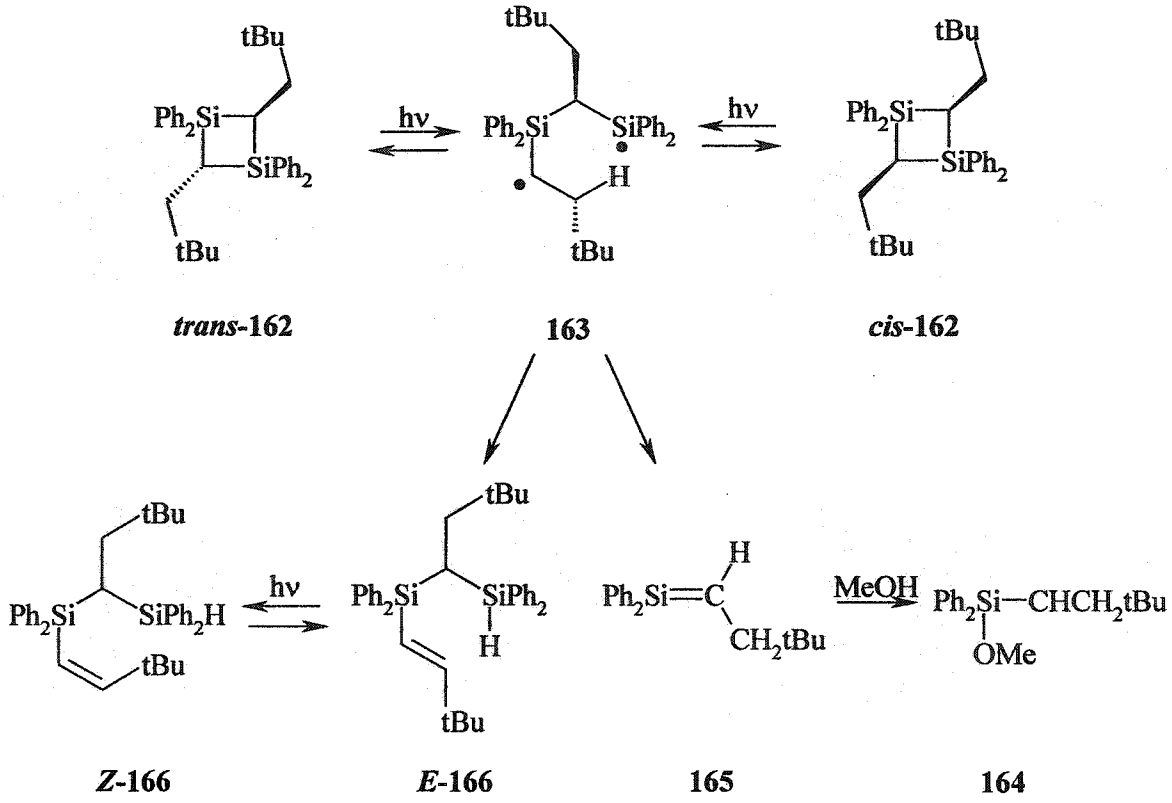

The results of Jones and coworkers show that biradical **163** undergoes fragmentation in competition with reclosure and H-abstraction. They do not, however, give meaningful information on the relative rate constants for these processes, because the product yields were reported at ~97% conversion of the starting material. The relative rates can be correlated with product yields only if the photolysis is monitored at much lower conversions of a single *cis* or *trans* isomer of **162**, otherwise it cannot be determined which isomer leads to formation of the products. For example, photolysis of

***trans*-162** up to ≤20% conversion results in a relatively low amount of ***cis*-162**.* Therefore, under these conditions, the amounts of biradical and subsequent products arising from photolysis of the *cis*-isomer are relatively low.

Also, the photolysis of the pure *cis* and *trans* isomers of **162** must be examined independently if this system is to be used to approximate the rate constant ratio $k_{M=C}$ / k_{RC}. There are two possible conformations of **163** that can lead to silene formation (Scheme 4.4). In order to determine the relative rate constants of interest, the biradical conformations must exist in rapid equilibrium. Unfortunately, there are no reported studies on organosilicon or germanium 1,4-singlet biradicals, so it is difficult to predict how these species might behave. Studies on the photolysis of ***cis*-** and ***trans*-162** are currently underway in our lab to address these problems systematically.

---

* I would like to thank my labmates Joanna Grinyer and Tom Owens for sharing their preliminary results with me on their photolysis of ***trans*-162**.

Scheme 4.4 Photochemical Interconversion of *Cis*- and *Trans*-162

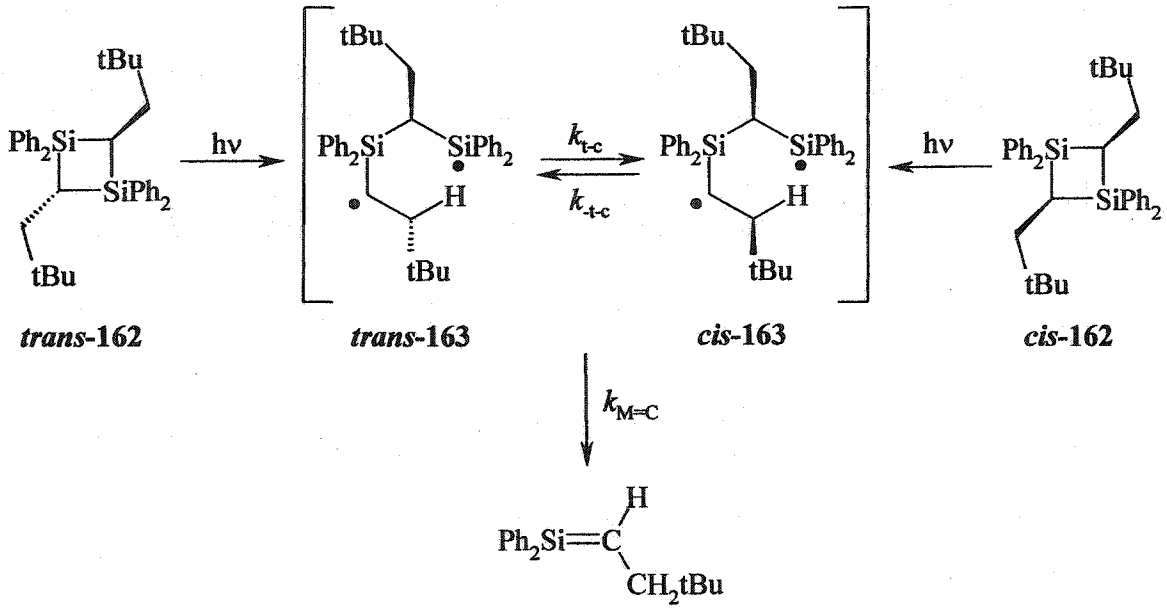

***trans*-162** ***trans*-163** ***cis*-163** ***cis*-162**

165

The photochemistry of the analogous germanium compound **33b** can be interpreted slightly more conclusively, but with great caution. The higher quantum yield for germene formation from **33b** suggests that β-scission ($k_{M=C}$) of **161b** might be occurring with reasonable efficiency relative to ring closure (k_{RC}). At this time it is not known what the actual relative rates are, but the results support the possibility that $k_{M=C} > k_{RC}$, which is what the slightly positive E_a for the stepwise dimerization of **31b** requires.

4.2.5 The Possibility of a Concerted Mechanism

Much of this discussion has been concerned with evaluating the reported results in the context of the stepwise dimerization mechanism proposed by Bernardi and coworkers (equation 4.3).[218] However, the observed activation energies are also consistent with a

concerted mechanism. Houk and Rondan have used *ab initio* calculations (RHF/3-21G) to study the cycloaddition reactions of dichlorocarbene and difluorocarbene with alkenes.[234] They showed that negative activation energies can result even for reactions that do not involve an intermediate. This type of behaviour can result if the concerted reaction is highly exothermic, and the $\Delta G^{\neq}$ term is dominated by entropy (Figure 4.7). Therefore, it is feasible that the dimerization of **31a** and **b** could proceed via a concerted mechanism similar to that proposed by Seidl et. al.[215]

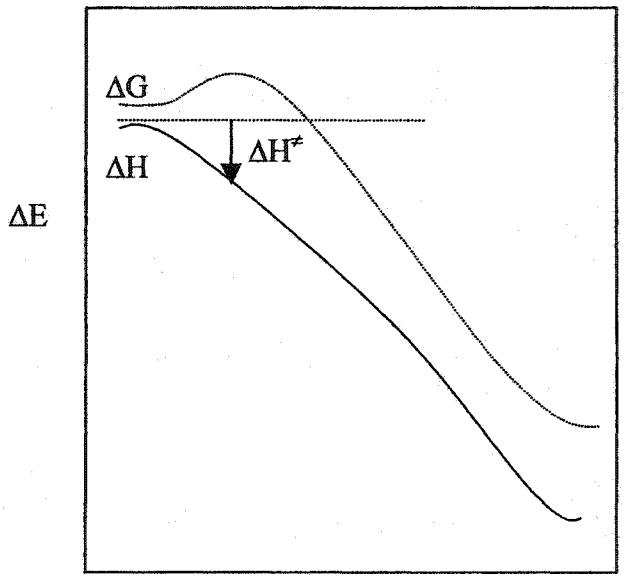

Figure 4.7 Hypothetical reaction coordinate diagram for the concerted dimerization of 1,1-diphenylmetallaenes. The solid line (—) represents the reaction curve for ΔH while the dotted line (- - - -) represents that for ΔG.

4.3 Summary

The absolute rate constants for dimerization of 1,1-diphenylsilene and 1,1-diphenylgermene have been determined in hexane solution at room temperature. Both species dimerize in head-to-tail fashion at close to the diffusion-controlled rates in hexane and are the fastest bimolecular reactions of 1,1-diphenylmetallaenes that have been studied. The activation energy for dimerization is slightly negative for 1,1-diphenylsilene and slightly positive for 1,1-diphenylgermene. At this point, none of the proposed mechanisms for silene dimerization can be ruled out. More rigorous experimental work is necessary to address this difficult problem (see Chapter 5).

Chapter 5

Conclusion

5.1 Implications of this Work

This work includes the first determination of an absolute rate constant measured for the rearrangement of an α-silylcarbene in solution. Although it is a significant contribution to the field of organosilicon reactive intermediates, it also contributes to the large amount of kinetic data known for carbenes in general, creating a link between the two fields. The rate constant for silene formation from the (trimethylsilyl)carbene is one of the largest known, and is exceeded only by the [1,2]-hydrogen migration in ethylidene (**90**).

The results for (trimethylsilyl)diazomethane (**84**) illustrate that irradiation in different regions of the absorption spectrum leads to different photochemical outcomes with good selectivities. Photolysis at 419 nm (in the n,π* band) leads to the exclusive formation of (trimethylsilyl)diazirine; photolysis at 351 nm results in formation of 1,1,2-trimethylsilene with no evidence of singlet (trimethylsilyl)carbene, suggesting that silene formation from the diazo compound occurs strictly via an excited state reaction.

The determination of absolute rate constants for the addition of nucleophiles to Wiberg's transient silene (1,1-dimethyl-2,2-bis(trimethylsilyl)silene) is an important

contribution to the systematic kinetic investigation of substituent effects on the reactivities of silicon-carbon double bonds. The determination of the absolute rate constant for Wiberg's transient silene has linked the very first kinetic investigation of silene reactivity with more recent studies. Furthermore, this work, along with previous investigations in our group,[102,104] have defined the effect of substituents on k_{MeOH} within the $5x10^7 - 1.5x10^{10}$ M^{-1} s^{-1} range. Now the values for k_{MeOH} can be predicted for silenes that react within this kinetic range. A good example of this was the successful prediction of k_{MeOH} for the other two silenes formed in the photolysis of **88a** and **b**: *E*- or *Z*-1,2-dimethyl-1,2-bis(trimethylsilyl)silene (***E/Z*-152**) or 1,1,2-trimethyl-2-pentamethyldisilanylsilene (**153**).

This work also includes the first study on the absolute kinetics of head-to-tail dimerization of a silene in the condensed phase, and the first study of any kind on the kinetics of germene dimerization. It is also the first determination of the Arrhenius parameters for the head-to-tail dimerization of silenes and germenes in the condensed phase. The results of this thesis are not able to support conclusively any of the three proposed mechanisms for dimerization of metallaenes. However, the results from the dimerization of 1,1-diphenylgermene do support a possible stepwise mechanism, though more work is necessary in this area to test this hypothesis. One way to examine this further would be to study the photochemistry of the germanium analogues of ***cis***- and ***trans*-162**.

5.2 Future Directions

The kinetics of methanol addition to Wiberg's transient silene in THF is intriguing and worth further investigation. Because of its potent electrophilicity, it is possible that this silene exists primarily as its solvent complex at room temperature. Such complexation has distinct effects on silene reaction mechanisms. The addition of more acidic nucleophiles to Wiberg's transient silene in THF might lead to initial protonation followed by nucleophilic attack, an observation that would be the first of its kind in silene chemistry.

The difficulty arises from finding a suitable precursor and technique for the investigation. Clearly, flash photolysis (248 nm) of (pentamethyldisilanyl)(trimethylsilyl)diazomethane (**88a**) is not the best method because the observation of spectral shifts of the transients are masked by photobleaching of the precursor. Furthermore, a clean source of **11a** is also desirable, since this study has shown that the overlapping absorption of the lower yielding silenes leads to problems in assigning the transients conclusively.

The challenge then becomes designing another method to determine the absolute kinetics for nucleophilic addition to **11a** in THF. Clearly, fast time-resolved techniques are required, suggesting that flash photolysis is still the best method. The UV spectrum of THF prohibits the use of a precursor that requires 193-nm excitation, because the solvent absorbs at wavelengths below 210 nm. With this criterion in mind, the design of a precursor becomes exceedingly difficult, because **11a** itself does not contain a suitable chromophore for excitation above 200 nm.

An alternative to studying **11a** is to study another electrophilic silene, such as 1,1-diphenyl-2,2-bis(trimethylsilyl)silene (**167**). Wiberg has generated this silene previously, using the thermal salt elimination method.[31,133] The 1,3-disilacyclobutane dimer (**168**) would be a good photochemical precursor to **167**, since irradiation at 248 nm might result in the formation of **167** as the single product, just as the photolysis of other 1,3-disilacyclobutanes has resulted in silene formation.[227,235] The dimer could be synthesized by generating the silene via the thermal salt elimination (**169**) in the absence of a nucleophilic trap (Scheme 5.1).

Scheme 5.1 Synthesis of 1,1,3,3-Tetraphenyl-2,2,4,4-Tetrakis(trimethylsilyl)-1,3-Disilacyclobutane (168) and the Photochemical Generation of 1,1-Diphenyl-2,2-bis(trimethylsilyl)silene (167)

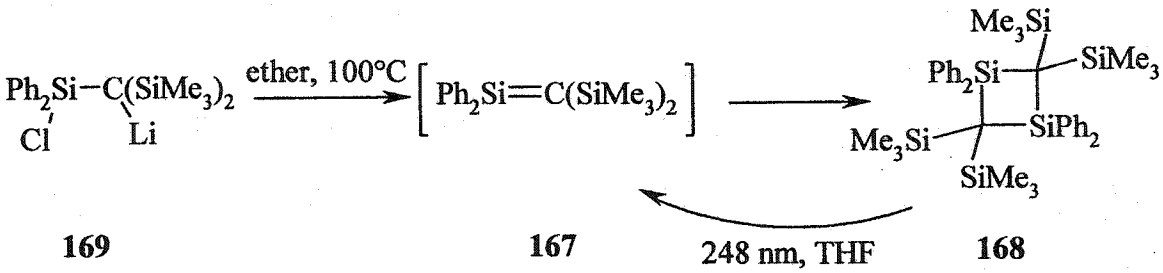

The determination of the mechanism for head-to-tail dimerization of metallaenes requires a metallaene precursor that does not depend on a biradical intermediate to generate the metallaene. However, if the metallaene contained a radical probe, such as a cyclopropyl ring at carbon, the products formed would shed light on the possibility of a biradical mechanism (Scheme 5.2). The generation of a 2-cyclopropylsilene (**171**) would be ideal, as the cyclopropyl group can serve as a "radical clock."[236,237] However, the

generation of a silene with a cyclopropyl group at carbon is likely to require a precursor that would be challenging to synthesize.

For example, thermolysis of the "anthracene-trapped silene" (**170**) would yield silene (**171**) that could dimerize with head-to-tail regiochemistry to give a biradical (**172**). This biradical can undergo ring closure to give the 1,3-disilacyclobutane (**173**) or the cyclopropyl ring will open and form products (**175** and **176**) that are consistent with the intermediacy of a second biradical (**174**). Formation of only head-to-tail dimer would support a concerted mechanism, unless ring closure is faster than cyclopropyl ring opening.

Scheme 5.2 Dimerization of 1,1-Dimethyl-2-cyclopropylsilene

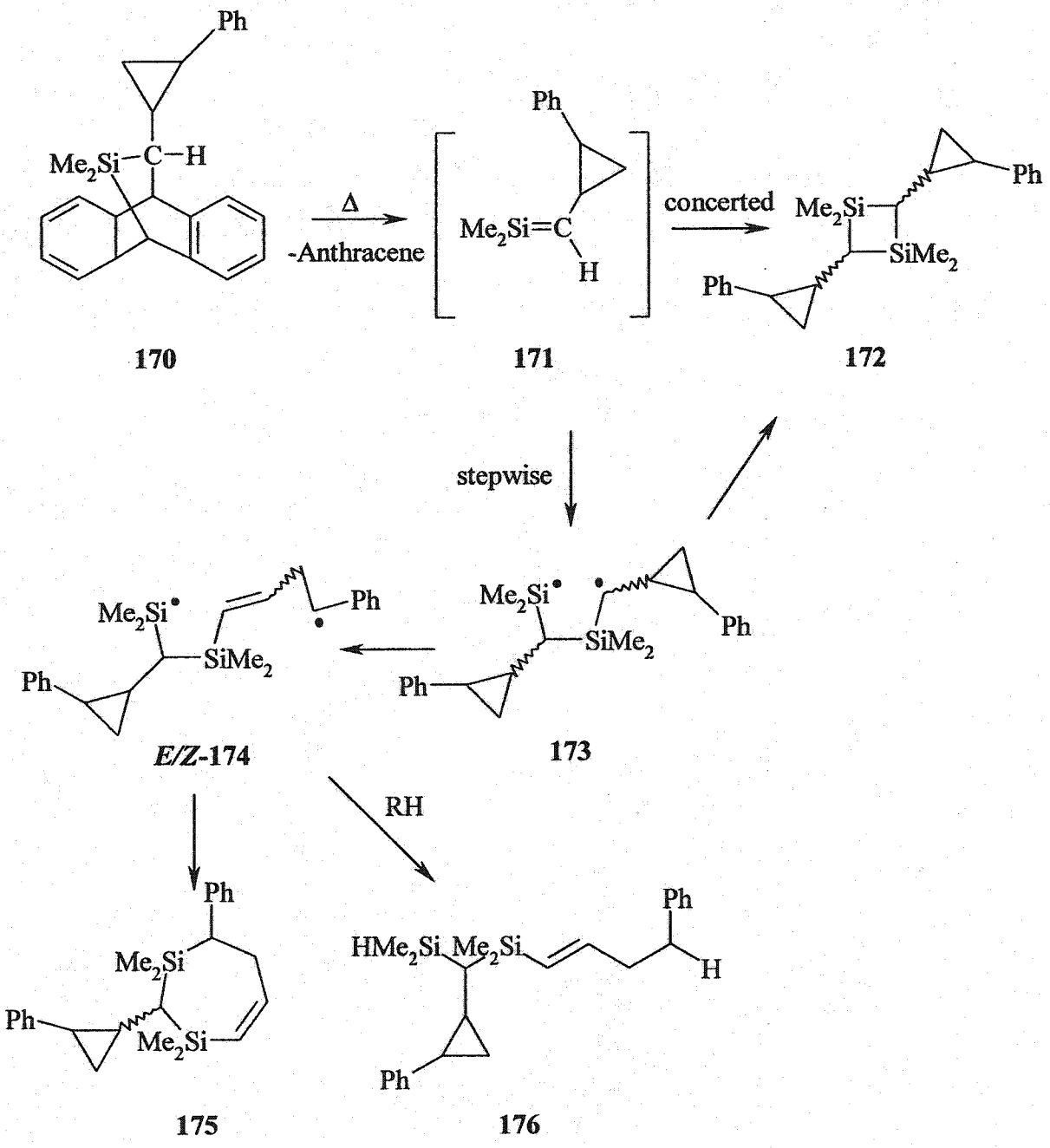

Chapter 6

Experimental

6.1 General

^{1}H and ^{13}C NMR spectra were recorded on Bruker AV200, or DRX500 NMR spectrometers in deuterated chloroform or cyclohexane-d_{12} solutions and are reported in parts per million downfield from tetramethylsilane using residual hydrogenated solvent resonances as the internal standard. Ultraviolet absorption spectra were recorded on a Perkin-Elmer Lambda 9 or Varian Cary 50 spectrophotometers. Low resolution mass spectra and GC/MS analyses were determined using a Hewlett-Packard 5890 gas chromatograph equipped with a HP-5971A mass selective detector and a DB-5 or DB-1701 fused silica capillary column (30 m x 0.25 mm; Chromatographic Specialties, Inc. or Agilent Technologies). Infrared spectra were recorded on a BioRad FTS-40 FTIR spectrophotometer and are reported in wavenumbers (cm^{-1}). Analytical gas chromographic analyses were carried out using a Hewlett-Packard 5890II+ gas chromatograph equipped with a flame ionization detector, Hewlett-Packard 3396A integrator, conventional heated splitless injector and either DB-1 or DB-1701 fused silica capillary columns (15 m x 0.20 mm; Chromatographic Specialties). Semi-preparative gas chromatographic separations were carried out using a Varian 3300 gas chromatograph equipped with a thermal conductivity detector and stainless steel column (3% OV-17 on

Chromosorb W, HP 80/100; 6' x 0.25"; Chromatographic Specialties, Inc.). Radial chromatographic separations employed a Chromatotron® (Harrison Research, Inc.), 2- or 4 mm silica gel 60 thick-layer plates, and hexanes as the eluant.

6.2 Commercial Reagents and Solvents

Hexane (EM Science, Omnisolv®) was distilled from sodium under dry nitrogen. Tetrahydrofuran (HPLC grade, Caledon) was refluxed for several days over potassium under dry nitrogen and distilled. Methanol (spectroscopic grade), ethanol (spectroscopic grade), 2-propanol (spectroscopic grade), *tert*-butyl alcohol (HPLC grade), methanol-O*d* and acetic acid, 1,3-dibromopropane, and hexamethyldisilane were used as received from Aldrich Chemical Co. Cyclohexanol and *tert*-butylamine (Aldrich) were distilled immediately prior to use. (Trimethylsilyl)diazomethane (**84**) was used as received (Aldrich) as a 2.0 M solution in hexanes for synthetic purposes. It was further purified by semi-preparative gas chromatography prior to its use in photochemical experiments. Pentane (reagent grade, Caledon), and diethyl ether (Caledon) were used as received. Diphenylgermanium dichloride and diphenyldichlorosilane (Gelest, Inc.) were used as received.

6.3 Nanosecond Laser Flash Photolysis

Nanosecond laser flash photolysis experiments employed the pulses from a Lambda-Physik Compex 100 excimer laser in conjunction with a home-built detection

system[238] or a Luzchem® LS-100 laser flash photolysis system. The laser was filled with F_2/Ar/Ne mixtures to provide pulses at 193 nm (12-25 ns, 30-70 mJ); with F_2/Kr/Ne mixtures to provide pulses at 248 nm (15-20 ns, 70-120 mJ); or with F_2/Xe/Ne mixtures to provide pulses at 351 nm (20-25 ns, 15 mJ). A Lumonics TE-861M exicimer laser was filled with Xe/HCl/Ne mixtures to provide pulses at 308 nm (15 ns, 45 mJ); or with N_2/He mixtures to provide pulses at 337 nm (6 ns, 5 mJ). The system incorporates a brass sample holder whose temperature is controlled by a VWR 1155 constant temperature circulating bath. Solution temperatures were measured with a Teflon-coated copper/constantan thermocouple inserted directly into the sample cell, and are considered accurate to ±0.1°C.

6.3.1 Determination of Bimolecular Rate Constants and Transient Absorption Spectra Under Flow Conditions

Solutions of **81a, 83, 87, 88a, 88b, 30a, 30b, 33a** and **33b** and were prepared at concentrations such that the absorbance at the excitation wavelength was ca. 0.7 (0.4 – 5 x10^{-3} M), and were flowed continuously through a 3 x 7 mm or 7 x 7 mm Suprasil flow cell connected to a calibrated 50 or 100 mL reservoir. The solutions were deoxygenated continuously with a stream of dry nitrogen. Oxygen quenching studies were carried out using a Matheson 600 gas proportioner to regulate the composition of oxygen/nitrogen mixtures that were bubbled continuously through the solution. Reagents were added directly to the reservoir by microlitre syringe as aliquots of standard solutions. Rate constants were calculated by least-squares analysis of decay rate vs. concentration data (6-15 points) that spanned at least a factor of five in the transient decay rate. Errors are

quoted as twice the standard deviation ($\pm 2\sigma$) obtained from the least-squares analysis in each case.

6.3.2 Pyridine Trapping of Trimethylsilylcarbene (124-s)

Mixtures of a hexane stock solution of (trimethylsilyl)diazomethane (2.0 M) or (trimethylsilyl)diazirine (2.0 M) with a stock solution of pyridine were made to total 2 mL with varying concentrations of pyridine. Each solution was saturated with argon for 30 min. in a 7 x 7 mm static quartz cell. Flash photolysis of (trimethylsilyl)diazomethane-pyridine mixtures with 351 nm or (trimethylsilyl)diazirine-pyridine mixtures with 337 or 308 nm. Maximum absorbances of the resulting ylides were measured at 370 or 390 nm for each of the pyridine-precursor solutions. Each measurement was taken one after the other to ensure constant light intensity for each concentration.

6.3.3 Determining Extinction Coefficients for 31a and 31b

Hexane solutions of 1,1-diphenylsilacyclobutane (**30a**, ca. 3×10^{-3} M) and 1,1-diphenylgermacyclobutane (**30b**, ca. 4×10^{-3} M) and an acetonitrile solution of benzophenone (**159**, ca. 5×10^{-4} M) were made up such that they were all optically matched at 248 nm ($A_{248nm} = 0.60 \pm 0.02$). All three solutions were degassed for one hour. Solutions of **30a** and **30b** were flowed through separate 3 x 7 mm sample cells (ca. 2-3 drops per second) while **159** was contained in a 3 x 7 mm static cell. Maximum absorbances of **31a** (325 nm), **31b** (325 nm) and $\mathbf{159}^{3*}$ (525 nm) were measured upon

flash photolysis of their respective precursors. The laser intensity was varied by a series of homemade screens of various optical densities, which were calibrated using the Varian Cary 50 spectrophotometer.

6.4 Preparation and Characterization of Compounds

(Trimethylsilyl)diazirine (87) was synthesized by photolysis of an deaerated solution (0.2 M) of **84** in pentane in a Rayonet Reactor fitted with 10 RPR-419X lamps (419 nm) for 4 hours. The progress of the reaction was followed by UV-spectroscopy and GC and continued to >97% conversion of **84**. The resulting solution was concentrated to ca. 2 M by slow, cautious distillation. The concentration of the distillate was determined by measuring its UV absorption spectrum. The extinction coefficient at 332 nm (ε_{332nm}= 48 L mol^{-1} cm^{-1}) was used to determine the approximate concentration of the distilled solution. The ^{1}H NMR and UV spectra of **87** compared favourably to reported literature data.[171] ^{1}H NMR ($CDCl_3$); δ -0.25 (s, 9H), δ 0.11 (s, 1H); $UV^{pentane}$ / nm (ε / L mol^{-1} cm^{-1}): 340 (39), 332 (48), 322 (43), 315 (35), and 308 nm (30).

(Trimethylsilyl)ketene (81a) and **(pentamethyldisilanyl)(trimethylsilyl)ketene (88b)** were provided by collaborators T. Tidwell and K. Sung and were prepared according to their previously published method.[239]

(Pentamethyldisilanyl)(trimethylsilyl)diazomethane (88a) was synthesized an adaptation of the literature procedure of Seyferth et al. for bis(trimethylsilyl)diazomethane.[194] (Trimethylsilyl)diazomethane (0.0088 mol) and 100 mL of dry pentane were added to a 2-necked, 250 mL round bottom flask fitted with a stir bar, condenser, nitrogen inlet and rubber septum. This solution was cooled to -78°C under a nitrogen atmosphere. n-Butyllithium (5 mL of a 1.6 M solution; 0.0088 mol) was added dropwise via syringe. At the completion of the addition, a light yellow precipitate had formed. The mixture was allowed to stir for 2 hours, while the temperature was maintained at < -20°C. At the end of the 2-hour period, the reaction was cooled to -78°C again and chloropentamethyldisilane (0.0088 mol, prepared from hexamethyldisilane according to the method of Sakurai[195], boiling point: 128-130; lit. b.p.131-132) was added dropwise to the solution, which resulted in the evolution of a white gas. The reaction was allowed to warm to room temperature overnight with stirring. The orange reaction mixture was then concentrated under reduced pressure and bulb-to-bulb distilled (0.02 mmHg) after three freeze-pump-thaw cycles, yielding a yellow liquid. This material was then purified by semi-preparative chromatography to yield 0.30 g (0.0012 mol, 16% yield) of **88a**, as a bright yellow liquid. The compound was identified by comparison of the following spectroscopic data to literature values[184]: ^{1}H NMR ($CDCl_3$) δ 0.0.106 (s, 9), 0.152 (s, 9), 0.179 (s, 6); IR (neat) 2955.3 (w), 2943.2 (w), 2040.5 (s), 1251.2 (m), 1221.5 (m), 922.8 (w), 836.7 (m), 790.9 (m); MS (EI) *m/z* = 244 (2), 216 (20), 201 (100), 185 (10), 171 (5), 141 (3), 130 (17), 113 (10), 73 (80), 59 (30), 45 (25).

1,1-Diphenylsilacyclobutane (30a) and 1,1-diphenylgermacyclobutane (30b) were synthesized according to the procedure of Leigh and Toltl.[90] The products were purified by radial chromatography followed by column chromatography using hexanes as the eluant, to >98% purity as measured by GC/FID. The compounds were identified by comparison of their ^{1}H NMR and mass spectra to previously reported data for these two compounds.[72,90,128]

1,1,3,3-Tetraphenyl-1,3-disilacyclobutane (33a) was synthesized from the photolysis of **30a**.[91] A solution of **30a** (0.250 g, 0.009 mol) in hexane (15 mL) was divided into two 1 x 10 cm quartz tubes, sealed with rubber septa and saturated with argon. Photolysis was carried out with 10 RPR-2357A lamps (254 nm) in a Rayonet reactor for six hours. The solvent was removed by rotary evaporation to yield a yellow oil. The product was purified by radial chromatography using hexane as the eluant to recover **30a**. Once the starting material was recovered, the eluant was changed to 10% methylene chloride in hexane. The methylene chloride was removed by rotoratory evaporation to yield a solid, white product. This material was recrystallized twice from pentane and identified as **33a**, by comparison of its ^{1}H NMR spectrum and melting point to previously reported data (m.p. 134-135°, lit. 135-136°[240]).

6.5 Steady-State Photolysis Methods

6.5.1 Analytical-Scale Photolyses of (Trimethylsilyl)diazomethane and –diazirine

A hexane solution containing (trimethylsilyl)diazomethane (**84**, 0.001 M) and *t*-butyl alcohol (0.15 M) was placed in a 3 mm x 10 mm quartz tube, sealed with a rubber septum and saturated with argon. Photolysis was carried out with 4 RPR-2537A low pressure mercury lamps (254 nm) in a Rayonet reactor and led to the formation of a single product up to 20-50% conversion of the starting material. The compound was identified as $\mathbf{144}_{t\mathrm{Bu}}$ by comparison of its retention time and mass spectrum to the spectroscopic data reported for $\mathbf{144}_{t\mathrm{Bu}}$ from the photolysis of **81a** in methanolic hexane, which was identified by coinjection of an authentic sample.[102] MS *m/z* = 160 (0.05), 145 (15), 131 (19), 89 (20), 87 (22), 75 (100), 61 (22), 59 (21), 45 (13).

A hexane solution containing (trimethylsilyl)diazomethane (**84**, 0.01 M) and *t*-butyl alcohol (0.3 M) was placed in a 1 cm x cm quartz UV cell, sealed with a rubber septum and saturated with argon. Photolysis was carried out with 8 RPR-4190A low pressure mercury lamps (419 nm) in a Rayonet reactor and led to the formation of a single product up to 90% conversion of the starting material. This compound was identified as **87** by comparing the UV-vis and ^{1}H NMR spectra to known literature values,[171] and to the spectroscopic data reported for **87** in section 6.4.

A hexane solution containing (trimethylsilyl)diazirine (**87**, 0.02 M) and *t*-butyl alcohol (0.3 M) was placed in a 3 mm x 10 mm quartz tube, sealed with a rubber septum and saturated with argon. Photolysis was carried out with 8 RPR-3000A lamps (300 nm)

in a Rayonet reactor and led to the exclusive formation of **144$_{tBu}$** up to 40% conversion of the starting material.

6.5.2 Analytical Scale Photolyses of (Pentamethyldisilanyl)(trimethylsilyl)-diazomethane and –ketene

A hexane solution containing **(pentamethyl)(trimethylsilyl)ketene (88b**, 0.003 M) and methanol or *tert*-butyl alcohol (0.02 M) was placed in a 3 mm x 10 mm quartz tube, sealed with a rubber septum and saturated with argon. Photolysis was carried out with a zinc resonance lamp (214 nm; Philips 93106E) and the course of the reaction was monitored by GC/MS (DB1701 column) between 5 and 20% conversion. One major product (**144$_R$**) and two minor ones were detected. The two minor products detected are **149$_R$** and **150$_R$**; it was later learned that **151$_R$** coelutes with **144$_R$** under these GC conditions. Continued photolysis of **88b** resulted in the formation of a variety of low molecular weight secondary photolysis products.

A hexane solution containing **(pentamethyl)(trimethylsilyl)diazomethane (88a**, 0.001 M) and methanol or *tert*-butyl alcohol (0.02 M) was placed in a 3 mm x 10 mm quartz tube, sealed with a rubber septum and saturated with argon. Photolysis was carried out with one or two RPR-2537A lamps (254 nm) in a Rayonet reactor and the course of the reaction was monitored by GC/MS (DB1701 column) up to 95% conversion. The longer wavelength excitation source used for **88a** allowed it to be taken to quite high conversions with no evidence for the formation of the low molecular weight secondary photolysis products observed in the photolysis of **88b**.

A solution of **88a** (0.024 M) in C_6D_{12} and 0.15 M methanol was placed in a quartz NMR tube, sealed with a rubber septum and saturated with argon. Photolysis to ca. 95% conversion by GC led to the observation of methoxysilane products in the ratio 77.8 : 5.8 : 8.9 : 7.6. When this product mixture was analyzed by GC/MS (DB-5 column), four products were observed in the ratio 79.6 : 7.9 : 4.5 : 8.7. The mass spectra of these products (Figure 3.4a-d) all exhibited molecular ions ($M^{+\bullet}$) of $m/z = 248$. The product formed in 8.7 % yield (8.9% by NMR) was assigned to $\mathbf{151_{Me}}$ on the basis of its stronger $M^{+\bullet}$-73 peak compared to those in the mass spectra of the other three products.

An NMR-scale photolysis of **88a** (0.024 M) in C_6D_{12} in the presence of *tert*-butyl alcohol (0.15 M) led to the observation of a single major product with resonances that compared favourably to those observed by Ando and Sekiguchi for $\mathbf{144_{Bu}}$.[184] When the same solution was analyzed by GC/MS (DB-5 column), three *tert*-butoxysilane products ($M^{+\bullet} = 290$) in the ratio 83.5 : 8.5 : 8.0 were observed. Presumably the fourth isomer coeluted with the major product ($\mathbf{144_{Bu}}$).

6.5.3 Preparative Scale Photolysis of 88a in the Presence of Methanol

A hexane solution containing **88a** (250 mg) and 0.2 M methanol was carried out in two 1 cm x 15 cm quartz tubes which were sealed with rubber septa and purged with argon. Photolysis of this mixture was carried to 90-95% conversion of **88a** as determined by GC. The crude photolysis mixture was stripped of solvent, and the resulting products were collected as mixtures by semi-preparative GC, taking two different cuts (Figure 3.5a and b) to produce mixtures of different compositions. Comparison of the ^1H NMR

spectra of the two mixtures in $CDCl_3$ allowed partial assignment of the NMR spectra of the three minor products.

144_{Me} (79.6%): ^{1}H NMR ($CDCl_3$), δ -0.5165 (s, 1H), 0.1021 (s, 18H), 0.1687 (s, 6H), 3.3709 (3H); MS *m/z* = 248 (0.5), 233 (100), 203 (7), 175 (2), 147 (3), 145 (4), 129 (20), 115 (5), 89 (5), 73 (13), 59 (12).

149_{Me} (5.8%): ^{1}H NMR ($CDCl_3$) δ 0.9775 (d, 3H), 3.4122 (s, 3H); MS *m/z* = 248 (4), 233 (100), 203 (7), 175 (48), 147 (11), 145 (14), 129 (23), 117 (11), 89 (30), 73 (46), 59 (30).

150_{Me} (7.6%): ^{1}H NMR ($CDCl_3$) δ 1.105 (d, 3H), 3.429 (s, 3H); MS *m/z* = 248 (8), 233 (90), 203 (10), 175 (100), 147 (28), 145 (26), 129 (26), 117 (26), 89 (60), 73 (81), 59 (54).

151_{Me} (8.9%): ^{1}H NMR ($CDCl_3$) δ 0.2061 (q, 1H), 1.0431 (d, 3H), 3.405 (s, 3H); MS *m/z* = 248 (3), 233 (11), 203 (3), 175 (100), 147 (3), 145 (5), 131 (5), 129 (5), 117 (7), 89 (24), 73 (24), 59 (17).

6.5.4 Competitive Trapping Experiments with 88a

A hexane solution containing **(pentamethyl)(trimethylsilyl)diazomethane (88a**, 1.3 M), *tert*-butyl alcohol (1.4 M) and cyclohexanol (1.4 M) or methanol (1.4 M) were placed in a 3 mm x 10 mm quartz tube, sealed with a rubber septum and saturated with argon. Photolysis was carried out with one or two RPR-2537A lamps (254 nm) in a Rayonet reactor and the course of the reaction was monitored by GC/MS (DB-1701

column) up to 95% conversion. The ratio of the major products ($\mathbf{144_{CHX}}$:$\mathbf{144_{Bu}}$ = 1.9±0.3) was determined from peak ratios from GC/FID analysis. Products were tentatively identified based on their mass spectra. $\mathbf{144_{CHX}}$: MS (EI) *m/z* = 316 (1), 301 (25), 219 (100), 203 (43), 187 (15), 133 (13), 129 (50), 83 (14), 73 (70), 57 (44), 41 (23). $\mathbf{144_{Bu}}$: MS (EI) *m/z* = 275 ($M^{+\bullet}$-15) (1), 219 (100), 203 (9), 187 (4), 161 (1), 143 (2), 129 (12), 113 (2), 99 (2), 85 (3), 73 (15), 57 (8).

6.6 Fluorescence Spectroscopy

Fluorescence emission spectra and lifetimes were determined using a Photon Technologies Inc. LS-100 spectrofluorimeter, which also enables lifetime determinations by time-correlated single-photon counting. Isooctane solutions of **30a,b** and **33a,b** (ca. $1x10^{-5}$ M, A<0.2 at λ_{ex}) were saturated with argon prior to measurement. The samples used for these experiments were of the highest purity (>99%), to minimize emission from any impurities. The excitation wavelength employed was 256 nm for all samples. The emission wavelengths varied, depending on the emission spectra (see Table 4.4). GC/FID analysis after the fluorescence experiments showed that no detectable decomposition of the samples occurred over the time of the experiment.

REFERENCES

(1) Bowry, V. W.; Ingold, K. U. *Acc. Chem. Res.* **1999**, *32*, 27-34.

(2) Lofgren, A.; Albertsson, A.-C.; Dubois, P.; Jerome, R. *Rev. Macromol. Chem. Phys.* **1995**, *C35*, 379-418.

(3) Gaspar, P. P. Silylenes; In *Reactive Intermediates, Vol. 3*; Jones, M. Jr., Moss, R. A., eds. John Wiley & Sons: New York, 1985; pp 333-427.

(4) Chatgilialoglu, C. *Chem. Rev.* **1995**, *95*, 1229-1251.

(5) Lopinski, G. P.; Moffat, D. J.; Wayner, D. D. M.; Wolkow, R. A. *J. Am. Chem. Soc.* **2000**, *122*, 3548-3549.

(6) Wojtyk, J. T. C.; Tomietto, M.; Boukherroub, R.; Wayner, D. D. M. *J. Am. Chem. Soc.* **2001**, *123*, 1535-1536.

(7) Sohn, H.; Calhoun, R. M.; Sailor, M. J.; Trogler, W. C. *Angew. Chem. Int. Ed. Engl.* **2001**, *40*, 2104-2106.

(8) Lambert, J. B.; Zhao, Y.; Zhang, M. *J. Phys. Org. Chem.* **2001**, *14*, 370-379.

(9) Pitzer, K. *J. Am. Chem. Soc.* **1948**, *70*, 2140-2145.

(10) Gusel'nikov, L. E.; Flowers, M. C. *J. Chem. Soc. ,Chem. Commun.* **1967**, 864-865.

(11) Kumada, M.; Tamao, K. *Adv. Organomet. Chem.* **1968**, *6*, 19-117.

(12) Gusel'nikov, L. E.; Nametkin, N. S. *Chem. Rev.* **1979**, *79*, 529-577.

(13) Raabe, G.; Michl, J. Multiple bonding to silicon; In *The chemistry of organic silicon compounds*; Patai, S., Rappoport, Z., eds. John Wiley & Sons: New York, 1989; pp 1015-1142.

(14) Brook, A. G.; Brook, M. A. *Adv. Organomet. Chem.* **1996**, *39*, 71-158.

(15) Muller, T.; Ziche, W.; Auner, N. Silicon-carbon and silicon-nitrogen multiply bonded compounds; In *The chemistry of organic silicon compounds, Vol. 2*; Rappoport, Z., Apeloig, Y., eds. John Wiley & Sons Ltd.: New York, 1998; pp 857-1062.

(16) Satge, J. *Adv. Organomet. Chem.* **1982**, *21*, 241-287.

(17) Barrau, J.; Escudie, J.; Satge, J. *Chem. Rev.* **1990**, *90*, 283-319.

(18) Escudie, J.; Couret, C.; Ranaivonjatovo, H.; Satge, J. *Coord. Chem. Rev.* **1994**, *130*, 427-480.

(19) Raabe, G.; Michl, J. *Chem. Rev.* **1985**, *85*, 419-509.

(20) Trinquier, G.; Malrieu, J. P. *J. Am. Chem. Soc.* **1981**, *103*, 6313-6319.

(21) Walsh, R. *J. Organomet. Chem.* **1972**, *38*, 245-248.

(22) Kudin, K. N.; Margrave, J. L.; Khabashesku, V. N. *J. Phys. Chem. A* **1998**, *102*, 744-753.

(23) Brown, W. H.; Foote, C. S. Alkenes II; In *Organic Chemistry*; Saunders College Publishing: Orlando, 1998.

(24) Auner, N. *J. prakt. Chem.* **1995**, *337*, 79-92.

(25) Morkin, T. L.; Owens, T. R.; Leigh, W. J. Kinetic studies of the reactions of Si=C and Si=Si double bonds; In *The chemistry of organosilicon compounds, Volume 3*; Rappoport, Z., Apeloig, Y., eds. John Wiley and Sons: New York, 2001; pp 949-1026.

(26) Wiberg, N.; Wagner, G. *Chem. Ber.* **1986**, *119*, 1455-1466.

(27) Wiberg, N.; Fischer, G.; Wagner, S. *Chem. Ber.* **1991**, *124*, 769-771.

(28) Wiberg, N.; Kim, C.-K. *Chem. Ber.* **1986**, *119*, 2966-2979.

(29) Wiberg, N.; Kim, C.-K. *Chem. Ber.* **1986**, *119*, 2980-2994.

(30) Wiberg, N. *J. Organomet. Chem.* **1984**, *273*, 141-177.

(31) Wiberg, N.; Link, M. *Chem. Ber.* **1995**, *128*, 1231-1240.

(32) Wiberg, N.; Link, M. *Chem. Ber.* **1995**, *128*, 1241-1250.

(33) Wiberg, N.; Hwang-Park, H.-S.; Lerner, H.-W.; Dick, S. *Chem. Ber.* **1996**, *129*, 471-478.

(34) Chan, T. H.; Wang, D. *Chem. Rev.* **1995**, *95*, 1279-1292.

(35) Couret, C.; Escudie, J.; Satge, J.; Lazraq, M. *J. Am. Chem. Soc.* **1987**, *109*, 4411-4412.

(36) Jones, P. R.; Lim, T. F. O. *J. Am. Chem. Soc.* **1977**, *99*, 2013-2015.

(37) Jones, P. R.; Lee, M. E.; Lin, L. T. *Organometallics* **1983**, *2*, 1039-1042.

(38) Jones, P. R.; Lee, M. E. *J. Am. Chem. Soc.* **1983**, *105*, 6725-6726.

(39) Jones, P. R.; Lee, M. E. *J. Organomet. Chem.* **1984**, *271*, 299-306.

(40) Auner, N.; Ziche, W.; Herdtweck, E. *J. Organomet. Chem.* **1992**, *426*, 1-22.

(41) Auner, N.; Seidenschwarz, C. *Z. Naturforsch.* **1990**, *45B*, 909-920.

(42) Auner, N.; Heikenwalder, C.-R.; Wagner, C. *Organometallics* **1993**, *12*, 4135-4140.

(43) Ziche, W.; Auner, N.; Behm, J. *Organometallics* **1992**, *11*, 2494-2499.

(44) Auner, N. *J. Organomet. Chem.* **1989**, *377*, 175-195.

(45) Auner, N. *J. Organomet. Chem.* **1987**, *336*, 83-103.

(46) Lowry, T. H.; Richardson, K. S. Pericyclic Reactions; In *Mechanism and Theory in Organic Chemistry*; Harper Collins Publishers: New York, 1987.

(47) Steinmetz, M. G. *Chem. Rev.* **1995**, *95*, 1527-1588.

(48) Ishikawa, M.; Fuchikami, T.; Kumada, M. *J. Organomet. Chem.* **1976**, *117*, C58-C62.

(49) Ishikawa, M.; Fuchikami, T.; Kumada, M. *J. Organomet. Chem.* **1978**, *149*, 37-48.

(50) Ishikawa, M.; Kumada, M. *Adv. Organomet. Chem.* **1981**, *19*, 51-95.

(51) Leigh, W. J.; Bradaric, C. J.; Sluggett, G. W.; Venneri, P.; Conlin, R. T.; Dhurjati, M. S. K.; Ezhova, M. B. *J. Organomet. Chem.* **1998**, *561*, 19-27.

(52) Conlin, R. T.; Bobbitt, K. L. *Organometallics* **1987**, *6*, 1406-1410.

(53) Kira, M.; Maruyama, T.; Sakurai, H. *J. Am. Chem. Soc.* **1991**, *113*, 3986-3987.

(54) Ishikawa, M.; Fuchikami, T.; Kumada, M. *J. Organomet. Chem.* **1976**, *118*, 139-153.

(55) Ishikawa, M.; Fuchikami, T.; Kumada, M. *J. Organomet. Chem.* **1976**, *118*, 155-160.

(56) Ishikawa, M.; Fuchikami, T.; Kumada, M. *J. Organomet. Chem.* **1977**, *133*, 19-28.

(57) Leigh, W. J.; Sluggett, G. W. *Organometallics* **1994**, *13*, 269-281.

(58) Leigh, W. J.; Sluggett, G. W. *J. Am. Chem. Soc.* **1994**, *116*, 10468-10476.

(59) Leigh, W. J.; Toltl, N. P.; Apodeca, P.; Castruita, M.; Pannell, K. H. *Organometallics* **2000**, *19*, 3232-3241.

(60) Ishikawa, M.; Nishimura, K.; Sugisawa, H.; Kumada, M. *J. Organomet. Chem.* **1980**, *194* , 147-158.

(61) Ishikawa, M.; Fuchikami, T.; Kumada, M. *J. Am. Chem. Soc.* **1977**, *99*, 245-247.

(62) Ishikawa, M.; Sugisawa, H.; Fuchikami, T.; Kumada, M.; Yamabe, T.; Kawakami, H.; Fukui, K.; Ueki, Y.; Shizuka, H. *J. Am. Chem. Soc.* **1982**, *104*, 2872-2878.

(63) Ishikawa, M.; Matsuzawa, S.; Sugisawa, H.; Yano, F.; Kamitori, S.; Higuchi, T. *J. Am. Chem. Soc.* **1985**, *107*, 7706-7710.

(64) Kerst, C.; Rogers, C. W.; Ruffolo, R.; Leigh, W. J. *J. Am. Chem. Soc.* **1997**, *119*, 466-471.

(65) Kerst, C.; Ruffolo, R.; Leigh, W. J. *Organometallics* **1997**, *75*, 5804-5810.

(66) Miracle, G. E.; Ball, J. L.; Powell, D. R.; West, R. *J. Am. Chem. Soc.* **1993**, *115*, 11598-11599.

(67) Brook, A. G.; Nyburg, S. C.; Abdesaken, F.; Gutekunst, B.; Gutekunst, G.; Kallury, R. K. M. R.; Poon, Y. C.; Chang, Y.; Wong-Ng, W. *J. Am. Chem. Soc.* **1982**, *104*, 5667-5672.

(68) Brook, A. G. The photochemistry of organosilicon compounds; In *The chemistry of organic silicon compounds*; Patai, S., Rappoport, Z., eds. John Wiley & Sons: New York, 1989; pp 965-1005.

(69) Brook, A. G.; Harris, J. W.; Lennon, J.; El Sheikh, M. *J. Am. Chem. Soc.* **1979**, *101*, 83-95.

(70) Brook, A. G.; Kallury, R. K. M. R.; Poon, Y. C. *Organometallics* **1982**, *1*, 987-994.

(71) Damrauer, R. *Organomet. Chem. Rev. A* **1972**, *8*, 67-133.

(72) Auner, N.; Grobe, J. *J. Organomet. Chem.* **1980**, *188*, 25-52.

(73) Auner, N.; Grobe, J.; Muller, T.; Rathmann, H. W. *Organometallics* **2000**, *19*, 3476-3485.

(74) Gusel'nikov, L. E.; Nametkin, N. S.; Vdovin, V. M. *Acc. Chem. Res.* **1975**, *8*, 18-25.

(75) Davidson, I. M. T.; Dean, C. E.; Lawrence, F. T. *J. Chem. Soc. ,Chem. Commun.* **1981**, *1981*, 52-53.

(76) Davidson, I. M. T.; Wood, I. T. *J. Chem. Soc. ,Chem. Commun.* **1982**, 550-551.

(77) Grobe, J.; Ziemer, H. *Z. Naturforsch. [B].* **1993**, *48*, 1193-1202.

(78) Davidson, I. M. T.; Fenton, A.; Ijadl-Maghsoodi, S.; Scampton, R. J.; Auner, N.; Grobe, J.; Tillman, N.; Barton, T. J. *Organometallics* **1984**, *3*, 1593-1595.

(79) Walsh, R. *Acc. Chem. Res.* **1981**, *14*, 246-252.

(80) Steinmetz, M. G.; Bai, H. *Organometallics* **1989**, *8*, 1112-1113.

(81) Golino, C. M.; Bush, R. D.; On, P.; Sommer, L. H. *J. Am. Chem. Soc.* **1975**, *97*, 1957-1958.

(82) Leigh, W. J.; Bradaric, C. J.; Sluggett, G. W. *J. Am. Chem. Soc.* **1993**, *115*, 5332-5333.

(83) Bradaric, C. J.; Leigh, W. J. *Can. J. Chem.* **1997**, *75*, 1393-1402.

(84) Leigh, W. J. *Pure Appl. Chem.* **1999**, *71*, 453-462.

(85) Barton, T. J.; Marquardt, G.; Kilgour, J. A. *J. Organomet. Chem.* **1975**, *85*, 317-325.

(86) Gordon, M. S.; Barton, T. J.; Nakano, H. *J. Am. Chem. Soc.* **1997**, *119*, 11966-11973.

(87) Becerra, R.; Walsh, R. Thermochemistry; In *The chemistry of organic silicon compounds*; Rappoport, Z., Apeloig, Y., eds. John Wiley & Sons: New York, 1998; pp 153-180.

(88) Khabashesku, V. N.; Kudin, K. N.; Tamas, J.; Boganov, S. E.; Margrave, J. L.; Nefedov, O. M. *J. Am. Chem. Soc.* **1998**, *120*, 5005-5016.

(89) Leigh, W. J.; Bradaric, C. J.; Kerst, C.; Banisch, J. H. *Organometallics* **1996**, *15*, 2246-2253.

(90) Toltl, N. P.; Leigh, W. J. *J. Am. Chem. Soc.* **1998**, *120*, 1172-1179.

(91) Toltl, N. P.; Stradiotto, M. J.; Morkin, T. L.; Leigh, W. J. *Organometallics* **1999**, *18* , 5643-5652.

(92) Brook, A. G.; Nyburg, S. C.; Reynolds, W. F.; Poon, Y. C.; Chang, Y.; Lee, J. S. *J. Am. Chem. Soc.* **1979** , *101*, 6750-6752.

(93) Apeloig, Y.; Bravo-Zhivotovskii, D.; Zharov, I.; Panov, V.; Leigh, W. J.; Sluggett, G. W. *J. Am. Chem. Soc.* **1998**, *120*, 1398-1404.

(94) Barton, T. J.; Kline, E. A.; Garvey, P. M. *J. Am. Chem. Soc.* **1973**, *95*, 3078-3078.

(95) Barton, T. J.; Kilgour, J. A.; Gallucci, R. R.; Rothschild, A. J.; Slutsky, J.; Wolf, A. D.; Jones, M. Jr. *J. Am. Chem. Soc.* **1975**, *97*, 657-658.

(96) Barton, T. J. *Pure Appl. Chem.* **1980**, *52*, 615-624.

(97) Sekiguchi, A.; Ando, W. *Chem. Lett.* **1986**, 2025-2026.

(98) Sekiguchi, A.; Sato, T.; Ando, W. *Organometallics* **1987**, *6*, 2337-2341.

(99) Oku, A.; Miki, T.; Ose, Y. *J. Phys. Org. Chem.* **1996**, *9*, 619-622.

(100) Brook, A. G. The photochemistry of organosilicon compounds; In *The chemistry of organic silicon compounds*; Rappoport, Z., Apeloig, Y., eds. John Wiley and Sons: New York, 1998; pp 1233-1310.

(101) Barton, T. J.; Hoekman, S. K. *J. Am. Chem. Soc.* **1980**, *102*, 1584-1591.

(102) Leigh, W. J.; Kerst, C.; Boukherroub, R.; Morkin, T. L.; Jenkins, S.; Sung, K.; Tidwell, T. T. *J. Am. Chem. Soc.* **1999**, *121*, 4744-4753.

(103) Apeloig, Y.; Karni, M. *J. Am. Chem. Soc.* **1984**, *106*, 6676-6682.

(104) Leigh, W. J.; Boukherroub, R.; Kerst, C. *J. Am. Chem. Soc.* **1998**, *120*, 9504-9512.

(105) Baines, K. M.; Brook, A. G. *Organometallics* **1987**, *6*, 692-696.

(106) Zhang, S.; Conlin, R. T.; McGarry, P. F.; Scaiano, J. C. *Organometallics* **1992**, *11*, 2317-2319.

(107) Bravo-Zhivotovskii, D.; Zharov, I.; Kapon, M.; Apeloig, Y. *J. Chem. Soc. ,Chem. Commun.* **1995**, 1625-1626.

(108) Brix, T.; Arthur, N. L.; Potzinger, P. *J. Phys. Chem.* **1989**, *93*, 8193-8197.

(109) Low, H. C.; John, P. *J. Organomet. Chem.* **1980**, *201*, 363-369.

(110) Gusel'nikov, L. E.; Konobeyevsky, K. S.; Vdovin, V. M.; Nametkin, N. S. *Dokl. Akad. Nauk. SSSR (Engl. transl.)* **1977**, *235*, 791-794.

(111) Walsh, R. Thermochemistry; In *The Chemistry of Organic Silicon Compounds*; Patai, S., Rappoport, Z., eds. John Wiley & Sons Ltd.: 1989; pp 371-391.

(112) Brix, T.; Bastian, E.; Potzinger, P. N. *J. Photochem. Photobiol. A:Chem.* **1989**, *49*, 287-297.

(113) Vatsa, R. K.; Kumar, A.; Naik, P. D.; Upadhyaya, H. P.; Pavanaja, U. B.; Saini, R. D.; Mittal, J. P.; Pola, J. *Chem. Phys. Lett.* **1996**, *255*, 129-133.

(114) Bastian, E.; Potzinger, P.; Ritter, A.; Schuchmann, H.-P.; von Sonntag, C.; Weddle, G. *Ber. Bunsenges. Phys. Chem.* **1980**, *84*, 56-62.

(115) Namavari, M.; Conlin, R. T. *Organometallics* **1992**, *11*, 3307-3312.

(116) Sakurai, H. Mechanism and structures in alcohol addition reactions of disilenes and silenes; In *The Chemistry of Organic Silicon Compounds*; Rappoport, Z., Apeloig, Y., eds. Wiley and Sons, Ltd: 1998; pp 827-855.

(117) Morkin, T. L.; Leigh, W. J. *Acc. Chem. Res.* **2001**, *34*, 129-136.

(118) Wiberg, N.; Wagner, G.; Muller, G. *Angew. Chem. Int. Ed. Engl.* **1985**, *24*, 229-230.

(119) Wiberg, N.; Wagner, G. *Chem. Ber.* **1986**, *119*, 1467-1476.

(120) Wiberg, N.; Wagner, G.; Muller, G.; Riede, J. *J. Organomet. Chem.* **1984**, *271*, 381-391.

(121) Wiberg, N.; Joo, K. S.; Polborn, K. *Chem. Ber.* **1993**, *126*, 67-69.

(122) Wiberg, N.; Fischer, G.; Schurz, K. *Chem. Ber.* **1987**, *120*, 1605-1606.

(123) Wiberg, N.; Schurz, K.; Fischer, G. *Chem. Ber.* **1986**, *119*, 3498-3501.

(124) Wiberg, N.; Wagner, S.; Fischer, G. *Chem. Ber.* **1991**, *124*, 1981-1983.

(125) Ishikawa, M.; Fuchikami, T.; Kumada, M. *J. Organomet. Chem.* **1977**, *127*, 261-272.

(126) Sluggett, G. W.; Leigh, W. J. *J. Am. Chem. Soc.* **1992**, *114*, 1195-1201.

(127) Bradaric, C. J.; Leigh, W. J. *J. Am. Chem. Soc.* **1996**, *118*, 8971-8972.

(128) Bradaric, C. J. "A mechanistic study of the reactions of 1,1-diarylsilenes and 1-silastyrenes." *Ph.D Thesis*, **1998**, McMaster University.

(129) Bradaric, C. J.; Leigh, W. J. *Organometallics* **1998**, *17*, 645-651.

(130) Lew, C. S. Q.; Brisson, J. R.; Johnston, L. J. *J. Org. Chem.* **1997**, *62*, 4047-4056.

(131) Ishikawa, M.; Fuchikami, T.; Sugaya, T.; Kumada, M. *J. Am. Chem. Soc.* **1975**, *97*, 5923-5924.

(132) Ishikawa, M.; Kikuchi, M.; Watanabe, K.; Sakamoto, H.; Kunai, A. *J. Organomet. Chem.* **1993**, *443*, C3-C5.

(133) Wiberg, N.; Link, M.; Fischer, G. *Chem. Ber.* **1989**, *122*, 409-418.

(134) Jones, P. R.; Bates, T. F.; Cowley, A. F.; Arif, A. M. *J. Am. Chem. Soc.* **1986**, *108*, 3122-3123.

(135) Leigh, W. J.; Bradaric, C. J.; Morkin, T. L.; Li, X. *Organometallics* **2001**, *20*, 932-936.

(136) Toltl, N. P.; Leigh, W. J. *Organometallics* **1996**, *15*, 2554-2561.

(137) Wiberg, N.; Wagner, G. *Angew. Chem. Int. Ed. Engl.* **1983**, *22*, 1005-1006.

(138) Kerst, C.; Boukherroub, R.; Leigh, W. J. *J. Photochem. Photobiol. A:Chem.* **1997**, *110*, 243-246.

(139) Kerst, C.; Byloos, M.; Leigh, W. J. *Can. J. Chem.* **1997**, *75*, 975-982.

(140) Wiberg, N.; Preiner, G.; Schieda, O. *Chem. Ber.* **1981**, *114*, 3518-3532.

(141) Moss, R. A. Absolute Kinetics of Intramolecular Alkylcarbene Reactions; In *Advances in Carbene Chemistry, Vol. I*; Brinker, U. H., ed. JAI Press Inc.: Greenwich, Connecticut, 1994; pp 59-88.

(142) Jackson, J. E.; Soundararajan, N.; Platz, M. S.; Liu, M. T. H. *J. Am. Chem. Soc.* **1988**, *110*, 5595-5596.

(143) Moss, R. A. *Pure Appl. Chem.* **1995**, *67*, 741-747.

(144) Platz, M. S.; Modarelli, D. A.; Morgan, S.; White, W. R.; Mullins, M.; Celebi, S.; Toscano, J. P. *Prog. React. Kinet.* **1994**, *19*, 93-137.

(145) Jensen, P.; Bunker, P. R. *J. Chem. Phys.* **1988**, *89*, 1327-1332.

(146) Irikura, K. K.; Goddard, W. A. I.; Beauchamp, J. L. *J. Am. Chem. Soc.* **1992**, *114*, 48-51.

(147) Moss, R. A.; Wlostowski, M.; Shen, S.; Krogh-Jespersen, K.; Matro, A. *J. Am. Chem. Soc.* **1988**, *110*, 4443-4444.

(148) Gallo, M. M.; Schaefer, H. F., III *J. Phys. Chem.* **1992**, *96*, 1515-1517.

(149) Richards, C. A. Jr.; Kim, S.-J.; Yamaguchi, Y.; Schaefer, H. F., III *J. Am. Chem. Soc.* **1995**, *117*, 10104-10107.

(150) a) Dixon, D. A.; Arduengo, A. J. I. *J. Phys. Chem.* **1991**, *95*, 4180-4182. b) Mueller, P.H.; Rondan, N.G.; Houk, K.N.; Harrison, J.F.; Hooper, D.; Willen, B.H.; Leibman, J.F. *J. Am. Chem. Soc.* **1981**, *103*, 5049-5052.

(151) Warkentin, J. Diamino-, Amino(oxy)-, Dioxy-, Amino(thio)-, Oxy(thio)-, and Dithiocarbenes; In *Advances in Carbene Chemistry, Vol. II*; Brinker, U. H., ed. JAI Press Inc.: Greenwich, Connecticut, 1998; pp 245-295.

(152) Kirmse, W. Carbenes and the OH Bond; In *Advances in Carbene Chemistry*; Brinker, U. H., ed. JAI Press Inc.: Greenwich, Connecticut, 1994; pp 1-57.

(153) Bonneau, R.; Liu, M. T. H. *J. Am. Chem. Soc.* **1990**, *112*, 744-747.

(154) Griller, D.; Nazran, A. S.; Scaiano, J. C. *J. Am. Chem. Soc.* **1984**, *106*, 198-202.

(155) Jackson, J. E.; Platz, M. S. Laser Flash Photolysis Studies of Ylide-Forming Reactions of Carbenes; In *Advances in Carbene Chemistry, Vol. I*; Brinker, U. H., ed. JAI Press Inc.: Greenwich, Connecticut, 1994; pp 89-160.

(156) Hadel, L. M. Laser Flash Photolysis; In *Handbook of Organic Photochemistry*; Scaiano, J. C., ed. CRC Press: Boca Raton, 1989; pp 279-292.

(157) Jackson, J. E.; Soundararajan, N.; White, W.; Liu, M. T. H.; Bonneau, R.; Platz, M. S. *J. Am. Chem. Soc.* **1989**, *111*, 6874-6875.

(158) Soundararajan, N.; Jackson, J. E.; Platz, M. S. *Tet. Lett.* **1988**, *29*, 3419-3422.

(159) Bonneau, R.; Liu, M. T. H. 1,2-Hydrogen Migration in Carbenes: Laser Flash Photolysis and Beyond; In *Advances in Carbene Chemistry, Vol. II*; Brinker, U. H., ed. JAI Press Inc.: Greenwich, Connecticut, 1998; pp 1-28.

(160) Miller, D. M.; Schreiner, P. R.; Schaefer, H. F., III *J. Am. Chem. Soc.* **1995**, *117*, 4137-4143.

(161) Modarelli, D. A.; Platz, M. S. *J. Am. Chem. Soc.* **1993**, *115*, 470-475.

(162) Evanseck, J. D.; Houk, K. N. *J. Phys. Chem.* **1990**, *94*, 5518-5521.

(163) Ma, B.; Schaefer, H. F., III *J. Am. Chem. Soc.* **1994**, *116*, 3539-3546.

(164) Evanseck, J. D.; Houk, K. N. *J. Am. Chem. Soc.* **1990**, *112*, 9148-9150.

(165) Platz, M. S. Issues and Challenges in the Chemistry of Alkylcarbenes; In *Advances in Carbene Chemistry, Vol.II*; Brinker, U. H., ed. JAI Press Inc.: Greenwich, Connecticut, 1998; pp 133-174.

(166) Chang, K.-T.; Shechter, H. *J. Am. Chem. Soc.* **1979**, *101*, 5082-5085.

(167) LaVilla, J. A.; Goodman, J. L. *Tet. Lett.* **1990**, *31*, 5109-5112.

(168) Moss, R. A.; Liu, W. *Chem. Commun.* **1993**, 1597-1599.

(169) Haszeldine, R. N.; Scott, D. L.; Tipping, A. E. *J. Chem. Soc. ,Perkin Trans. I* **1974**, 1440-1443.

(170) Kreeger, R. L.; Shechter, H. *Tet. Lett.* **1975**, 2061-2064.

(171) Chapman, O. L.; Chang, C.-C.; Kolc, J.; Jung, M. E.; Lowe, J. A.; Barton, T. J.; Turney, M. L. *J. Am. Chem. Soc.* **1976**, *98*, 7844-7846.

(172) Chedekel, M. R.; Skoglund, M.; Kreeger, R. L.; Shechter, H. *J. Am. Chem. Soc.* **1976**, *98*, 7846-7848.

(173) Closs, G. L.; Coyle, J. D. *J. Am. Chem. Soc.* **1962**, *84*, 4350.

(174) Celebi, S.; Leyva, S.; Modarelli, D. A.; Platz, M. S. *J. Am. Chem. Soc.* **1993**, *115*, 8613-8620.

(175) Yamamoto, N.; Bernardi, F.; Bottoni, A.; Olivucci, M.; Robb, M. A.; Wilsey, S. *J. Am. Chem. Soc.* **1994**, *116*, 2064-2074.

(176) Meier, H. Diazirine-Diazoalkane Interconversions; In *Chemistry of Diazirines*; Liu, M. T. H., ed. CRC Press, Inc.: Boca Raton, Florida, 1987; pp 1-18.

(177) Seburg, R. A.; McMahon, R. J. *J. Am. Chem. Soc.* **1992**, *114*, 7183-7189.

(178) Lowe, G.; Parker, J. *Chem. Commun.* **1971**, 1135-1136.

(179) Erni, B.; Khorana, H. G. *J. Am. Chem. Soc.* **1979**, *102*, 3888-3896.

(180) Frey, H. M.; Penny, D. E. *J. Chem. Soc. , Faraday Trans.* **1977**, 2011-2024.

(181) Brunner, J.; Senn, H.; Richards, F. M. *J. Biol. Chem.* **1980**, *255*, 3313-3318.

(182) Hoffmann, R. *Tetrahedron* **1966**, *22*, 539-545.

(183) Bonneau, R.; Liu, M. T. H. *J. Am. Chem. Soc.* **1996**, *118*, 7229-7230.

(184) Sekiguchi, A.; Ando, W. *Organometallics* **1987**, *6*, 1857-1860.

(185) Griller, D.; Majewski, M.; McGimpsey, W. G.; Nazran, A. S.; Scaiano, J. C. *J. Org. Chem.* **1988**, *53*, 1550-1553.

(186) Goddard, J. D.; Yoshioka, Y.; Schaefer, H. F., III *J. Am. Chem. Soc.* **1980**, *102*, 7644-7650.

(187) Sulzbach, H. M.; Platz, M. S.; Schaefer, H. F., III; Hadad, C. M. *J. Am. Chem. Soc.* **1997**, *119*, 5682-5689.

(188) Moss, R. A.; Jones, M. Jr. Carbenes; In *Reactive Intermediates, Vol. 2*; Jones, M. Jr., Moss, R. A., eds. John Wiley & Sons: New York, 1981; pp 59-131.

(189) Moss, R. A. *Acc. Chem. Res.* **1989**, *22*, 15-21.

(190) White, W. R. I.; Platz, M. S. *J. Org. Chem.* **1992**, *57*, 2841-2846.

(191) Pezacki, J. P.; Pole, D. L.; Warkentin, J.; Chen, T.; Ford, F.; Toscano, J. P.; Fell, J.; Platz, M. S. *J. Am. Chem. Soc.* **1997**, *119*, 3191-3192.

(192) Platz, M. S.; Huang, H.; Ford, F.; Toscano, J. P. *Pure Appl. Chem.* **1997**, *69*, 803-807.

(193) Wiberg, N.; Preiner, G.; Schieda, O. *Chem. Ber.* **1981**, *114*, 2087-2103.

(194) Seyferth, D.; Flood, T. C. *J. Organomet. Chem.* **1971**, *29*, C25-C28.

(195) Sakurai, H.; Tominaga, K.; Watanabe, T.; Kumada, M. *Tet. Lett.* **1966**, 5493-5497.

(196) Murov, S. L.; Carmichael, I.; Hug, G. L. *Handbook of photochemistry*; Dekker: New York, 1993.

(197) Sakurai, H. *J. Organomet. Chem.* **1980**, *200*, 261-286.

(198) Sakurai, H.; Sugiyama, H.; Kira, M. *J. Phys. Chem.* **1990**, *94*, 1837-1843.

(199) Kira, M.; Miyazawa, T.; Sugiyama, H.; Yamaguchi, M.; Sakurai, H. *J. Am. Chem. Soc.* **1993**, *115*, 3116-3124.

(200) Pitt, C. G.; Bock, H. *J. Chem. Soc. Chem. Commun.* **1972**, 28-29.

(201) McDiarmid, R. *J. Phys. Chem.* **1980**, *84*, 64-70.

(202) Ohno, K.; Okamura, K.; Yamakado, H.; Hoshino, S.; Takami, T.; Yamauchi, M. *J. Phys. Chem.* **1995**, *99*, 14247-14253.

(203) Khvostenko, V. I.; Zykov, B. G.; Yuriev, V. P.; Mironov, V. F.; Kovel'zon, G. I.; Panasenko, A. A.; Sheludyakov, V. D.; Gailyunas, I. A. *J. Organomet. Chem.* **1981**, *218*, 155-158.

(204) The Sadtler Standard Spectra. Sadtler Research Laboratories, Inc. **1966**, #129.

(205) Nemeth, G. I.; Selzle, H. L.; Schlag, E. W. *Chem. Phys. Lett.* **1993**, *215*, 151-155.

(206) Sakurai, H.; Kumada, M. *Bull. Chem. Soc. Jpn.* **1964**, *37*, 1894-1895.

(207) Espenson, J. H. *Chemical kinetics and reaction mechanisms*; McGraw-Hill, Inc.: New York, 1995; pp 15-45.

(208) Atkins, P. W. *The Elements of Physical Chemistry*; W.H.Freeman: New York, 1993.

(209) *CRC Handbook of Chemistry and Physics*; CRC Press: Boca Raton, 1995; pp 6-241.

(210) Wiberg, N.; Wagner, G. *Chem. Ber.* **1986**, *119*, 1467-1476.

(211) Leigh, W. J. and Li, X. *Organometallics*, **2001**, In Press.

(212) Przbytek, J. T. *High-Purity Solvent Guide*; Burdick and Jackson Laboratories, Inc.: Muskegon, MI, 1980.

(213) Damrauer, R.; Williams, D. R. *J. Organomet. Chem.* **1974**, *66*, 241-247.

(214) Ahlrichs, R.; Heinzmann, R. *J. Am. Chem. Soc.* **1977**, *99*, 7452-7456.

(215) Seidl, E. T.; Grev, R. S.; Schaefer, H. F., III *J. Am. Chem. Soc.* **1992**, *114*, 3643-3650.

(216) Bernardi, F.; Bottoni, A.; Olivucci, M.; Robb, M. A.; Venturini, A. *J. Am. Chem. Soc.* **1993**, *115*, 3322-3323.

(217) Bernardi, F.; Bottoni, A.; Olivucci, M.; Venturini, A.; Robb, M. A. *J. Chem. Soc., Faraday Trans.* **1994**, *90*, 1617.

(218) Venturini, A.; Bernardi, F.; Olivucci, M.; Robb, M. A.; Rossi, A. *J. Am. Chem. Soc.* **1998**, *120*, 1912-1913.

(219) Carmichael, I.; Hug, G. L. *Appl. Spectrosc.* **1987**, *41*, 1033-1038.

(220) Wintgens, V.; Johnston, L. J.; Scaiano, J. C. *J. Am. Chem. Soc.* **1988**, *110*, 511-517.

(221) Carmichael, I.; Hug, G. L. Spectroscopy and intramolecular photophysics of triplet states; In *CRC handbook of organic photochemistry, Vol. I*; Scaiano, J. C., ed. CRC Press: Boca Raton, 1989; pp 369-404.

(222) Carmichael, I.; Hug, G. L. *J. Phys. Chem. Ref. Data* **1986**, *15*, 1-250.

(223) Leigh, W. J.; Boukherroub, R.; Bradaric, C. J.; Cserti, C. C.; Schmeisser, J. M. *Can. J. Chem.* **1999**, *77*, 1136-1147.

(224) Gusel'nikov, L. E.; Potapov, V. K.; Volnina, E. A.; Orlov, V. Yu.; Vdovin, V. M.; Nametkin, N. S. *Dokl. Akad. Nauk. SSSR* **1976**, *229*, 753-755.

(225) Nagase, S.; Kudo, T. *Organometallics* **1984**, *3*, 324-325.

(226) Nagase, S.; Kudo, T.; Ito, K. Structures, Stability, and reactivity of doubly bonded compounds containing silicon or germanium; In *Applied Quantum Chemistry*; Smith, V. H. Jr., Schaefer, H. F., Morokuma, K., eds. D. Reidel: Dordrecht, 1986; pp 249-267.

(227) Jung, I. N.; Pae, D. H.; Yoo, B. R.; Lee, M. E.; Jones, P. R. *Organometallics* **1989**, *8*, 2017-2019.

(228) Yoo, B. R.; Lee, M. E.; Jung, I. N. *Organometallics* **1992**, *11*, 1626-1632.

(229) Carpenter, B. K. *Acc. Chem. Res.* **1992**, *25*, 520-528.

(230) Pedersen, S.; Herek, J. L.; Zewail, A. H. *Science* **1994**, *266*, 1359-1364.

(231) Chatgilialoglu, C.; Ingold, K. U.; Lusztyk, J.; Nazran, A. S.; Scaiano, J. C. *Organometallics* **1983**, *2*, 1332-1335.

(232) Lew, C. S. Q.; McClelland, R. A. *J. Am. Chem. Soc.* **1993**, *115*, 11516-11520.

(233) Turro, N. J. *Modern Molecular Photochemistry*; Benjamin/Cummings: Menlo Park, 1978, p. 135.

(234) Houk, K. N.; Rondan, N. G.; Mareda, J. *Tetrahedron* **1985**, *41*, 1555-1563.

(235) Dhanya, S.; Kumar, A.; Vatsa, R. K.; Saini, R. D.; Mittal, J. P.; Pola, J. *J. Chem. Soc., Far. Trans.* **1996**, *92*, 179-183.

(236) Horner, J. H.; Tanaka, N.; Newcomb, M. *J. Am. Chem. Soc.* **1998**, *120*, 10379-10390.

(237) Newcomb, M.; Choi, S.; Horner, J. H. *J. Org. Chem.* **1999**, *64*, 1225-1231.

(238) Leigh, W. J.; Workentin, M. S.; Andrew, D. *J. Photochem. Photobiol. A:Chem.* **1991**, *57* , 97-109.

(239) Sung, K.; Tidwell, T. T. *Organometallics* **1997**, *16*, 78-85.

(240) Jutzi, P.; Langer, P. *J. Organomet. Chem.* **1980**, *202*, 401-409.